

The Effects of Surface Modification on Properties of Solid Lubricant Additives

By

Yang Jiao

A thesis submitted to the University of Hertfordshire in partial fulfilment
of the requirement of the degree of Doctor in Philosophy

The programme of research was carried out in the School of Engineering
& Technology, University of Hertfordshire, UK

September 2017

Abstract

Three different fine-particles (lanthanum fluoride nanoparticles, cerium oxide nanoparticles and zinc borate submicron particles) were modified and tested on the purpose of study the effects of surface modified fine-particles when they used as lubricant additives in liquid paraffin. The modified fine-particles were examined and characterised by a FT-IR spectroscopy and a zeta-potential measurer. The tribological performances of surface modified fine-particles were invalided by a pin-on-disc test rig under various experimental environments. The worn surfaces on post-tested pin were analysed by AFM, SEM and a nano-indentation tester.

The results indicated Hexadecyltrimethoxysilane (HS) modified lanthanum fluoride nanoparticles and HS modified cerium oxide nanoparticles all shown better dispersibility than unmodified lanthanum fluoride nanoparticles and unmodified cerium oxide nanoparticles in liquid paraffin (LP). HS modified lanthanum fluoride nanoparticles and HS modified cerium oxide nanoparticles also have been approved that they can improve the tribological properties of LP significantly under various working conditions. The formation of tribo-films on the worn scar is the key mechanism of friction and wear reduction. On the other hand, surface modified zinc borate submicron particles have not demonstrated great potential as an oil lubricant additive under various working conditions.

HS, as a particle surface modifier, could improve the performance of fine-particle oil lubricant additives impressively. The positive effects of HS on both dispersibility and tribological performance of surface modified fine-particles were observed.

Acknowledgement

I would like to express my appreciation to my supervisor team Dr. Yongkang Chen and Dr. Guogang Ren. I could never finish this PhD without their guide and help. Especially my first supervisor, Dr. Chen, thank him for always support me and always be helpful. I know he sacrificed his own holiday many times just for providing me feedbacks in time. I appreciate everything he did to me from the bottom of my heart.

I also would like to thank my mother, my father and Miss Yang Hu, thank you for your unconditioned love, support and patience, I did this PhD not only for myself but also for you all too.

I would like to thank all my colleagues and friends, I will never finish my PhD without their helps and encourages. Especially, I would like to express my appreciation to Dr Chuanli Zhao and Dr Adil Loya for their professional opinions and technical supports.

Last but not least, I would like to give a special thanks to Miss Liming Feng. Thank you for having such a beautiful soul.

Table of Contents

Abstract	I
Acknowledgement	II
Table of Contents	III
List of Figures	IX
List of Tables	XIV
List of Publications	XVI
Nomenclature	XVII
Chapter 1 Introduction	1
1.1 Introduction	1
1.2 Aims and objectives of the project	2
1.3 Thesis outline	3
Chapter 2 Friction and Wear	4
2.1 Introduction	4
2.2 Wear	4
2.2.1 Wear mechanisms	4
2.2.2 Measurement techniques of wear.....	8
2.3 Friction	8
2.3.1 Introduction.....	8
2.3.2 Mechanism of sliding friction of metal.....	10
2.3.3 Adhesion friction	11

2.3.4	Deformation term of friction.....	12
2.3.5	Other terms of mechanism of friction.....	15
2.3.6	Friction transition during sliding contact.....	16
2.4	Summary	18
Chapter 3 Lubrication and Lubricant Additives		19
3.1	Introduction	19
3.2	The regimes of fluid lubrication.....	19
3.3	Boundary lubricating films.....	22
3.3.1	Solid-like boundary films	23
3.3.2	Fluid-like boundary films	25
3.3.3	Replenishment.....	26
3.4	Stribeck curve.....	26
3.5	Previous studies of lubricant additives.....	27
3.5.1	Inorganic lubricant additives.....	28
3.5.2	Organic lubricant additives	33
3.6	Base oils	34
3.7	Summary	35
Chapter 4 Surface Modification on Solid Lubricant Additives		37
4.1	Introduction	37
4.2	Basic principles of surface modification of particle materials.....	37
4.3	Other approaches to improving oil solubility of particle materials.....	38

4.4	Surface modification agents	39
4.5	Previous studies of surface modified particles as lubricant additives	42
4.6	Summary	44
Chapter 5 Materials and Experimental Methods		45
5.1	Introduction	45
5.2	Materials.....	45
5.2.1	Properties of fine-particles	45
5.2.2	Surface modification agents.....	51
5.2.3	Base oils	51
5.3	Experimental methods and apparatus.....	52
5.3.1	Sample characterisation	53
5.3.2	Tribological testing	55
5.3.3	Surface characterisation	59
5.4	Preparation of surface modified particles.....	63
5.5	Preparation of suspensions	64
5.6	Summary	65
Chapter 6 Effects of Surface Modified Cerium Oxide Nanoparticles in Liquid Paraffin.....		67
6.1	Introduction	67
6.2	Experimental preparations.....	67
6.2.1	Characterisation of surface modified cerium oxide nanoparticles.....	67

6.2.2	Pin-on-disc test.....	67
6.2.3	Characterisation of the worn surfaces.....	68
6.3	Results and discussion.....	70
6.3.1	Characterisation of CeO ₂ nanoparticles.....	70
6.3.2	Dispersibility of modified and unmodified cerium oxide nanoparticles.....	71
6.3.3	Anti-wear behaviour.....	76
6.4	Characterisation of the tribo-film.....	80
6.4.1	AFM and Nano-indentation results.....	80
6.4.2	SEM observations and EDS analysis.....	85
6.5	Summary.....	87
Chapter 7 Effects of Surface Modified Zinc Borate Submicron Particles in Liquid Paraffin.....		89
7.1	Introduction.....	89
7.2	Experimental preparation.....	89
7.2.1	Characterisation apparatus.....	89
7.2.2	Procedures and experimental conditions for pin-on-disc tests.....	90
7.2.3	Preparations of lubricant samples.....	91
7.2.4	Characterisation of samples.....	92
7.3	Results and discussion.....	94
7.3.1	Dispersibility of surface modified zinc borate submicron particles.....	94

7.3.2	Wear property of surface modified zinc borate submicron particles in LP.....	97
7.3.3	Coefficient of friction	100
7.4	Summary	101
Chapter 8 Effects of Surface Modified Lanthanum Fluoride Nanoparticles in Liquid Paraffin.....		103
8.1	Introduction	103
8.2	Experimental preparations.....	104
8.2.1	Sample characterisation	104
8.2.2	Pin-on-disc testing	104
8.3	Results and discussions	105
8.3.1	Dispersibility and stability	105
8.3.2	Results of tribological tests	109
8.3.3	Characterisation of one typical worn surfaces	121
8.4	Summary	125
Chapter 9 Discussion.....		127
9.1	Introduction	127
9.2	Effects of surface modified cerium oxide nanoparticles in liquid paraffin	127
9.3	Effects of surface modified zinc borate ultrafine particles in liquid paraffin	129

9.4 Effects of surface modified lanthanum fluoride nanoparticle in liquid paraffin132

9.5 The role of the tribo-film..... 134

Chapter 10 Conclusions and Suggestions for Future Work.....135

10.1 Introduction135

10.2 Conclusions 135

10.2.1 Dispersibility of surface modified particles in an organic solvent135

10.2.2 Effects of surface modified particles on tribological performance of liquid paraffin136

10.2.3 Effects of surface modified particles on formation of tribo-film.....137

10.3 Suggestions for future work138

References.....140

List of Figures

Figure 2-1 An illustration of the principles of Amonton-Coulomb model of friction [47].	11
Figure 2-2 An illustration of a conical asperity slides through a softer body [57].	13
Figure 2-3 An illustration of a spherical asperity slides through a softer body [57].	15
Figure 2-4 Typical curve shapes of running-in reported by Blau [64], Vertical axis: friction force; Horizontal axis: Number of cycles.	17
Figure 3-1 Schematic of different boundary films on a solid surface [83].	22
Figure 3-2 A schematic of boundary lubrication mechanism of surfactant monolayer on the metal surface [17].	24
Figure 3-3 Crystal structure of molybdenum disulphide [90].	25
Figure 3-4 A typical schematic of the Stribeck curve [99].	26
Figure 3-5 A schematic diagram of the chemical structure of triacylglycerides [151].	35
Figure 4-1 Chemical formula of Hexadecyltrimethoxysilane.	40
Figure 4-2 Chemical formula of polyisobutylene succinimide [115].	41
Figure 4-3 Chemical formula of carboxylic acids.	41
Figure 5-1 A transmission electron microscopy (TEM) micrograph of lanthanum fluoride nanoparticles employed in this project.	47
Figure 5-2 A transmission electron microscopy (TEM) micrograph of cerium oxide nanoparticles employed in this project.	48

Figure 5-3 A transmission electron microscopy (TEM) micrograph of zinc borate ultrafine powders employed in this project.....50

Figure 5-4 Fourier transform infrared spectroscopy (Perkin-Elmer Spectrum 100) employed in University of Hertfordshire.....54

Figure 5-5 Dynamic Light Scattering (DLS) (Malvern Zetasizer-Nano Series) employed in University of Hertfordshire.....55

Figure 5-6 A representation of pin-on-disc tester’s basic working principle.57

Figure 5-7 The POD 2 pin-on-disc tester (Teer Coatings Ltd.) employed in this study.57

Figure 5-8 A typical photography of wear track on pre-tested sample disc.60

Figure 5-9 The SEM employed in this study.61

Figure 5-10 The atomic force microscope employed in this study.....62

Figure 5-11 The Nano-indentation tester in University of Hertfordshire.63

Figure 6-1 FT-IR spectra of: (a) unmodified CeO₂ nanoparticles; (b) OA; (c) HS; (d) OA modified CeO₂ nanoparticles; (e) HS modified CeO₂ nanoparticles.70

Figure 6-2 Status of the sedimentation of the lubricant samples at the different periods after the sample preparation: at zero hour: (a-1) LP + CeO₂, (b-1) LP + OA-CeO₂, (c-1) LP +HS-CeO₂, and at the 48th hour: (a-2) LP + CeO₂, (b-2) LP + OA-CeO₂, (c-2) LP +HS-CeO₂.....76

Figure 6-3 Optical micrographs of wear scars lubricated using: (a) LP, (b) LP with CeO₂ nanoparticles, (c) LP with OA modified CeO₂ nanoparticles, (d) LP with HS modified CeO₂ nanoparticles, (e) LP with OA, (f) LP with HS.78

Figure 6-4 Effect of different lubricant additives on volume loss of the bearing balls.
79

Figure 6-5 Morphologies of the tribo-film generated by LP with HS modified CeO₂ nanoparticles: (a) optical image, (b) AFM surface topographic image, (c) 3D AFM surface topographic image.81

Figure 6-6 Indentation curves obtained at different domains on the worn surface lubricated by LP with HS modified CeO₂ nanoparticles: (a) on substrate, (b) on tribo-film.....82

Figure 6-7 AFM surface topographic images of the worn surfaces lubricated with different lubricants: (a) LP; (b) LP with unmodified CeO₂ nanoparticles; (c) LP with OA modified CeO₂ nanoparticles; (d) LP with HS modified CeO₂ nanoparticles.84

Figure 6-8 SEM images and EDS patterns of worn surfaces lubricated with LP with HS modified CeO₂ nanoparticles: (a) worn surface morphology, (b, c) magnified SEM image, (d) EDS patterns of the substrate, (e) EDS patterns of the tribo-film.....86

Figure 7-1 FTIR spectra of: (a) Unmodified zinc borate submicron particles; (b) OA; (c) HS; (d) OA zinc borate submicron particles; (e) HS zinc borate submicron particles.93

Figure 7-2 Images of wear scars taken by optical microscope and WSD measurements of, (a) LP; (b) 1% ZB +LP; (c) 1% OA-ZB + LP; (d) 1% HS-ZB + LP.98

Figure 7-3 Images of wear scars taken by optical microscope and WSD measurements of, (a) LP; (b) 0.5% ZB + LP; (c) 0.5% OA-ZB + LP; (d) 0.5% HS-ZB + LP.99

Figure 7-4 Coefficient of friction versus time curves of 1% HS-ZB + LP, 1% OA-ZB + LP, 1% ZB + LP and LP recorded during pin-on-disc test under Experimental Condition (ii)..... 100

Figure 7-5 Coefficient of friction versus time curves of 0.5% HS-ZB + LP, 0.5% OA-ZB + LP, 0.5% ZB + LP and LP recorded during pin-on-disc test under Experimental Condition (iii)..... 101

Figure 8-1 Status of the sedimentation of the lubricant samples at the different periods after the sample preparation: at 00 hour: (a-1) LP + LaF₃ (1% wt), (b-1) LP + HS-LaF₃ (1% wt), and at the 48th hour: (a-2) LP + LaF₃ (1% wt), (b-2) LP + HS- LaF₃ (1% wt). 108

Figure 8-2 WSD values obtained after pin-on-disc tests with an applied loading of 10 N..... 110

Figure 8-3 Optical micrographs of wear scars (pin balls) with WSD measurements. 111

Figure 8-4 Optical micrographs of wear scars (pin balls) with WSD measurements. 112

Figure 8-5 Optical micrographs of wear scars (pin balls) with WSD measurements. 113

Figure 8-6 Optical microscope images and WSD measurements of wear scars on the pin-ball lubricated by 1% HS-LaF₃ + LP, taken at different period during the pin-on-disc test, (a) 1100s after test started; (b) 2500s after test started; (c) 3600s after test started..... 114

Figure 8-7 Coefficient of friction versus time curves of 1% HS-LaF₃ + LP, 1% LaF₃ + LP and LP recorded during pin-on-disc tests..... 116

Figure 8-8 Images of wear scars (pin balls) with WSD measurements, taken by optical microscope. 119

Figure 8-9 Coefficient of friction versus time curves of 1% HS-LaF₃ + LP, 1% LaF₃ + LP and LP recorded during pin-on-disc tests..... 120

Figure 8-10 The images of worn surface of pin-ball (1% HS-LaF₃, 30 N, 3600s); (a) optical image; (b) AFM topography; (c) AFM 3-D view..... 122

Figure 8-11 (a) Load versus depth curves of tribo-film and substrate; (b) An AFM image of the indent that left by a Berkovich tip of nano-tester on tribo-film; (c) An AFM image of the indent that left by a Berkovich tip of nano-tester on substrate.... 124

List of Tables

Table 5-1 A list of properties of unmodified LaF ₃ nanoparticles.	46
Table 5-2 A list of properties of unmodified CeO ₂ nanoparticles.	48
Table 5-3 A list of properties of unmodified zinc borate submicron particles.	50
Table 5-4 A list of properties of HS.....	51
Table 5-5 A list of properties of OA.....	51
Table 5-6 A list of mechanical properties of AISI52100 steel.	58
Table 5-7 A list of calculation results of Hertz pressure under different loading conditions.....	59
Table 6-1 Different formulations with pure LP as control fluid.....	69
Table 6-2 The mean values of conglomerate size and Zeta-potential readings of CeO ₂ nanoparticles dispersed in methanol.	72
Table 6-3 The standard deviations of conglomerate size results of cerium oxide nanoparticles dispersed in methanol. (Unit:nm)	74
Table 6-4 The standard deviations of Zeta-potential results of cerium oxide nanoparticles dispersed in methanol. (Unit:mV)	74
Table 6-5 A comparison of mechanical properties of the tribo-film and the substrate.	83
Table 6-4 Quantified elemental analysis on the worn surface shown in Figure 6-8....	87
Table 7-1 The settings of experimental conditions.....	90
Table 7-2 Sample code and definition of associated fluid.....	91

Table 7-3 Assignment of absorption bands and corresponding wave numbers from the FTIR spectrums shown in Figure 7-1.92

Table 7-4 Conglomerate size and zeta-potential readings of ZB, OA-ZB and HS-ZB.95

Table 7-5 The standard deviations of conglomerate size results of zinc borate submicron-particles dispersed in methanol. (Unit:nm).....96

Table 7-6 The standard deviations of Zeta-potential results of of zinc borate submicron-particles dispersed in methanol. (Unit:mV).....97

Table 8-1 Experimental conditions of pin-on-disc test..... 104

Table 8-2 Different formulations with pure LP as controlled fluid. 105

Table 8-3 Conglomerate size and Zeta-potential of CeO₂ nanoparticles dispersed in methanol with a concentration of 0.05%. 106

Table 8-4 The standard deviations of conglomerate size results of lanthanum fluoride nanoparticles dispersed in methanol. (Unit:nm) 107

Table 8-5 The standard deviations of Zeta-potential results of lanthanum fluoride nanoparticles dispersed in methanol. (Unit:mV) 107

Table 8-6 Hardness of tribo-film and substrate obtained by nano-indentation tester.. 123

Table 9-1 A comparison of WSD measurements between published results and results presented in section 7.3..... 130

List of Publications

[1] C. Zhao, Y. K. Chen*, Y. Jiao, A. Loya and G. G. Ren, The preparation and tribological properties of surface modified zinc borate ultrafine powder as a lubricant additive in liquid paraffin, *Tribology International*, 70, 156 (2014).

[2] C. Zhao, Y. Jiao, Y. K. Chen* and G. G. Ren, The tribological properties of zinc borate ultrafine powder as a lubricant additive in sunflower oil, *Tribology Transactions*, 57 (3), 425 (2014).

Nomenclature

Abbreviations

AFM atomic force microscope

CeO₂ cerium oxide nanoparticle

DDP dialkyl-dithiophosphate

DLS dynamic light scattering

EDS the energy dispersive spectroscopy

EHA 2-ethyl hexoic acid

EP extreme pressure

ESFD ethanol supercritical fluid drying technique

FTRI Fourier transform infrared spectroscopy

HS hexadecyltrimethoxysilane

HS-CeO₂ hexadecyltrimethoxysilane modified cerium oxide nanoparticle

HS-ZB hexadecyltrimethoxysilane modified zinc borate submicron particle

HS- LaF₃ hexadecyltrimethoxysilane modified lanthanum fluoride nanoparticle

LaF₃ lanthanum fluoride nanoparticle

LP liquid paraffin

OA oleic acid

OA-CeO₂ oleic acid modified cerium oxide nanoparticle

OA-ZB oleic acid modified zinc borate submicron particle

PAG polyalkylene glycol

PAO poly-alpha-olefin

SEM scanning electron microscope

TCP tricresyl phosphate

TEM transmission electron microscopy

TXP trixylyl phosphate

WSD wear scar diameter

ZB zinc borate submicron particle

ZDDP dialkyl dithiophosphate

Chapter 1 Introduction

1.1 Introduction

The recent breakthrough in technology and chemistry of fine-particles has allowed the synthesis of micro-sized, even nano-sized solid particles. Some fine-particle materials could offer superior lubrication qualities to the base oil and enhance the effectiveness of lubricant systems as solid lubricant additives [1-7]. Compared with liquid organic lubricant additives, the advantages of inorganic solid lubricant additives can be listed as follows: 1) better stability under high and low temperature, 2) sulphur, phosphorus and chlorine free, more environments friendly, 3) no induced corrosion on the surface of working components [5, 8]. Although there are some disadvantages of inorganic solid lubricant additives, such as the poor stability and dispersibility in organic solvents. However, since the recent development of surface modification technology, these disadvantages could be compensated by conducting surface modification on particle surfaces.

Surface modification of solid inorganic lubricant additives could attach hydrocarbon chains to the surface of particle. These hydrocarbon chains provide better interactions with the hydrocarbon solvent and therefore, improve the dispersibility of particles [9]. The most often seen surface modification agents such as oleic acid (OA), decanoic acid, dialkyl-dithiophosphate (DDP) and 2-ethyl hexoic acid (EHA) have been extensively studied during the past decade. In particular, in the field of tribology, excellent tribological performance of the particles which were modified by aforementioned surface agents has been reported. For examples, results have indicated that surface modified ceria oxide [10], titanium oxide [2], zinc sulphide [11], copper

[12], molybdenum disulphide [13] and palladium [14] have improved the tribological performance of base lubricants significantly. However, the investigation of relatively newer surface modification agents, such as hexadecyltrimethoxysilane (HS), is seldom. Many of fine-particles such as lanthanum fluoride nanoparticle, cerium oxide nanoparticle and zinc borate ultrafine particle have shown great potential as oil lubricant additives [7, 15-19]. However, the effects of using surface modified fine-particles as lubricant additives under various working conditions are still unknown.

In this study, HS has been selected as a surface modification agent. Three types of fine-particle materials that have different particle sizes (lanthanum fluoride nanoparticle, cerium oxide nanoparticle and zinc borate ultrafine particle) were synthesised and modified by HS.

1.2 Aims and objectives of the project

This research aimed to study the effects of surface modified solid lubricant additives on liquid paraffin and to explore the potential of HS as a surface modification agent of solid lubricant additive. These aims were achieved through following objectives:

- Synthesis HS and OA modified CeO₂, zinc borate and LaF₃ particles
- Study the tribological effects of surface modified particles on liquid paraffin under various working conditions
- Explore the tribological mechanisms of lubricant and surface modified particles through analysis of wear scars and tribo-films
- Evaluate the performance of surface modification agent and surface modified particles as lubricant additives via comparing results

1.3 Thesis outline

This thesis contains ten chapters in total with five major components: literature reviews, experimental methods, test results, discussion and conclusions.

The literature reviews are divided into three chapters regarding the topic for a clearer view. Chapter 2 provides an understanding of basic theories of wear and friction. The tribological measurement techniques have also been presented in this part of the thesis. Chapter 3 is a review of lubrication mechanisms and previous studies of lubricant additives. Chapter 4 has summarised fundamental theories of surface modification and characteristics of different surface modification agents.

The detailed information of test methods and experimental apparatus are presented in chapter 5. The specifications of materials and test procedures have also been listed there.

Test results of surface modified CeO₂, zinc borate and LaF₃ are presented in chapters 6, 7 and 8 respectively. The effects and mechanisms of surface modified particles in liquid paraffin have been discussed in chapter 9. Eventually, the final chapter of this thesis presents conclusions that based on all findings from this research. The suggestions of future work are also listed in chapter 10.

Chapter 2 Friction and Wear

2.1 Introduction

Tribology is the science that embraces friction, wear and lubrication [20, 21]. Under most of the circumstances, low friction and less wear are usually desirable[22]. Lubrication of a tribo-pair is the most common approach to reduce friction or wear, and the main purpose of applying lubricant additives is to help the lubrication system to decrease friction or wear more efficiently. Basic tribological theories are the foundation of studying mechanisms of lubricant and lubricant additives. In order to investigate the tribological performance of lubricant additives and to explore experimental methods, a study of principles and measurement techniques of friction and wear is essential. This chapter presents the basic mechanisms and measurement techniques of friction and wear as a part of the literature review.

2.2 Wear

2.2.1 Wear mechanisms

Wear is the phenomenon that normally occurs in a sliding, rolling, or impact motions between two solid rubbing surfaces which lead to deformation or material loss from one or both surfaces [21]. In many cases, wear leads to damage of working component and even mechanical failure under many of circumstances [23]. Generally speaking, wear is undesirable in industry. Wear is a response of a system which is affected by many factors such as working conditions and material properties. Low wear is not always associated with the presence of a low coefficient of friction. In

some cases low coefficient of friction occurs associated with significant wear losses and vice versa [24].

Adhesive wear, abrasive wear, fatigue wear and tribo-chemical wear are four principal types of wear mechanisms [25]. They are named based on their material removal mechanisms. These wear mechanisms appear either alone or as a combination and could cause aggressive material loss on the mating surfaces.

2.2.1.1 Adhesive wear

Adhesive wear is normally a result of the adhesive bonding between asperities on two flat rubbing surfaces under the sliding contact. The possibility of occurring adhesive wear is high if two rubbing surfaces are made of an identical material since the adhesive and bonding is strong in such situation [26]. During the sliding contact, asperities are sheared and compressed unceasingly and crack, plastic deformation and fragment transfer occurs on two rubbing surfaces respectively. As the sliding continues, more and more fragment are generated and transferred between two surfaces. Then an accumulation takes place, some of the accumulated fragments fall off from rubbing surfaces and become wear particles [24, 27]. This process can be aggravated under a high loading and high sliding speed. Surfaces worn by adhesive wear normally have high roughness and grooves. Adhesive wear can happen whether the surfaces are lubricated or not. In another word, adhesive wear can never be eliminated [28, 29]. However, severe adhesive wear can be reduced or minimised by applying a lubricant which can form a protective tribo-film. Many lubricants that contain organic lubricant additives can react with working environment speedily and form tribo-films to prevent adhesive [8, 30, 31]. However, some studies indicated that the active chemicals in organic additives could be corrosive to the rubbing surfaces

and shorten service length of working parts [8, 32]. Inorganic lubricant additives would be a suitable alternative to reduce corrosion since inorganic lubricant additives are normally more chemically stable [5, 8].

2.2.1.2 Abrasive wear

The definition of abrasive wear has been described by Bhushan as follows:

'Abrasive wear occurs when asperities of a rough, hard surface or hard particles slide on a softer surface and damage the interface by plastic deformation or fracture [33].'

Generally, abrasive wear could be categorised into two types, two-body abrasive wear and three-body abrasive wear [34, 35]. Two body abrasive wear occurs when relatively harder surface slides on a softer surface. Grinding, cutting and machining are typical examples of two-body abrasive wear [26]. Three body abrasive wear occurs when one or both surfaces are abraded by grits or particles that are trapped between two surfaces or embedded on a softer surface [26, 36]. The abrasive grits must have a higher hardness than at least one of the surfaces. In this case, the relative harder surface of two surfaces plays a role as a third body. Examples of three-body abrasive could be found in mechanical operations such as free-abrasive lapping and polishing [26]. Normally abrasive grooves that are caused by abrasive wear of particles or asperities from the harder surface can be observed on the worn scar. Micro-cutting can be the main mechanism of the generation of wear debris. The hardness and size of particles could exert a strong influence on the degree of abrasive wear [37]. During a sliding process, three-body abrasive wear normally is a consequence of adhesive wear since the debris generated by adhesive wear could be

trapped between surfaces and become abrasive grits [26]. Therefore, in some cases, particle lubricant additives may cause abrasive wear if the hardness of particles reaches a certain level.

2.2.1.3 Fatigue wear

Fatigue wear is a result of a very high loading that repeats a large number of times during sliding and rolling process. When the applied load exceeds the fatigue strength of the material, fatigue happens [38]. Fatigue starts with cracks beneath the contact surfaces and then spreads while the loading cycles continue. When the amount of cracks developed to a critical level, the material above cracks will be removed and fatigue wear happens. The observation of crack formation and flaking of surface materials are important to the characterisation of fatigue wear [39]. Fatigue wear occurs with or without lubrication and in some cases, improper lubrication may accelerate fatigue wear [40].

2.2.1.4 Chemical (corrosive) wear

Chemical wear is a result of friction in a corrosive environment. Normally, surfaces will be covered by a layer that formed by a chemical product of corrosion. This layer can protect the surfaces from further corrosions. However, once the sliding takes place on the surfaces, the protective layer can be damaged and the beneath material will be exposed. So, the corrosive elements in the environment could react with surfaces continuously [41]. The degree of chemical wear depends on how energetic the chemical reactions are [42]. Since the chemical wear requires both chemical reactions and rubbing, to reduce the influence of chemical wear, corrosive

environment such as high temperature and high humidity should be avoided during experiments.

2.2.2 Measurement techniques of wear

The purpose of a wear test usually is to simulate a specific condition or environment and to evaluate wear properties of the test specimens. Measurement of wear is a very important part of all wear tests because it is one of the major factors to evaluate the tribological property of materials. The nature of wear is a removal or volume loss of materials and therefore, the volume measurement and mass measurement are two common direct measure methods [43]. The volume loss of materials can be calculated based on the measurement of a wear scar or wear track. There are mainly three ways to collect the dimensions data, such as wear scar diameter (WSD), surface profile or mass losses. Microscopy approach is normally used to measure WSD and observe worn surface and wear track. A smaller WSD means less material loss of the worn surface and the anti-wear property of lubricants can be evaluated by comparing the values the WSD [44]. The surface profile can be obtained by a surface profilometry which is more accurate. For known density materials, a volume loss also can be calculated from a mass loss. Mass loss can be measured by using a precision balance directly [45].

2.3 Friction

2.3.1 Introduction

Friction force is the resistive tangential force in the opposite direction of a sliding or rolling motion during a contact when a body moves over another tangentially. The resistance to motion is called friction [46]. Friction force plays either positive or

negative role under different circumstances. For instance, brake device of vehicles has been designed to maximise the friction. But in wheel bearings, high friction is undesirable [46]. Friction leads to an unavoidable energy loss and wear and therefore in most of sliding or rotating components of machinery applications, low friction is expected. Different from hardness, plasticity or other material properties, friction is a response of the system. High friction happens if two clean solid surfaces are sliding over each other. However, friction can be reduced dramatically if the contact surfaces are separated by chemical films or adsorbents. Static friction F_s is the minimum value of the force that starts a relative motion of a solid body. The force that is required to continue this motion is called the kinetic friction force or dynamic friction force (F_k) [47].

Leonardo da Vinci and Guillaume Amontons are pioneers who described and explored two basic rules of friction [48]. They are:

- The ratio of the friction force (F) to the normal load (W) is called coefficient of friction (μ), and μ is independent of normal load [48].

$$F = \mu W \qquad 2.3.1 - 1$$

- The friction force or coefficient of friction is independent of the nominal area of contact.

In 1785, Coulomb added the third rule based on these two rules mention above:

- The coefficient of friction (or friction force) is independent of the sliding velocity once motion commences [49].

These three rules that build the foundation of tribology are entirely empirical. However, during experimental practices, it was observed that the first two rules were not applied to many cases. Bhushan emphasised that:

' μ is strictly constant only for a given pair of sliding materials under a given set of operating conditions (temperature, humidity, normal pressure and sliding velocity). Many materials show dependence of normal load, sliding velocity and apparent area on the coefficients of static and kinetic friction in dry and lubricated contacts.' [50]

Therefore, for tests which on purpose to measure the coefficient of friction, the test conditions must be controllable.

2.3.2 Mechanism of sliding friction of metal

Amontons and Coulomb, two pioneers in tribology have pointed out that metallic friction is caused by the mechanical interaction of asperities on contacting surfaces, in other word the surface roughness of metal has been considered as the dominating cause of friction [50]. Fig. 2-1 shows an illustration of Amonton-Coulomb model of friction. This friction model was established based on Amontons and Coulomb's theory, and also is probably one of the earliest friction models [51]. Assuming two surfaces that both have sawtooth geometry asperities are sliding over each other under the normal load W from position A to position B, the coefficient of friction μ is equal to $\tan \theta$ (shown in Fig. 2-1) since the work done by the friction force is equal to the work done against W [47]. However, Amontons and Coulomb's theory did not include the mechanisms of energy dissipation. Since friction is a dissipative process, it is pointed out by many scholars that this theory is inaccurate under many circumstances [50].

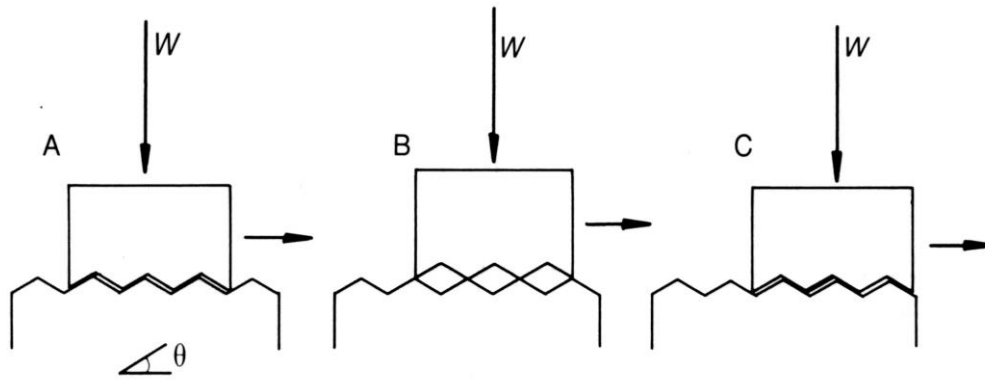


Figure 2-1 An illustration of the principles of Amonton-Coulomb model of friction [47].

Bowden and Tabor firstly suggested that the dominant mechanism for the friction of metals was plastic deformation such as adhesion and ploughing (deformation of metal). This theory soon becomes one of the widely accepted friction theories [52]. Therefore, an equation can be written as follows,

$$F = F_a + F_d \quad 2.3.2 - 1$$

where F is the total intrinsic friction force of a system, F_a is the forces required to shear adhered junctions and F_d is the force needed to continue the deformation [53]. The adhesion term of friction and deformation term of friction will be discussed in next two sections.

2.3.3 Adhesion friction

Bowden and Tabor defined that the adhesion friction force (F_a) equals to the product of the true contact area (A_r) and the average shear strength of dry contact (τ) as the equation below.

$$F_a = A_r \tau \quad 2.3.3 - 1$$

For the case of a partial lubricated contact,

$$F_a = A_r [\alpha \tau_a + (1 - \alpha) \tau_l] \quad 2.3.3 - 2$$

and

$$\tau_l = \frac{\eta_l V}{h} \quad 2.3.2 - 3$$

where τ_a is the average shear strengths of the dry contact; τ_l is the average shear strengths of the lubricant film; α is the fraction of unlubricated area; η_l is the absolute viscosity of the lubricant; V is the relative sliding velocity and h is the liquid film thickness [54]. Adhesion friction could dominate the overall friction force in some cases, especially for the contacts that conducted under humid environments [54].

2.3.4 Deformation term of friction

In Bowden and Tabor classic theory of friction, the deformation term of friction has not been described as the primary component of friction. However, in the later study published by Tabor and Greenwood, deformation term of friction is considered as one of the dominant components of friction when a solid surface slides over another [55]. Bhushan suggested that two types of interaction could happen during the sliding. From the microscopic point of view, the interaction is considered as the plastic deformation and displacement of the asperities. Macroscopic interaction occurs when a harder surface contacts a softer one. The asperities of the harder material normally will plough into the softer surface and generate grooves via plastic deformation. Wear

particles trapped between sliding surfaces can also cause ploughing on one or both of the surfaces. The ploughing may lead to fracture, tear or fragmentation of material [21]. The further study from Rigney and Hirth revealed the significance of plastic deformation in metal to metal contact from the angle of energy dissipation [56]. Their work attempted to quantify the contribution of plastic deformation through calculation of plastic work done in a certain region.

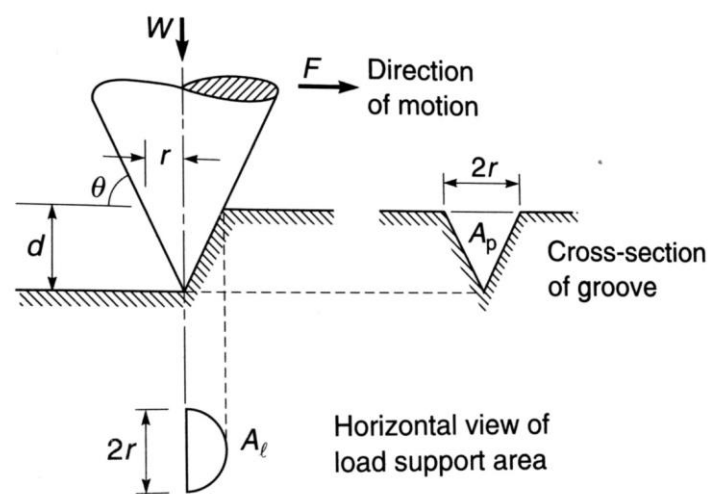


Figure 2-2 An illustration of a conical asperity slides through a softer body [57].

The calculation of deformation (ploughing) component of the friction force for conical and spherical asperities has been done by Bhushan [53]. As shown in Fig. 2-2, assuming an asperity that has conical shape slide over a softer body with an attack angle of θ , the horizontal projection of the asperity contact A_l (the load supporting area) can be calculated by the equation 2.3.4-1 where r is the radius of load supporting area.

$$A_l = \frac{1}{2} \pi r^2 \quad 2.3.4-1$$

The vertical projection of asperity contact A_p (the friction force supporting area) is where d is the depth of the cross-section groove:

$$A_p = \frac{1}{2}(2rd) = r^2 \tan\theta \quad 2.3.4-2$$

If the yielding of the body is assumed isotropic and that its yield pressure is p , the tangential force W and the normal load F are [58]:

$$W = pA_l \quad 2.3.4-3$$

$$F = pA_p \quad 2.3.4-4$$

Hence, the expression for μ_p is,

$$\mu_p = \frac{F}{W} = \frac{A_p}{A_l} \quad 2.3.4-5$$

Therefore,

$$\mu_p = \frac{2 \tan\theta}{\pi} \quad 2.3.4-6$$

Generally, the value of μ_p will not exceed to 0.1 since the slopes of real surfaces are never greater than 10° [59].

The contact between a spherical asperity and a softer body is shown in Fig. 2-3, with R is the radius of asperity, the expression for μ_p can be written as:

$$\mu_p = \frac{A_p}{A_t} = \frac{4}{3\pi} \frac{r}{R} \quad 2.3.4-7$$

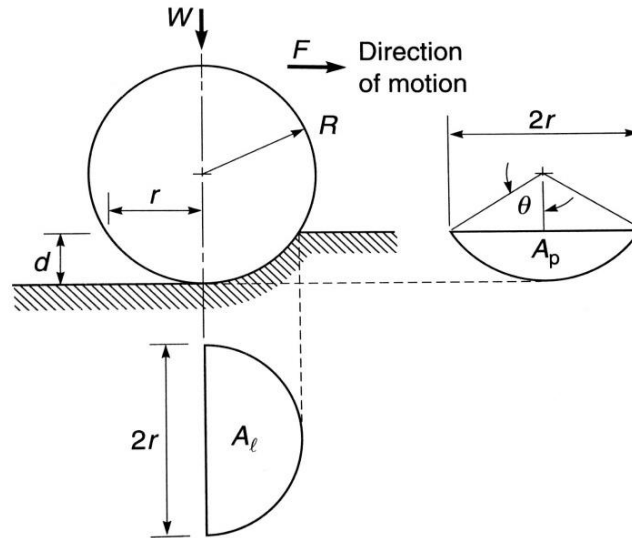


Figure 2-3 An illustration of a spherical asperity slides through a softer body [57].

Suh and Sin developed the model and the expression of μ_p by including the ploughings which were caused by wear. They claimed that the width of ploughing groove is normally greater in comparison of the radius of spherical asperity [60]. The asperities or wear particles that have relatively high value of θ such as abrasive materials normally lead to high ploughing component of friction. However, for most engineering surfaces, the ploughing component has been considered relatively small since the θ normally is small [61].

2.3.5 Other terms of mechanism of friction

The friction behaviour can also be affected by other factors such as grain boundary effects and crystallographic structure of a material [61]. Buckley found that the coefficient of friction was influenced by the grain boundaries in a material. As a result of a series of friction experiments, Buckley observed that grain boundaries could lead

to the accumulation of dislocations and then result in strain hardening of the surficial layers. This strain hardening will increase the resistance of sliding and therefore, affect the anti-friction performance of the material [62]. Rabinowicz attributed that there was a relationship between the number of slip planes and tribological performance of materials. His observation demonstrated that the primary reason that hexagonal close-packed metal had a lower coefficient of friction and better anti-wear performance than face-centred cubic metal is that hexagonal close-packed metal has less number of slip planes [63].

2.3.6 Friction transition during sliding contact

Friction transition is a phenomenon that happens in most of sliding tests, such as pin-on-disc tests since the friction force is not always stable or maintained at a certain level during sliding processes. The fluctuation of the friction force during the beginning period of a sliding contact between an unworn tribo-pair is called running-in. The friction force soon will be stabilised and fluctuations will be stopped as the system becomes steady. A change of condition of mating surfaces leads to such friction transition. This friction transition could happen multiple times in a tribo-system during running-in. Running-in has a strong influence on the life span and performance of a sliding system such as gear boxes or brake systems. In order to reduce the chance of system failure, an appropriate running-in should be given. Surfaces will become smoother since high asperities will be worn off or smoothed out during the running-in. Also running-in leads to removal of oxidation films of surfaces and generation of the steady film and this creates an excellent environment for a better mating of contact surfaces.

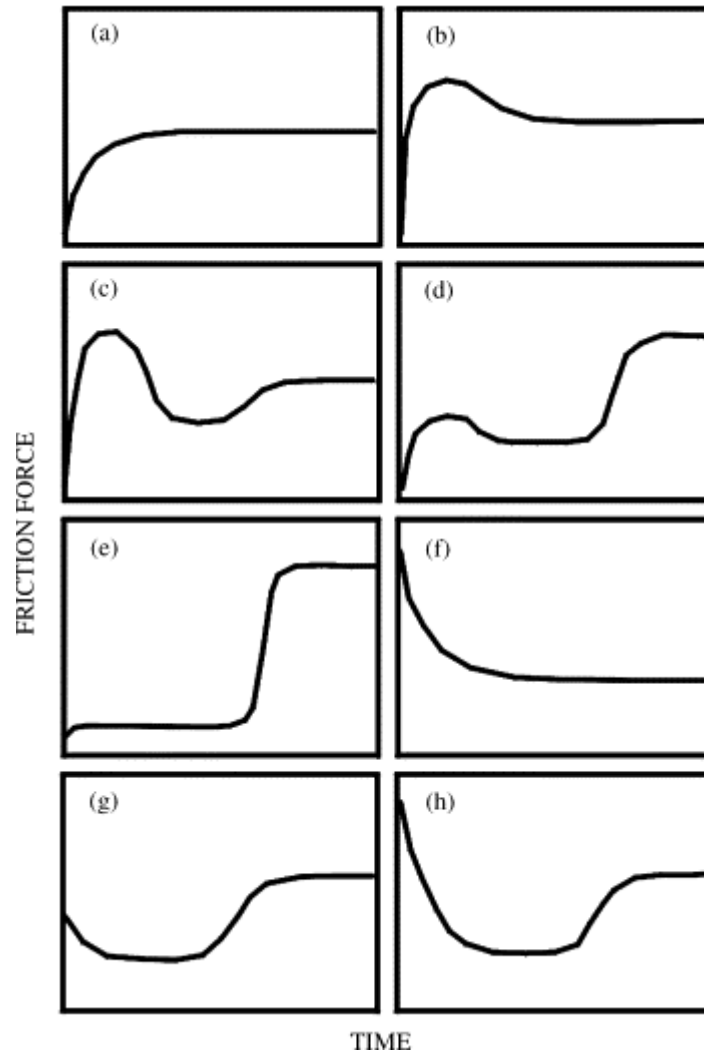


Figure 2-4 Typical curve shapes of running-in reported by Blau [64], Vertical axis: friction force; Horizontal axis: Number of cycles.

Fig. 2-4 shows eight typical friction running-in curves which have been sorted and reported by Blau based on previous studies. He did a thorough review of different types of friction transition. He pointed out that running-in is a complex process which is influenced by how the energy in the tribo-system is partitioned [64, 65]. Fig. 2-4 (b) is the typical running-in curve of boundary lubrication or unlubricated metal to metal contact. The coefficient of friction decreased after the initial growth caused by the roughness of surfaces. Once the surfaces become relatively smooth and uniform, the coefficient of friction starts to drop and stable [64].

2.4 Summary

This chapter presented a review of basic theories and mechanisms of wear and friction. The calculation method of wear and friction has been summarised. It has been noticed that the testing environment of a tribological test has a strong influence on the accuracy of the results.

Chapter 3 Lubrication and Lubricant Additives

3.1 Introduction

Lubricant has been used to reduce wear and friction for over two thousand years [24, 66]. The general mechanism of lubricant is to generate a layer between contact surfaces that has relatively lower shear strength [67]. A lubricant could be either fluid (e.g. vegetable oil and mineral oil, etc.) or solid (e.g. polymer and tungsten, etc.). Lubricant additives are the substances that are able to improve the tribological performance or to provide additional properties of the base lubricants [68]. This chapter included a literature review of basic lubrication theories and the regimes of different lubrication conditions. The results from previous studies of several types of lubricant additives and base oils have been summarised and presented in this chapter too.

3.2 The regimes of fluid lubrication

Lubrication has various forms that could be identified by the thickness of lubrication film. There are four common regimes of fluid film lubrication which are hydrodynamic, elastohydrodynamic, mixed and boundary lubrication [69].

Hydrodynamic lubrication is also called fluid film lubrication. Hydrodynamic can be observed when contact surfaces are completely separated by a lubricant film. The thickness of this film is normally larger than 0.25 μm , sometimes could reach to 500 μm [69, 70]. The hydrodynamic lubrication is an ideal lubrication condition since a relatively thicker lubrication film carries the primary load and prevents solid to solid

in contact directly. The lowest coefficient of friction in the hydrodynamic lubrication could be smaller than 0.003 [71].

Elastohydrodynamic lubrication is actually a particular type of hydrodynamic lubrication. In some cases of hydrodynamic lubrication, the lubrication is significantly enhanced by the elastic deformation of the contact surfaces, therefore this term of hydrodynamic lubrication is called elastohydrodynamic lubrication [72]. In elastohydrodynamic lubrication, the load is mainly carried by the lubrication film also. However, it is observed that the actual contact between asperities may occur in the certain isolated area [73]. Elastohydrodynamic lubrication could be induced by harsh working condition, such as heavy load or the highly deformable materials of contact surfaces [74]. The typical thickness of lubrication film of elastohydrodynamic lubrication is normally between 0.025 μm to 5 μm [73].

When a system is dominated by both hydrodynamic lubrication/elastohydrodynamic lubrication and boundary lubrication at the same time, the lubrication regime of this system is called mixed lubrication. In a mixed lubrication, more solid contacts may be observed compared with hydrodynamic/elastohydrodynamic lubrication, however, some area of surfaces will be protected by a partial hydrodynamic film [73].

The first one who used the term of boundary lubrication was W. B. Hardy. In 1922 , Hardy described boundary lubrication in his published work as following [75, 76]:

'In what is often called complete lubrication, the kind of lubrication investigated by Towers and Osborne Reynolds, the solid surfaces are completely floated apart by the lubricant. There is, however, another kind of lubrication in which the solid faces are near enough to influence directly the physical properties of the lubricant. This is the

condition found with 'dry' or 'greasy' surfaces. What Osborne Reynolds calls 'boundary conditions' then operate and the friction depends not only on the lubricant, but also on the chemical nature of the solid boundaries. Boundary lubrication differs so greatly from complete lubrication as to suggest that there is a discontinuity between the two states.'

As stated by Hardy, boundary lubrication is a regime between hydrodynamic lubrication and dry contact. His theory is very fundamental, however, his theory did not consider the lubricated surfaces which normally come with a protective boundary film [76].

Since then, many scholars have done excellent research work on boundary lubrication with advanced methods and techniques. In 1993, Spike published a review paper on the topic about boundary lubrication where boundary lubrication was defined as *'a chemical or physical interaction between the rubbing surfaces and components of a liquid or vapour lubricant which results in localized surface films with physical properties different from both the rubbing surfaces and the bulk lubricant and which thereby influence friction, wear or seizure behaviour'* [77].

Nowadays, the boundary lubrication has been recognised as a consequence of the formation of low shear strength films due to the physical adsorption or tribo-chemical reaction on the lubricated surfaces. These so-called boundary films or tribo-films could separate solid rubbing surfaces and reduce the solid contact, therefore decrease the chance of formation of adherent high friction junctions [78].

Different lubrication regimes could appear in different stages of a sliding process based on the working condition of components [79]. Some designs of sliding systems

aim to maintain the operating condition within the hydrodynamic and mixed lubrication regimes as long as possible since the formation of lubricant film could result in a desirable tribological performance. However, a combination of low speed, low viscosity and high load will cause boundary lubrication [80]. During the beginning and stopping stage of a sliding process, if the sliding components carry a very high load, boundary lubrication can be the dominant regime [81]. The boundary lubrication can lead to higher friction and wear compared with other regimes of lubrication. The addition of boundary lubricant additives that may form boundary lubricating film is essential to extend the durability of working parts under boundary lubrication [82].

3.3 Boundary lubricating films

Swalen has systematically reviewed the different types of boundary lubrication films and classified those films regarding parameters, such as chemical, physical properties, aggregate state and film thickness.

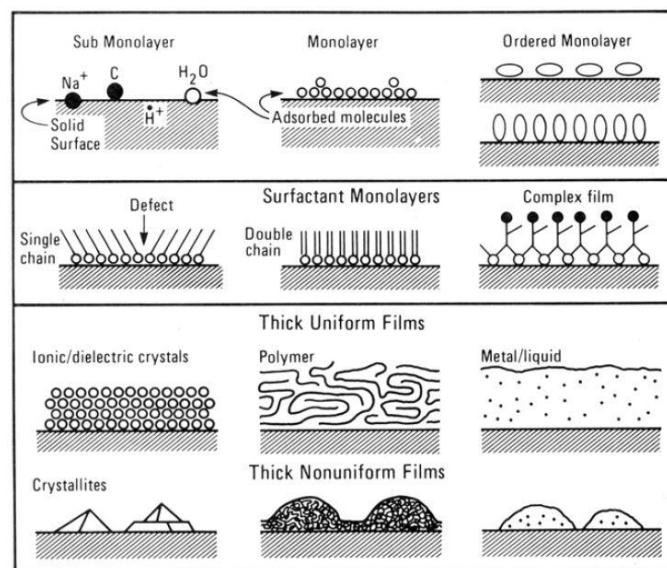


Figure 3-1 Schematic of different boundary films on a solid surface [83].

Fig. 3-1 is a schematic view of different boundary films on a solid surface [83]. But generally, boundary films could be divided into two categories regarding their physical states: fluid-like boundary films and solid-like boundary film [84].

3.3.1 Solid-like boundary films

Generally, solid-like boundary films are a consequence of chemical reactions between lubricant additives and contact surfaces which can be strongly influenced by environmental factors such as temperature and humidity [85]. During a contact, these films will be worn off and new films will be generated due to the continuous chemical reaction and physical interaction. The process of film generation and film removal is a dynamic equilibrium between materials loss and interactions of additive and surfaces [86]. The most seen solid-like film types including metal oxide films, surfactant monolayers, and molybdenum disulphide films are given as follows [82].

Oxide film

An oxide film will be formed on the surface of metals once the exterior of reactive metals (e.g. ferrous) react with the element in an environment. The oxide films are relatively easier to be worn off if the load is sufficiently high [78]. However, before they are abraded, those oxides could reduce the coefficient of friction moderately. Strong adhesion and junction growth occurs when two clean, identical metals are rubbed together. This will result in extremely high friction. Most metal oxides are much less adhesive than the metals, thus the oxide film on the metal surface could decrease the coefficient of friction as a boundary lubrication film [87]. Air sometimes plays a role as a gaseous boundary lubricant on metal surfaces since air could react to the newly exposed metal and form oxide film continuously during the rubbing.

Surfactant monolayers

Surfactant monolayers are composed of long-chain surfactant molecules which contain a polar group attached to non-polar hydrocarbon chain [88]. This polar end and metal surfaces are normally connected via the Van der Waal attraction forces or chemical bonding. Meanwhile, the hydrocarbon group protruded from the surface and gives lower shear strength than metal or metal oxide on the metal surface [89]. The long chain structure of the hydrocarbon group could reduce adhesion of asperities, therefore, reduce friction and wear. The disadvantage of using these surfactants is that these adsorbed monolayers can often be easily desorbed or melt at high temperatures [83].

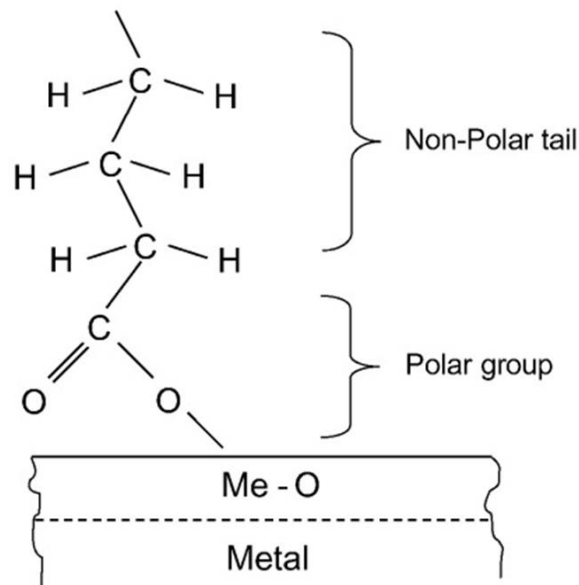


Figure 3-2 A schematic of boundary lubrication mechanism of surfactant monolayer on the metal surface [17].

Molybdenum disulphide films

Molybdenum disulphide films are formed by soluble, organo-molybdenum additives [90]. These films are thin layers of MoS₂ which can result in a very low coefficient of

friction, this can be attributed to the crystalline structure of the films of layer lattice similar to graphite as shown in Fig. 3-3 and they can be sheared very easily [91]. Molybdenum disulphide films appear to form only on the tops of the rubbing asperities and their formation is thus stimulated by rubbing [92].

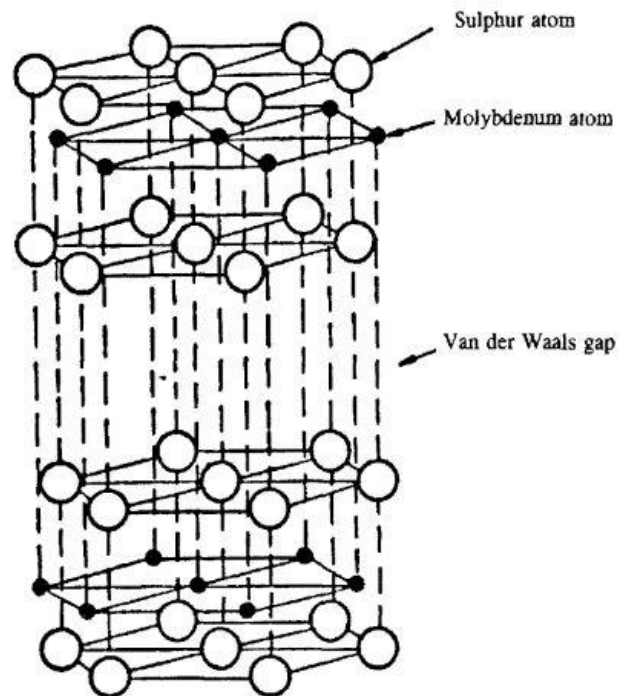


Figure 3-3 Crystal structure of molybdenum disulphide [90].

3.3.2 Fluid-like boundary films

Fluid-like boundary films could be formed when the polar viscosity index improver polymers are added to mineral oils. They are adsorbed on metal surfaces to form monolayers with much higher concentration than the bulk solution [93]. This boundary film affects friction at low speeds when the film thickness is more or less as the diameter of the polymer molecules [77].

Fluid-like boundary film can also be observed when polar and non-polar components that have different viscosity are mixed. As reported by Spike, a thin fluid-like boundary film was formed as a consequence of mixing mineral oil and highly viscous polar ester [94].

3.3.3 Replenishment

All boundary films mentioned above have a significant self-replenishing characteristic since these films can be reformed on rubbing surfaces by adsorption or reaction when they are damaged by rubbing [95, 96]. This is a crucial advantage of boundary lubricant compared with solid coatings or treatments.

3.4 Stribeck curve

Stribeck curve is a plot of the friction and other variables including the viscosity of lubricant, rotating speed and load which influence the thickness of lubricant film [97]. Fig.3-4 is an illustration of a typical schematic of the Stribeck curve where η is the fluid viscosity, V is the relative speed of the surfaces, and P is the load on the interface per unit bearing width [98].

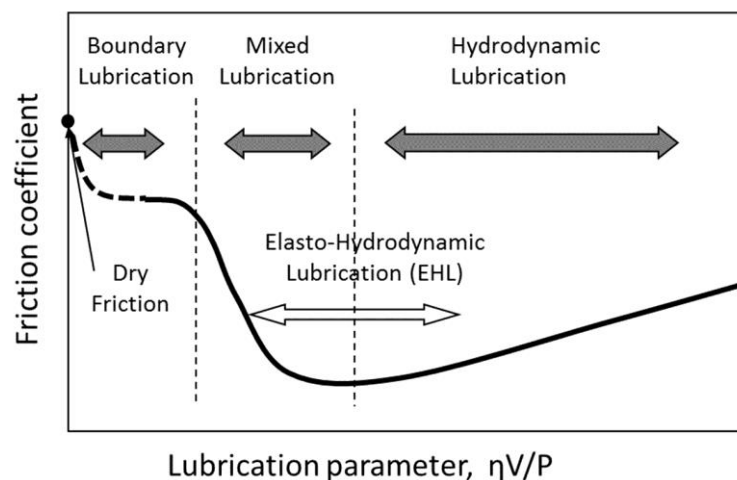


Figure 3-4 A typical schematic of the Stribeck curve [99].

It can be seen in Fig. 3-4 that the different regimes of lubrication have different domains of the curve. As shown in Fig. 3-4, the vertical axis of the Stribeck curve is the coefficient of friction. The horizontal axis shows the lubrication parameter ($\frac{\text{Speed} \times \text{Viscosity}}{\text{Load}}$) [75, 99]. Stribeck curve is generally used to demonstrate the transitions between lubrication regimes. Also, some studies have used the Stribeck curve to explain how variations in the coefficient of friction are associated with the changes in thickness of lubricant film [100].

3.5 Previous studies of lubricant additives

Lubricant additives are substances to advance lubricity and durability of lubricant. Usually, they are added to oils in quantities of small weight ratios. Their application has gained a general acceptance since 1940's. After a development for several decades, a great variety of additives has been widely applied in almost all kinds of lubricants. Meanwhile, the function of additives becomes more and more various. Nowadays every additive in one lubricant plays a different role according to the unique function of each type of additives such as friction reduction, anti-wear, extreme pressure resistance improving, anti-oxidation, anti-corrosion, debris control, foam control and etc [101]. However, the most common purpose of employing lubricant additives is to improve the tribological performance (anti-wear, anti-friction) of the base oil.

There are many ways to classify additives. On the basis of chemical properties, they can be roughly divided into organic additives and inorganic additives. Most of the inorganic additives are fine solid particles. Organic lubricant additives, such as zinc dialkyl dithiophosphate (ZDDP), tricresyl phosphate (TCP) and trixylyl phosphate

(TXP), generally contain chemical active elements to induce tribo-chemical reactions. The tribo-chemical reactions could form the boundary films that reduce friction and wear significantly [5, 31, 79, 102-105]. However, as pointed out, some of the chemically active elements, such as sulphur, phosphorus, chlorine and polar groups that contained in organic lubricant additives will cause corrosive wear to the tribo-pair under harsh working conditions, and the manufacturing process of those organic additives may lead to irreversible damage to the environment [8, 106].

The great potential of inorganic lubricant additives on improving the performance of base lubricant has been proven by many studies [2, 107-110]. However, the intrinsic poor dispersibility of inorganic lubricant additives in the organic solvents is the biggest obstruct of a wide application of inorganic additives in the industry [5, 8]. The previous studies of lubricant additives will be covered regarding their nature of chemical components and presented in next few sections of this chapter.

3.5.1 Inorganic lubricant additives

Rare-earth compound

The study of the rare-earth compounds as lubricant additives has received much attention since 60's [111]. The rare-earth fluorides such as LaF_3 and CeF_3 were investigated systematically by many scholars during the early stage. Sliney has discovered the friction reduction capability of solid lubricant LaF_3 and CeF_3 under a wide temperature range up to 1000 °C in air and argon. It was pointed out that rare-earth fluorides are better-performed lubricant additives and film former compared with rare-earth oxides under high temperature [111]. Further study was carried on by Aldorf. His work indicated that LaF_3 and CeF_3 can improve tribological properties of

ester-based lubricating base oil [112]. The anti-corrosion and anti-wear ability of a phenolic/epoxy-resin-MoS₂ bonded solid film can be advanced by LaF₃ and CeF₃ [113, 114]. In order to improve the poor solubility of rare-earth fluorides in oil, researchers put their attention on surface modification techniques. The succinimide modified LaF₃ nanoparticles have been synthesised and tested in liquid paraffin by Wang and Zhang [115]. It was reported that the load-carrying capacity and anti-wear ability of liquid paraffin were increased significantly by adding succinimide modified LaF₃ nanocluster. In another study, Wang and his colleagues reported that remarkable improvement of wear resistance and anti-pressure performance in lithium grease was observed when oleic acid capped CeF₃ nanoparticles were tested [116]. However, the author noticed that the information on effects of surface modified rare-earth fluoride particles as lubricant additives was insufficient. Although the great potential of surface modified rare-earth LaF₃ nanoparticles as a lubricant additive has been proved, the effects of surface modified LaF₃ nanoparticles on oil lubricant under various working conditions are unknown.

In recent years, many results of tribological tests of using fine particle rare-earth oxide compounds as lubricant additives have been published. A typical example is the CeO₂ nanoparticles. It was observed by Gu that the anti-wear property and the friction reduction property of 40CD oil were improved by 33.5% and 32% respectively by adding CaCO₃ and CeO₂ nanoparticles [117]. Ru [118] and Evans [17] reported that CeO₂ nanoparticle had excellent ability to improve anti-wear property and chemical erosion resistance of the base lubricant. In order to improve the dispersibility of CeO₂ nanoparticles, an attempt to synthesise surface modified CeO₂ nanoparticles has been made by Veriansyah. It was reported that the dispersibility of surface modified CeO₂ nanoparticles in ethylene glycol was improved by maximum 100% [10]. However,

only a little information about using solely CeO₂ nanoparticle as a lubricant additive has been found. Also, the studies regarding the lubricity of lubricating oils when surface modified CeO₂ nanoparticle was applied as lubricant additives were seldom reported.

Metal borate

The studies of zinc borate [18, 119, 120], titanium borate [121], magnesium borate [122-124] and lanthanum borate [3, 125] have been carried out in recent years. Great tribological performance for these nano-sized metal borate lubricant additives has been reported. Hu did a series of investigation on titanium borate [121], lanthanum borate [3] and magnesium borate nanoparticles [123]. A significant decrease of the coefficient of friction and wear scar diameter has been found. The tribological mechanism of metal borate nanoparticles has been described by Hu as well. Hu and his colleagues pointed out that the great improvement on lubricity of base oil was attributed to the deposition of metal borate nanoparticles and the tribo-film formed by chemical reactions which were triggered by adding metal borate nanoparticles. B₂O₃, FeB and Fe₂B were observed on the worn surface as the products of these tribo-chemical reactions [3, 30, 121, 123].

On the other hand, surface modification techniques have been used to improve the performance of borate fine particle as lubricant additives. The tribological performance of oleic acid modified cerium borate nanoparticles as a lubricant additive has been reported by Kong [126]. The dispersity of cerium borate nanoparticles in oil has been improved successfully by the surface modification. The coefficient of friction of the base oil was decreased sharply by adding oleic acid modified cerium borate nanoparticles.

It was also found that the surface modification has a positive effect on borate ultra-fine particles. Zhao investigated the friction reduction property of zinc borate submicron particles in sunflower oil [68]. An over 14% reduction in coefficient of friction was obtained when sunflower oil with 0.5%wt zinc borate submicron particles was tested. Formation of tribo-films on the post-test worn surfaces was observed. Another investigation has shown that as a solid lubricant additive, surface modified zinc borate submicron particles could improve the tribological property of liquid paraffin [127]. In this work, the zinc borate submicron particles were modified by surface modification agents oleic acid (OA) and hexadecyltrimethoxysilane (HS). The HS modified zinc borate in liquid paraffin with a concentration 0.5%wt has demonstrated the best anti-wear performance attributed to the formation of tribo-films. These results have indicated the great potential of surface modified zinc borate submicron particles as a solid lubricant additive. However, Zhao's study did not include any information about the performance of surface modified zinc borate particles under different test conditions such as different loading conditions or different concentrations of the zinc borate additives. As discussed in Chapter 2, the tribological mechanisms could be strongly affected by the experimental environment. Therefore, it is necessary to evaluate the performance of lubricant additive under different testing conditions since the real working condition of lubricant is various.

Metal oxide

Over past decades, metal oxide nanoparticles have received much attention as lubricant additives. Many studies of the tribological behaviour of metal oxide nanoparticles such as Fe₂O₃ [128], SiO₂ [4], Al₂O₃ [129], TiO₂ [130, 131], ZnO [132], CuO [133] and ZrO₂ [1] have been conducted. The results from those studies have

indicated that the tribological performance of lubricating oils can be improved significantly with an appropriate using of metal oxide nanoparticles under certain conditions. In particular, Hernández has investigated the tribological properties of CuO [109, 133], ZnO [132] and ZrO₂ [1]. The results he obtained indicated that all those metal oxides particles he tested had relatively considerable friction and wear reduction ability as well as anti-pressure performance in oil lubricant. It was pointed out that the raising of deposition on wear surfaces was a consequence of the increasing on nanoparticle concentration in base oil. High deposition levels on wear surface do not necessarily lead to extraordinary friction and wear reduction values [1]. However, under a specific concentration, low deposition levels on wear surface give better friction and wear elimination capacity [1]. It has also reported that ZnO nanoparticles can only reduce wear under extreme pressure (EP) condition rather than under other working conditions [132]. The anti-wear and friction reducing properties of TiO₂ were investigated by Hu. Hu believes the tribo-chemical reactions that induced by the deposition of TiO₂ nanoparticles on rubbing surface is the dominate mechanism of anti-wear and friction reduction of the TiO₂ nanoparticles added lubricant. Diboron trioxide was observed on the worn scar as a product of the tribo-chemical reaction [121]. Similar to the metal borate particles as a lubricant additive, the primary tribological mechanisms of the metal oxide particles as a lubricant additive are the deposition effect and tribo-chemical reaction.

In a short, inorganic fine particles have great potential for improving the lubricity of base lubricants. The poor solubility and stability of inorganic solid lubricant additives in oil could be improved by employment of surface modified particles. The tribological mechanism of solid inorganic lubricant additives is forming the tribo-film through either physical effect such as deposition or chemical effect such as tribo-

chemical reaction. However, some materials such as lanthanum fluoride, cerium oxide and zinc borate have not been studied systemically. Therefore, there is a need for a further investigation of the effects of surface modification on inorganic lubricant additive.

3.5.2 Organic lubricant additives

The earliest research of organic lubricant additives can be traced back to 1960's [106, 134-136]. Nowadays, organic lubricant additives have been widely applied in the industry. Typical examples of organic lubrication additives are Zinc dialkyldithiophosphate (ZDDP), tricresyl phosphate (TCP), trixylyl phosphate (TXP) and dilauryl phosphate. Many results have shown that these organic compounds have extraordinary performance as lubricant additives which may improve properties such as anti-wear, anti-oxidation or load carrying capacity of the base lubricant [31, 104, 137-139]. The tribological mechanisms of organic lubricant additives are complex. One common view is the active elements and polar groups in the organic additives could help the formation of a boundary film on the worn surface. As mentioned earlier in this chapter, the boundary film can resist the local contact pressure as well as providing well protection for friction surfaces [8, 31]. However, the using of organic lubricant additive could accelerate corrosion. The pollution caused by manufacturing and using organic lubricant additives is a big concern too since the active elements could easily react with the environment and surface of working component [8, 102, 140]. Another disadvantage of organic lubricant additives is that they are unstable under the high temperature environment. For example, it was reported that the ZDDP started to lose efficiency once the testing temperature was over 200°C [32]. On the contrary, it has been reported that inorganic rare-earth

compounds can obtain the relatively lower coefficient of friction at 1000°C in air [113].

3.6 Base oils

Base oils comprise of hydrocarbon compounds, which are molecules bound to elements that produce lubricants. There are three main types of lubricating base oils: mineral oil, synthetic oil and vegetable oil. Paraffin is derived from mineral base oil and it has been considered as the most popular lubricating oil [2, 11, 16, 115, 141-144]. The manufacturing process of liquid paraffin can remove unwanted substances, such as sulphur, odours and wax [66]. Synthetic oils such as poly-alkylene glycol (PAG) and poly-alpha-olefin (PAO) also have been widely applied [107, 145]. However, some of the synthetic oils were considered as pollution source since they are not biodegradable [146]. Mineral oils and synthetic oils generally are relatively inexpensive and easy to produce in massive quantities.

Vegetable oils have drawn much of attentions again with renewable and biodegradable features in recent years [147, 148]. The major components of the most of the vegetable oils are triacylglycerides. As shown in Fig. 3-5, triacylglycerides are glycerol molecules with three long chain fatty acids attached to the hydroxy groups through ester linkages [147]. In vegetable oil triglycerides, the length of the fatty acids is very close. Normally the length of each fatty acid is between 14 and 22 carbons long and it will depend on unsaturation levels of fatty acid [146, 149]. This special structure gives many tribological advantages to vegetable oil. However, many defects of vegetable oils are caused by triglyceride structure, such as low oxidation stability and poor performance under low temperature. [147, 150].

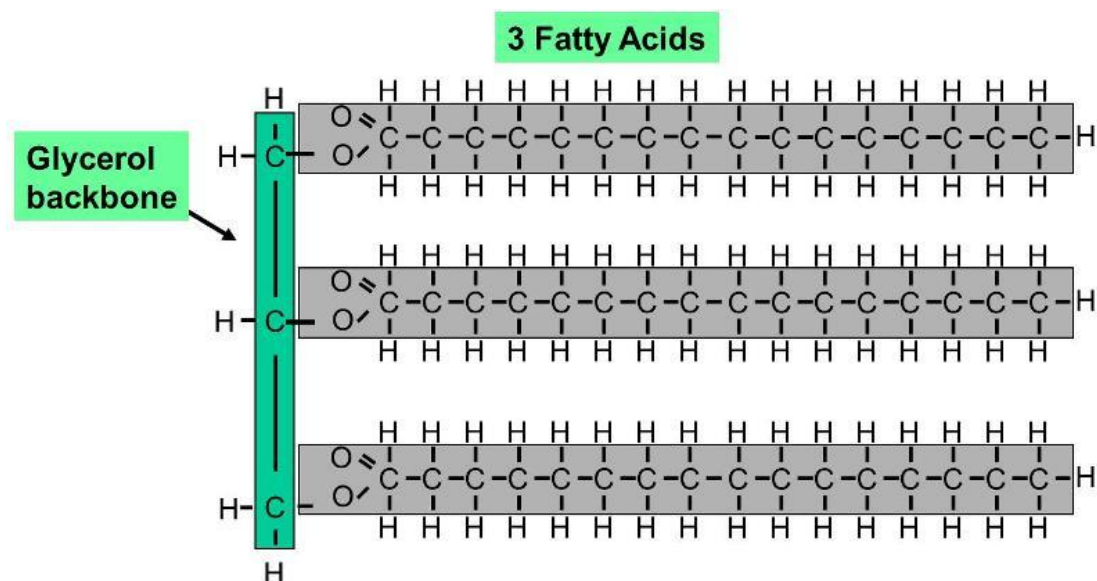


Figure 3-5 A schematic diagram of the chemical structure of triacylglycerides [151].

3.7 Summary

In this chapter, the basic theories of lubrication, such as regimes of fluid lubrication and Stribeck curve, have been reviewed. The previous studies of the tribological performance of different types of lubricant additives have been summarised. The formation of the protective boundary film (or tribo-film) is the dominant mechanism of lubricant to deliver satisfactory tribological performance. According to previous experimental results reviewed in this chapter, the addition of particle lubricant additive could help a lubrication system to generate healthy tribo-film. The tribo-film could be formed through either physical deposition or tribo-chemical reactions. The widely applied organic lubricant additives which contain active elements were pointed out that could be harmful to the environment and shorten the durability of working parts. Inorganic lubricant additives are more environment friendly, compared with organic lubricant additives, but their poor dispersibility in organic solvent obstructed the broad application of inorganic lubricant additives in industry. The development of

surface modification techniques may provide the solution to intrinsic poor solubility and stability of inorganic lubricant additives in organic solvents. The potential of further investigation on surface modified inorganic lubricant additives has been noticed since many materials have not been studied thoroughly such as lanthanum fluoride, cerium oxide, and zinc borate. Therefore, a study of surface modification method and surface modification agents is essential. The survey regarding surface modification of particle materials has been conducted and will be presented in Chapter 4 as a part of the literature review of this thesis.

Chapter 4 Surface Modification on Solid

Lubricant Additives

4.1 Introduction

As mentioned in chapter 3, many solid inorganic particles have excellent tribological properties such as rare-earth metal compounds and borates. However, their intrinsic poor dispersibility and stability in organic hydrocarbon based oils have limited their practical application as lubricant additives, since ineffectual dispersibility and stability of additives normally lead to poor performance or even lose efficacy of lubricants [24, 66]. With developments in surface modification techniques in recent years, more and more scholars pay their attention back to the studies of inorganic lubricant additives since the synthesis of oil soluble inorganic lubricant additives becomes possible.

In this chapter, the basic principles of surface modification of particle materials were reviewed. The characteristics of several surface modification agents were studied. The previous studies of surface modified particles as lubricant additives were summarised.

4.2 Basic principles of surface modification of particle materials

Surface modification is a widely used method to make fine-particles more soluble in organic media. Compared with using surfactants, surface modification has a less effect on the viscosity [9]. Surface modification technique could bring or change properties of the particles. Those properties could be physical, chemical or even biological properties. Generally, surface modification of particle materials is the process that attaches long hydrocarbon chain with high molecular weight to surfaces

of particles, therefore, makes those particles more soluble and stable in hydrocarbon solvents [81]. The organic layer on the surfaces of particles could reduce interactions between particles and decrease the size of conglomerated particles. In particular, for the case of solid inorganic lubricant additive, the surface modification is a great approach to achieve long-term stability and superior dispersity of particles in lubricant systems. The dispersion of surface modified particles can be conducted by physical agitators and no assist of additional surfactant is needed [68].

4.3 Other approaches to improving oil solubility of particle

materials

Using surfactants is another very effective and economic approach to improving dispersibility and stability of particle materials in organic solvent. The single surfactant molecule generally has been designed as a combination of two different ends, one hydrophobic end (the tail) with a long-chain hydrocarbon and the other end with a hydrophilic group (the head). Regarding the composition of the head, there are generally four types of surfactants [152]:

- 1) Non-ionic surfactants without charge groups in their heads (include polyethene oxide, alcohols, and other polar groups).
- 2) Anionic surfactants with negatively charged head groups (anionic head groups include long-chain fatty acids, sulfosuccinates, alkyl sulphates, phosphates, and sulfonates),
- 3) Cationic surfactants with positively charged head groups (cationic surfactants may be protonated long-chain amines and long-chain quaternary ammonium compounds).
- 4) Amphoteric surfactants with zwitterionic head groups (charge depends on pH).

Surfactants can lower the interfacial tension between two phases, no matter liquid phase/solid phase or two liquids. Once the surfactants have been added into a lubricant system that contains inorganic fine particles and organic media, the heads of surfactant molecules can be attached to the particle surface thus an organic oleophilic layer can be formed on the particle surface. By generating the layer effectively between particle surfaces and base oil fluid, even a small quantity of surfactant is able to influence the inter-surface properties of whole lubricant system significantly. However, the application of surfactants could also bring negative influence to the lubricant system. For instance, the surfactants could cause generation of foams when the lubricant system is working under high temperature, the foams could reduce the performance of lubricant [153]. Also, Kopperud reported that the viscosity of base oil could be affected significantly by the amount of surfactant [154].

4.4 Surface modification agents

Silanes

Silane or silicon hydride is the name of any of a series of covalently bonded compounds containing only the elements silicon and hydrogen. The silanes have the similar chemical structure of alkanes but much less stable [155]. During the surface modification, silanes could react with the hydroxyl group on the surface of particle and bond to the particles. These reactions have been described as a process of four steps [156].

‘Initially, hydrolysis of the three labile groups occurs. Condensation to oligomers follows. The oligomers then hydrogen bond with OH groups of the substrate. Finally during drying or curing, a covalent linkage is formed with the substrate with

concomitant loss of water. At the interface, there is usually only one bond from each silicon of the organosilane to the substrate surface. The two remaining silanol groups are present either in condensed or free form.'

Hexadecyltrimethoxysilane (HS) is one of the typical and relatively new silanes surface modification agent. The chemical formula of HS is shown in Fig. 4-1. The HS modified particles could be generated by the sol-gel method which is a universe method of particle synthesis [157]. It was reported that HS modified metal oxide nanoparticles demonstrated superior dispersibility in hydrocarbon solvents [158]. Remarkable potential of HS modified zinc borate submicron particles as a solid lubricant additive in liquid paraffin have been observed [7]. However, the tribological behaviour of HS modified nanoparticle as lubricant additive is seldom.

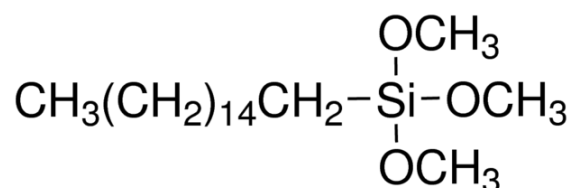


Figure 4-1 Chemical formula of Hexadecyltrimethoxysilane.

Succinimide

Succinimide is a nitrogen-containing surface modification agent. The superior anti-wear ability of liquid paraffin was observed when polyisobutylene succinimide modified LaF₃ nanoparticles were used as a lubricant additive [115]. It was also reported, as a lubricant additive, succinimide modified lanthanum hydroxide nanoparticles demonstrated remarkable improvement on the friction-reduction, anti-wear and extreme pressure properties of liquid paraffin [16, 159]. Fig. 4-2 shows the chemical formula of polyisobutylene succinimide.

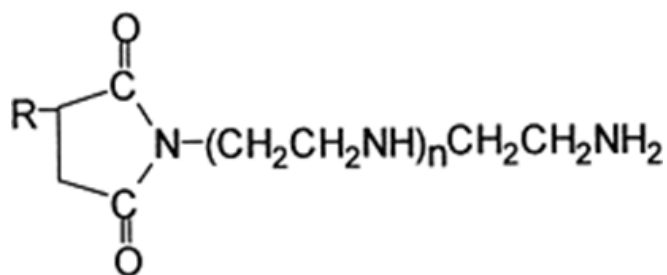


Figure 4-2 Chemical formula of polyisobutylene succinimide [115].

Carboxylic acids

Any organic compound that contains only one carboxylic group (-COOH) is called carboxylic acid, such as oleic acid and stearic acid. Fig.4-3 shows the chemical formula of carboxylic acids.

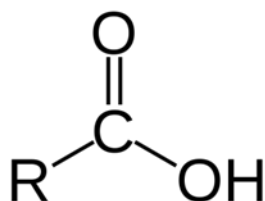


Figure 4-3 Chemical formula of carboxylic acids.

Carboxylic acids have been widely used as surface modification agents due to their promising performance. Many investigations and positive results of tribological behaviours of carboxylic acids modified particles as lubricant additives have been published [2, 4, 160-163]. During the modification, one end of the carboxylic acid is able to attach to the surface of a particle via a covalent bond which is a product of the reaction between carboxylic group (from carboxylic acids) and hydroxyl on the surface of particles. The great interactions between the carbon chains on the other end of the carboxylic acids and the hydrocarbon oil is the crucial factor of improving the dispersibility of modified particles [164].

4.5 Previous studies of surface modified particles as lubricant additives

In spite of the fact that many inorganic fine-particles have great potential to be used as lubricant additives [1, 2, 4, 128, 129, 132, 133, 162], their application in industry is limited because of their intrinsic poor dispersibility in hydrocarbon oils. Many studies were focused on surface modification of fine-particles using suitable modification agents in order to improve the dispersibility of those particles in a lubricant system. Various types of inorganic particles have shown their superior performance as lubricant additives after surface modifications were conducted. The successful syntheses of surface modified Al_2O_3 [165, 166], SiO_2 [4, 142], Fe_3O_4 [167], MoS_2 [13, 168, 169], ZnO [170], LaF_3 [115, 171] and Y_2O_3 [172] nanoparticles has been reported, and the improvement on tribological performance of lubricating oil has also been observed when these surface modified nanoparticles were added. In particular, some typical studies have been listed below.

Surface modified rare-earth particles

A series of investigations on surface modified rare-earth particles have been carried out by Zhang. The outstanding tribological performance of succinimide modified rare-earth nanoparticles has also been discovered [16, 115, 143]. Veriansyah made an attempt to synthesise surface modified CeO_2 nanoparticles in methanol. It was observed that the dispersibility of surface modified CeO_2 nanoparticles could be improved by 100% in ethylene glycol [10].

Surface modified metal particles

Kolodziejczyk has modified Pd nanoparticles with tetraalkylammonium chains. Significant improvement of friction reduction and the anti-wear ability of base lubricant was observed when the surface modified Pd nanoparticle was added into the base lubricant [14]. Zhou reported that dialkyl-dithiophosphate (DDP) modified Cu nanoparticle had greater oil dispersibility compared with unmodified Cu nanoparticles [12]. Yu reported that higher oil temperature could give surface modified Cu particles better tribological performance [173].

Surface modified metal oxide particles

Tribological performance of oleic acid (Cis-9-octadecenoic) modified TiO₂ in water has been explored by Gao. Gao synthesised surface modified TiO₂ nanoparticles by using a sol–gel method. Their results proof that oleic modified TiO₂ performed great in both friction-wear reduction and load-carrying capacity [162]. Similar results could be found in works contributed by Yu [174] and Xue [2]. Tetrafluorobenzoic and 2-ethyl hexoic acid have been introduced as a surface modifier in their works.

Surface modified metal borate particles

Results from Dong indicated that with an optimal content of zinc borate nanoparticle in 500 SN base oil, the coefficient of friction was decreased and the highest maximum non-seized load was obtained [18]. Similar improvements in wear resistance and load carrying capacity can be found when the titanium borate nanoparticle in 500 SN oil was tested [121]. It was reported that the friction reducing ability of base oil has been

enhanced by adding magnesium borate nanoparticles prepared by ethanol supercritical fluid drying technique [123].

Based upon the above studies, it is suggested that surface modification could be employed to most of the inorganic fine-particles. It can be said that surface modification is a mature method to improve dispersibility and tribological performance of inorganic fine-particles as lubricant additives. The effects of some most often seen surface agents such as oleic acid and succinimide have been studied by many scholars. However, the studies of new surface modification agent are seldom, for example, hexadecyltrimethoxysilan. Also, there is a lack of investigation on properties of the same material that modified by different surface modification agents.

4.6 Summary

The basic principles of surface modification method and material characteristic of surface modification agents are summarised in this chapter. According to results from previous studies, surface modification can be applied to most type of inorganic fine-particles as an approach to improve particles' oil solubility, stability and tribological performance as lubricant additives. It has been found that the surface modification agent such as hexadecyltrimethoxysilane has not attracted enough attention.

Chapter 5 Materials and Experimental Methods

5.1 Introduction

According to literature, suitable materials and experimental methods of this project have been chosen. The detailed specifications of materials and brief introductions of experimental apparatus are given in this chapter. Also, the procedure of particle surface modification and sample preparation are provided in order to offer a clear view of preparation work required by the pin-on-disc experiments.

5.2 Materials

5.2.1 Properties of fine-particles

- Lanthanum fluoride nanoparticles

Lanthanum fluoride (LaF_3) could appear as clear or yellow crystals. Like many other rare-earth compounds, lanthanum fluoride features high melting point, low hardness, hexagonal crystal allotrope and good resistance to thermal and chemical attack [175]. LaF_3 nanoparticles are often used as an ion-selective electrode for the detection and measurement of fluoride ions in solutions [176].

The potential of using LaF_3 nanoparticles as lubricant additives has been explored by many studies. For example, Sliney [114] applied LaF_3 nanoparticle as an anti-wear and extreme pressure additive in lubricating grease. Results indicate that LaF_3 nanoparticles demonstrated excellent performance as lubricant additives under high temperature. The loading capacity of the grease was increased significantly. Similar investigations have been conducted in paraffin oil too. It was reported that

pyridinium dialkyl dithiophosphate (PyDDP) modified LaF₃ nanoparticles were synthesised and evaluated with a four-ball test rig, remarkable improvements on tribological performances of paraffin oil were observed [175].

However, the surface modification agents used by previous studies contains sulphur (S) and phosphorus (P). As addressed in the chapters 2 and 3, lubricants with active elements are not environment friendly and may shorten the durability of the components. In this study, unmodified LaF₃ nanoparticles of 40-60 nm diameters and 99.9% purity were supplied by Henan Wangwu Co.,Ltd, China. S and P free oil-soluble surface modified LaF₃ nanoparticles were synthesised based on the unmodified LaF₃ nanoparticles. The properties of original unmodified LaF₃ particles were listed in Table 5-1. A TEM image of LaF₃ nanoparticles from supplier was shown in Fig 5-1.

Table 5-1 A list of properties of unmodified LaF₃ nanoparticles.

Properties	
Density	5.936 g/cm ³
Molar Mass	195.90 g/mol
Average Particle Size	40-60 nm
Purity	99.9%
Melting Point	1493 °C

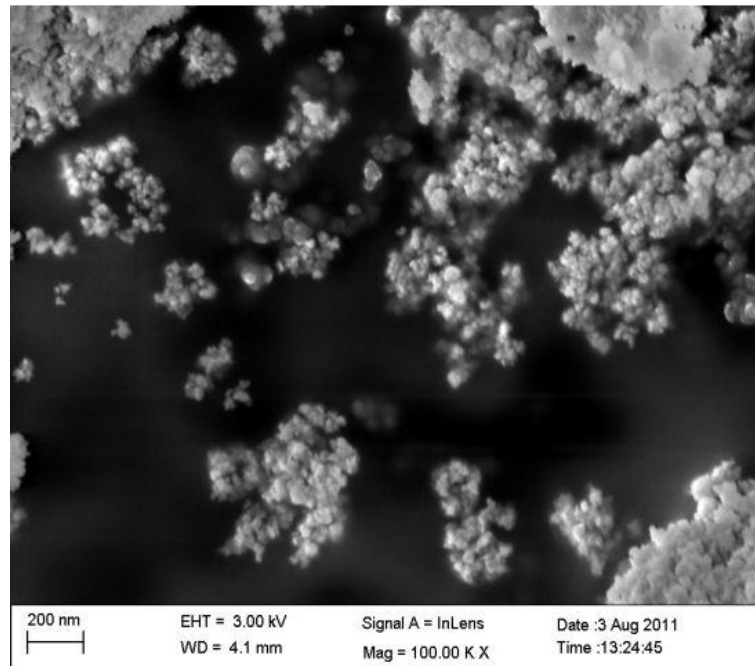


Figure 5-1 A transmission electron microscopy (TEM) micrograph of lanthanum fluoride nanoparticles employed in this project.

- Cerium oxide nanoparticles

According to the literature study, it is reported that both anti-friction property and anti-wear property of water-based cerium dioxide nanofluids can be improved significantly if CeO_2 nanoparticles are well dispersed in the nanofluids [177]. When a mixture of CeO_2 nanoparticles and CaCO_3 nanoparticles was tested in 40CD oil, the anti-wear property and the friction reduction property of 40CD oil were improved by 33.5% and 32% respectively by adding CaCO_3 and CeO_2 nanoparticles in 40CD oil [117]. An attempt to synthesise surface modified CeO_2 nanoparticles in methanol has been made. It was observed that the dispersibility of surface modified CeO_2 nanoparticles in ethylene glycol could be doubled [10]. However, relatively fewer researches have been effectuated when solely CeO_2 nanoparticles have been tested as lubricant additives. Little information can be found in the tribological properties of

lubricants when surface modified CeO₂ nanoparticles are applied as lubricant additives.

Unmodified CeO₂ nanoparticles of 20-40 nm diameters and 99.9% purity were supplied by Shandong Yitong Co.,Ltd, China. Surface modified CeO₂ nanoparticles were synthesised in lab. The properties of unmodified CeO₂ particles were listed in Table 5-2. Fig. 5-2 illustrates a typical TEM image of CeO₂ nanoparticles.

Table 5-2 A list of properties of unmodified CeO₂ nanoparticles.

Properties	
Density	7.132 g/cm ³
Molar Mass	172.13 g/mol
Average particle size	20-40 nm
Purity	99.97%
Melting Point	2600 ° C

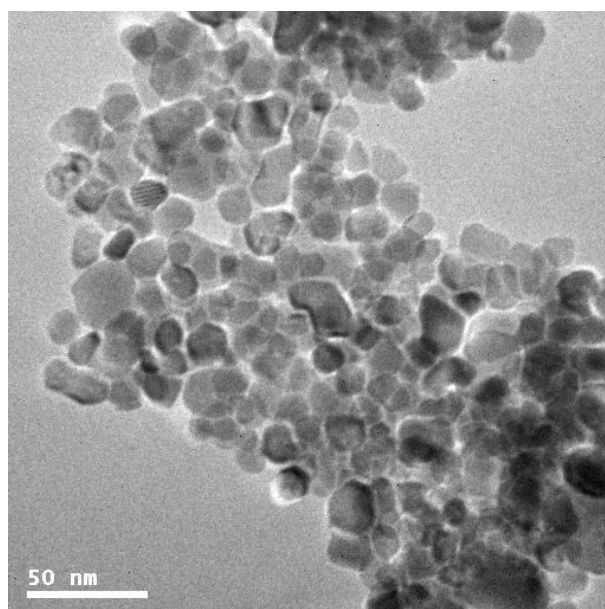


Figure 5-2 A transmission electron microscopy (TEM) micrograph of cerium oxide nanoparticles employed in this project.

- Zinc borate submicron particle

Zinc borate is a white crystalline or amorphous powder insoluble in water. Zinc borate has relatively high melting point and low toxicity. A number of variants of zinc borate exist, differing by the zinc/boron ratio and the water content, such as $2\text{ZnO}\cdot 3\text{B}_2\text{O}_3\cdot 3.5\text{H}_2\text{O}$, $2\text{ZnO}\cdot 3\text{B}_2\text{O}_3$, $4\text{ZnO}\cdot \text{B}_2\text{O}_3\cdot \text{H}_2\text{O}$, $4\text{ZnO}\cdot 6\text{B}_2\text{O}_3\cdot 7\text{H}_2\text{O}$, $2\text{ZnO}\cdot 2\text{B}_2\text{O}_3\cdot 3\text{H}_2\text{O}$. Zinc borate has been mainly used as a flame retardant in plastics and cellulose fibres, paper, rubbers and textiles in the industry. Zinc borate also could be used as paints, adhesives, and pigments [178]. Compared with bigger sized particles, nano-sized zinc borate particles feature higher strength-hardness, higher diffusivity, higher plasticity-flexibility, lower density, lower elastic modulus, higher electric resistance, higher specific heat, higher thermal coefficient of expansion, lower thermal conductivity and better soft magnetic property [179]. According to those features, nano-sized zinc borate particles have been widely used in high mechanical property required environments, absorption of light and heat, non-linear optics, special conductors, catalysts, sensor and lubricant additives [178, 180, 181]. Zinc borate nanoparticles can be prepared by ethanol supercritical fluid drying technique (ESFD) [18]. ESFD is a universal technique for preparation of inorganic nanoparticles. This method is applied widespread recent years. There are many researchers using this technique to prepare and investigate the tribological response of nanoparticles, and excellent lubricating performance has been reported [18, 121, 123, 182]. However, the expensive and complicated preparation process of nanoparticles hinders their mass application. Compared with nanoparticles, submicron size particles have won their attention in industrial application due to relatively low cost and simple preparation process although submicron size particles are more thermodynamically unstable in liquid media. In this study, unmodified zinc borate ($2\text{ZnO}\cdot 2\text{B}_2\text{O}_3\cdot 3\text{H}_2\text{O}$) with a

particle size of 500-800 nm and 99.9% purity were supplied by Shandong Jiqing Chemical Co.,Ltd, China. Surface modified CeO₂ nanoparticles were synthesised in lab. The detailed property of unmodified zinc borate submicron particles has been listed in Table 5-3. As shown in Fig. 5-3, it is a typical transmission electron microscopy (TEM) micrograph of a zinc borate ultrafine powder with around 700nm height and 400nm width.

Table 5-3 A list of properties of unmodified zinc borate submicron particles.

Properties	
Density	3.64 g/cm ³
Molar Mass	313.754 g/mol
Average particle size	500-800 nm
Purity	99.9%
Melting Point	980 ° C

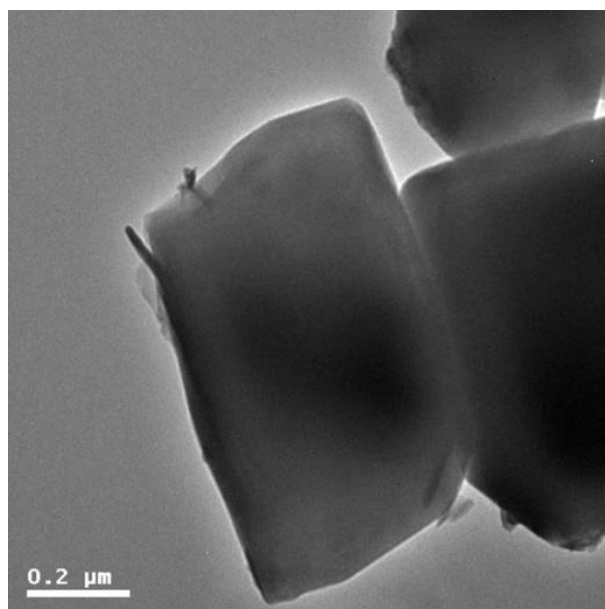


Figure 5-3 A transmission electron microscopy (TEM) micrograph of zinc borate ultrafine powders employed in this project.

5.2.2 Surface modification agents

- Hexadecyltrimethoxysilane (HS)

Hexadecyltrimethoxysilane ($C_{19}H_{42}O_3Si$) of 95% purity (*Gelest, Inc.*) with the flash point of 122°C has been used. Other properties of HS have been listed in Table 5-4.

Table 5-4 A list of properties of HS.

Properties	
Grade	Technical
Assay	$\geq 85\%$ (GC)
Impurities	Isomers
Density	0.89 g/mL at 20 °C
Purity	95%
Flash point	122°C

- Oleic acid (OA)

Oleic acid ($C_{18}H_{34}O_2$) (*Sigma-Aldrich, Inc.*) with the flash point of 113°C has been employed. Other properties of OA have been listed in Table 5-5.

Table 5-5 A list of properties of OA.

Properties	
Grade	Technical
Assay	$\geq 99\%$ (GC)
Form	Viscous liquid
Density	0.89 g/mL at 25 °C
Purity	98%
Flash point	113°C

5.2.3 Base oils

Liquid paraffin (LP) is one of the most widely applied lubricating base oil. LP has also been used intensely for science studies especially tribological studies as testing

oil. Pure liquid paraffin (LP) (Kerax Ltd, UK) that has a flash point of 220 °C, a viscosity of 24 mPa·s at 40 °C and 4.8 mPa·s at 100 °C is employed in this study as testing base oil.

5.3 Experimental methods and apparatus

According to the extensive literature review, the experimental studies of the tribological performance of surface modified particle as lubricant additive can be roughly divided into two stages: tribological test and characterisation. Main purposes of using lubricant additives are to improve friction reduction ability and anti-wear ability. Therefore, tribological tests have been designed to evaluate tribological properties of experiment samples in two aspects: friction reduction ability and anti-wear ability. Characterisation is about observing and analysing. The purpose of characterisation is to observe morphologies of tested substance as well as to find out any surface property changes that may be caused by adding additives. Element distribution and chemical analysis are also very important for the understanding interaction between a friction pair, in addition, to explain the mechanism of additives. The object of characterisation can be the worn surfaces of samples or surface modified additives and information which gathered in the first stage. In this research, the chemical bonding between the nanoparticles and modification agents were verified by FTIR spectrometer. The reduction in particle agglomeration size associated with the improved dispersibility in organic solvent was measured with a Zeta potential equipment. The friction reduction abilities and anti-wear properties of materials were tested by a pin-on-disc test rig through recording coefficient of friction and the measurement of wear scar diameter (WSD). An optical microscope was employed to observe and measure WSD of metal balls and wear tracks width of the

metal discs. Colour alterations were observed on the worn surface by optical microscope when different lubricants were applied. Changes of the mechanical property of tribo-films that associated with worn surface colour alteration were examined by using a nano-indentation tester and SEM equipped with EDS.

5.3.1 Sample characterisation

Once the surface modification of particles has been done, it is important to make sure the surface modification has been carried out correctly and successfully. Fourier transform infrared spectroscopy (FTIR) can analyse chemical bonding between particles and surface modification agents. Therefore any differences in chemical structure between original and modified particles would be reflected by the FTIR results. The results of surface modification of particles can also influence agglomeration size and dispersibility. Agglomeration size of particles could be measured by Dynamic Light Scattering (DLS) directly. The zeta potential is a key indicator of the stability of colloidal dispersions. The magnitude of the zeta potential indicates the degree of electrostatic repulsion between adjacent, similarly charged particles in the dispersion. Therefore, zeta-potential results can embody the improvement of dispersibility indirectly.

- Fourier transform infrared spectroscopy

Fourier transform infrared spectroscopy (FTIR) was employed to investigate the surface modification carried out on the solid lubricant additives as shown in Fig. 5-4. The Infrared spectroscopy measurements were conducted using a Perkin-Elmer Spectrum 100 FTIR Spectrometer. Samples were prepared as powder-pressed KBr

pellets. The spectra were collected in the wave range from 600 to 4000 cm^{-1} with a resolution of 4 cm^{-1} in a transmission mode.



Figure 5-4 Fourier transform infrared spectroscopy.

- Zeta-potential & Dynamic Light Scattering

Particle conglomerate size in organic solvent was measured using Dynamic Light Scattering (DLS) (Malvern Zetasizer-Nano Series) (Fig. 5-5). Zeta-potential is also known as an important parameter that affects the stability of suspension. Zeta-potential of the suspensions that contain particles was obtained to reflect the magnitude of the repulsion between particles. In this study, all samples have been measured three times repeated. The average results and deviations are presented in later chapters.



Figure 5-5 Dynamic Light Scattering (DLS).

5.3.2 Tribological testing

There are many methods to determine the tribological performance of materials such as pin-on-disc, four-ball, pin-on-cylinder, block-on-disc, thrust washers and crossed cylinder. Pin-on-disc test rig has been selected for the tribological tests of this project. The pin-on-disc tester measures the friction and sliding wear properties of dry or lubricated surfaces of a variety of bulk materials and coating. The pin-on-disc tester consists of a rotating disc of the material to be tested against a stationary sphere, usually made of cemented carbide, referred to as the pin. The normal load, rotational speed, and the wear track diameter are all set by the user prior to the pin on disc test. Friction reduction and anti-wear properties are two main parameters of a lubricant system. Pin-on-disc test rig could record coefficient of friction automatically and generate wear scar and wear tracks. Most pin on disc testers are computer controlled and store the measured friction versus time or distance plots for future reference.

When the friction is monitored during the pin on disc test the friction starts at it is the highest level but after a certain amount of time (or running in) the friction drops to a steady state level. Pin-on-disk tester is mostly applied in previous studies [183, 184], thus, in order to make this experiment comparable to former results a pin-on-disk tester and close test conditions have to be employed.

- Pin-on-disk test rig

Fig. 5-6 shows a representation of basic principle for pin-on-disk tester which is one of the mostly used tribology testers. The letter 'F' represents force or load; this force will be applied on the pin when the disc is rotating while testing. A pin on disc tribometer consists of a stationary "pin" under an applied load in contact with a rotating disc. The pin can have any shape to simulate a specific contact, but spherical tips are often used to simplify the contact geometry. In this study, the shape of the pin is spherical too. The coefficient of friction is determined by the ratio of the frictional force to the loading force on the pin. It has been widely used to exam the lubricating properties of lubricant and its interactions with the substrate. Wear and friction reduction can be obtained by using pin-on-disk tester. The measurement of WSD and wear tracks width can reflect the anti-wear ability of lubricant [58].

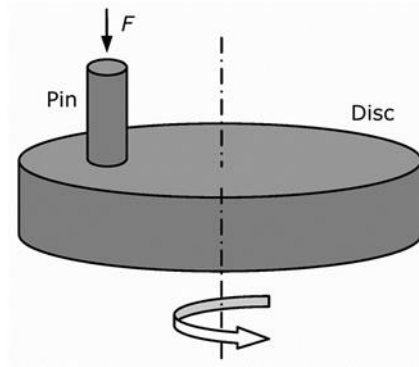


Figure 5-6 A representation of pin-on-disc tester's basic working principle.

Fig. 5-7 shows the pin-on-disc test rig which was employed in this research. For all tests that included in this study, a bearing ball of 5 mm diameter was used as the pin in a test was made of AISI52100 chrome steel with HRC of 59-61. The disc was made of the identical material, with 27 mm diameter and 3 mm thickness. The detailed mechanical properties of AISI52100 steel are listed in Table 5-6. Prior to each test, the discs were grounded and polished to a mirror finish and a uniform surface roughness R_a of 15 nm was achieved. Before each test, both the pins (bearing balls) and the discs were cleaned with toluene in an ultrasonic water bath for five minutes to eliminate any potential grease on the surface, and then a further cleaning with acetone was carried out for five minutes. Each lubricant sample is tested for three times.

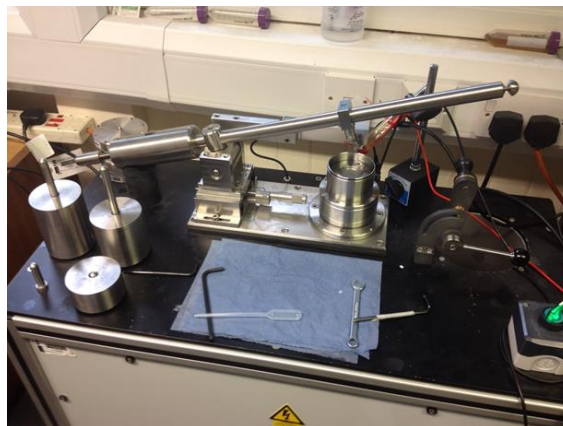


Figure 5-7 The POD 2 pin-on-disc tester.

Table 5-6 A list of mechanical properties of AISI52100 steel.

	AISI52100 Chrome Steel
Elastic modulus	200 G Pa
Poisson's ratio	0.30
Hardness, Vickers	848

The initial Hertz contact pressure of the pin-disc tribo-pair was calculated by using the equations in Johnson's book. For the case of a spherical pin statically contact onto a flat surface, the radius of point contact circle α can be expressed as equation 5.3.2-1 [185, 186]:

$$\alpha = \left(\frac{3WR}{4E} \right)^{\frac{1}{3}} \quad 5.3.2-1$$

where W is the load, R is the relative curvature. For the case of ball-on-flat contact, R is equal to the radius of the ball which is 5mm in this study. E is the reduced modulus which can be determined by:

$$\frac{1}{E} = \left(\frac{1 - \nu_1^2}{E_1} + \frac{1 - \nu_2^2}{E_2} \right) \quad 5.3.2-2$$

where ν_1, ν_2 are the poisson's ratios of pin ball and the disc respectively, and E_1 and E_2 are their elastic modulus. The maximum contact pressure P_m at the axis of contact could be determined by the follows equation:

$$P_{max} = \frac{3W}{2\pi\alpha^2} = \left(\frac{6WE^2}{\pi^3 R^2}\right)^{\frac{1}{3}} \quad 5.3.2-3$$

therefore, the initial mean Hertz contact pressure cross the contact area can be expressed as:

$$P_m = \frac{2}{3}P_{max} = \frac{W}{\pi\alpha^2} \quad 5.3.2-4$$

The calculation results are listed in Table 5-7.

Table 5-7 A list of calculation results of Hertz pressure under different loading conditions.

	$W=10\text{N (G Pa)}$	$W=30\text{N (G Pa)}$
P_{max}	0.98	1.41
P_m	0.65	0.94

5.3.3 Surface characterisation

The characterisations of post-test surfaces have been conducted by a SEM equipped with EDS, an AFM and a nano-indentation machine. SEM scans a specimen surface with its high-energy electron beam, there are several types of beams can be selected, such as X-rays, backscattered electrons, secondary electrons, specimen current and transmitted electrons. Caused by the unique properties of each type of beams, SEM is able to give a maximum resolution of around 5nm depends on the size of electron beam [187]. Fig. 5-8 is a typical example of SEM photograph of wear track on a pre-

tested sample disc. The Energy Dispersive Spectroscopy (EDS) is an analytical technique used in harmony with the SEM. EDS is used for the chemical characterisation of a specimen used in concert with SEM for compositional microanalysis. It is useful for material characterisation since it can perform qualitative and semi-quantitative microanalysis on a specimen from a relatively low ($\sim 25X$) to high magnification ($\sim 20,000X$) [58]. An atomic force microscope (AFM) was used to observe the morphology of the tribo-film generated on worn surfaces. Mechanical properties of the worn surfaces were determined using a Nano-indentation/scratching tester. Nano-indentation tester is designed to provide surface mechanical characterisation data by indenting or scratching to depths at the nanometres-micron scales. Nano-indentation/scratching tester can be used to examine the mechanical property of worn surfaces with a thickness on Nano-scale. The topography of testing sample before and after the test can be compared using scratching function. The mechanical properties and thickness of boundary layer on the worn surface will be obtained using indentation function. It will further prove the existence of boundary layer and help explain its friction and wear reduction mechanism.

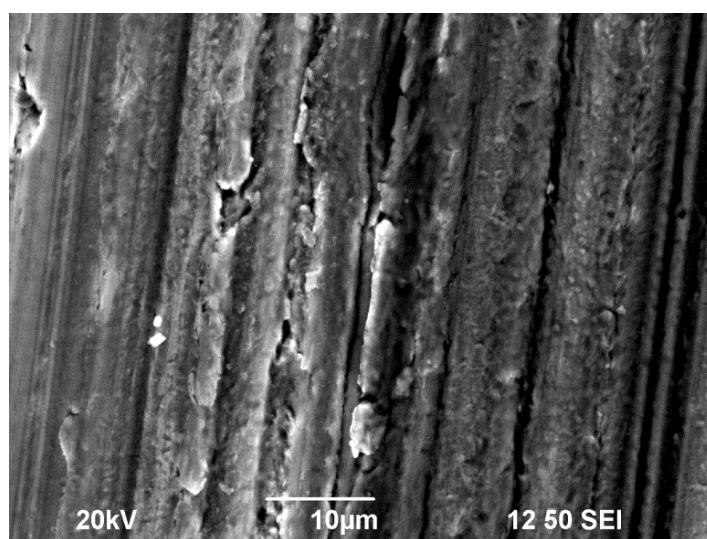


Figure 5-8 A typical photograph of wear track on pre-tested sample disc.

- Scanning electron microscope (SEM)

The solid lubricant additives and wear scars of the pins (bearing balls) after the Pin-on-disc tests were inspected using scanning electron microscopy (SEM) which shows in Fig. 5-9. Tested bearing ball was first ultrasonically cleaned in acetone for five minutes, and then mounted onto SEM sample substrates using carbon conductive adhesive tabs. The typical accelerating voltage was set at 5-20 kV, and the working distance was around 6 mm. A thin layer of gold coating on the examining object was sometime necessary to improve the conductivity of the sample. A sputter coater, Emitech SC7620, equipped with a gold target was set at 75 mA for 30 seconds to do the coating process. Also, conductive silver paint was used to ensure an electrical conductivity from the surface to the sample stub.

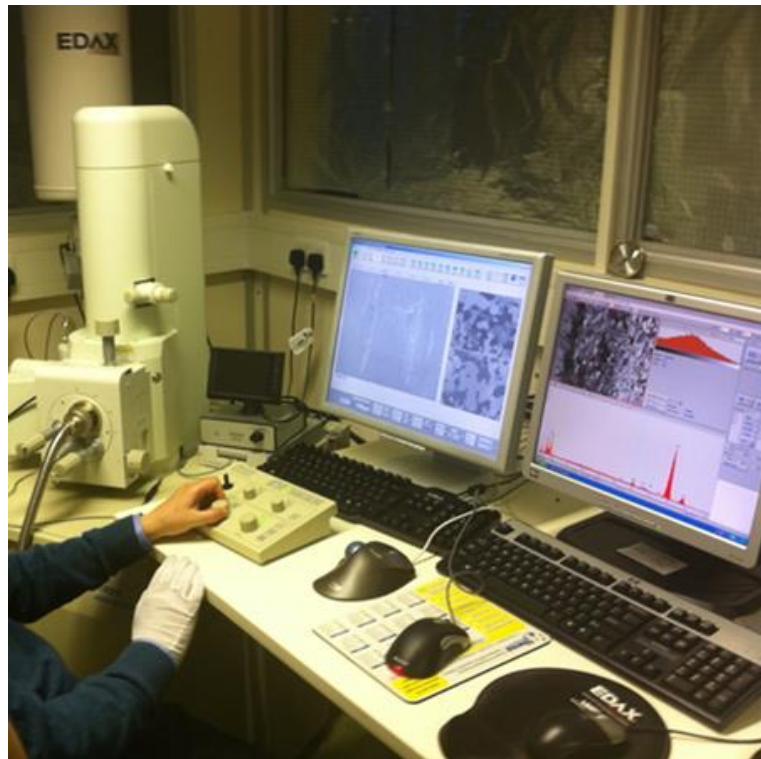


Figure 5-9 The SEM employed in this study.

- Atomic force microscopy

The AFM used in this study was a Multi-Mode scanning probe microscope, ‘Nanosurf Easyscan 2’ (Fig. 5-10), from Nanosurf (Liestal, Switzerland). In the observation, the three-dimensional image of the object surface can be constructed via a tip scanning across the surface under static force in contact mode. Contact force was set to be 20 nN to avoid any scratching damage when the probe was driven crossing the object surface. A silicon probe with a 5 nm-diameter tip was used in the AFM observation, and all images were captured at 512 ×512 pixel resolution at a scanning rate of 1 Hz.



Figure 5-10 The atomic force microscope employed in this study.

- Nano-indentation machine

Mechanical properties of the tribo-film were determined using a Nano-indentation device, ‘nano tester’, from Micro Material Ltd (Wrexham, UK) (Fig. 5-11). A Berkovich probe with a tip diameter of 50nm was employed for the experiment.

Supported by an onboard microscope, the ‘nano tester’ is able to carry out indentation on a specific point. All indentation experiments were conducted inside an environmental chamber, and a constant temperature of 20 degree Celsius was maintained. The ‘nano tester’ is also capable of generating topography of a surface under ‘scanning mode’. This function was employed to determine the wear track depth in the first series of the experiments. In this study, nine indents (three by three matrixes) have been conducted on each sample every time during the tests. The raw data have been collected and processed by the software automatically by using Oliver–Pharr data analysis [188]. The indentation results for each sample which presented in later chapters are an average value of the raw date from nine positions.

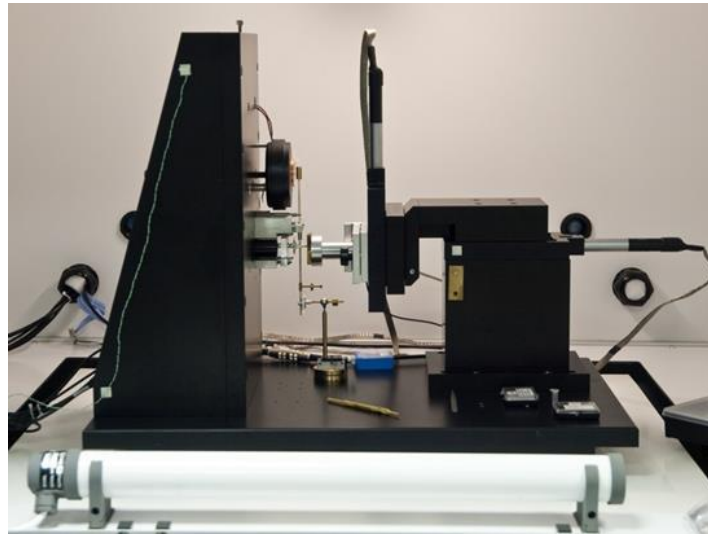


Figure 5-11 The Nano-indentation tester employed in this study.

5.4 Preparation of surface modified particles

The surface modification method and procedure of all particles in this project are identical. Each time, one surface modification process has only one type of particles

and one surface modification agent involved. Oleic acid (OA) and Hexadecyltrimethoxysilane (HS) were used as the surface modification agents. 2.78 g of particles (one from $ZnBO_3$, CeO_2 and LaF_3) were firstly dispersed in a 40ml mixed solution of ethanol and water (volume ratio 1:1) using a high shear homogenizer at a rotary speed of 15000 rpm for 10 minutes. A suitable amount of modifier (either OA or HS) dissolved in 10 ml of absolute alcohol was then added to the first dispersion. Subsequently, the mixture was heated to 70°C and maintained at this temperature with vigorous stirring for 4 hours. Then, the suspension was centrifuged at a speed of 8000 rpm for 10 minutes and the white precipitate was collected. The obtained precipitate was rinsed with distilled water and ethanol alternately and centrifuged repeatedly in order to remove the excessive modifier. Finally, the thoroughly washed precipitate was dried in a vacuum oven at 40°C for 6 hours and the surface modified particles were obtained.

5.5 Preparation of suspensions

In order to test the tribological performance of particles, all particles were combined with liquid paraffin separately and mixed into suspensions. All additives (either particles or modifiers) were dispersed in LP with an ultrahigh shear homogenizer at the speed of 20k rpm for 20 minutes. The suspensions have a variety of concentrations. Some coupling agents have excellent tribological properties when they were used as lubricant additives [189-191]. In order to validate if the effect of applying coupling agents on the anti-wear results of surface modified particles could be eliminated, OA and HS were combined with LP separately and tested with a pin-on-disc rig. When either OA or HS was added into LP alone as an additive, the concentration of additive was 0.1% in weight fraction.

5.6 Summary

Three different particles: lanthanum fluoride nanoparticles, cerium oxide nanoparticles and zinc borate submicron particles have been chosen as the experimental sample materials. Hexadecyltrimethoxysilane (HS) and oleic acid (OA) were used as surface modification agents in order to modify particles. Liquid paraffin was used as base lubricating oil. The experiment has three stages: sample characterisation, tribological tests and surface characterisation. All the particle samples were characterised by a Fourier transform infrared spectroscopy and a zeta-potential & dynamic light scattering equipment before the pin-on-disc tests in order to verify the surface modification. For the pin-on-disc tests, particles were dispersed into liquid paraffin and homogenised as suspension samples. After each pin-on-disc test, the worn surface of post-test disc was characterised by a SEM equipped with EDS, an AFM and a nano-indentation machine. The surface modification and preparation of suspension followed an identical procedure respectively.

Chapter 6 Effects of Surface Modified Cerium

Oxide Nanoparticles in Liquid Paraffin

6.1 Introduction

In this chapter, the effects of surface modification of CeO₂ nanoparticles on the properties of LP were studied. The surfaces of CeO₂ nanoparticles were modified with OA and HS coupling agents in order to improve their dispersibility in lubricant oil. The chemical bondings between the nanoparticles and modification agents were verified by a FTIR spectrometer. A reduction in particle agglomeration size associated with the improved dispersibility of CeO₂ nanoparticles was measured with a zeta potential equipment (Malvern Zetasizer Nano ZS). The anti-wear properties of the unmodified and modified CeO₂ nanoparticles in LP were investigated using a pin-on-disc tester. Worn surfaces of pre-tested pin ball were also examined by AFM and SEM equipped with EDS. The HS modified CeO₂ nanoparticles exhibited smaller conglomerate size in organic solvents and much greater improvement on anti-wear property in LP.

6.2 Experimental preparations

6.2.1 Characterisation of surface modified cerium oxide nanoparticles

The conglomerate size and zeta-potential measurements of all lubricant samples were obtained by using Dynamic Light Scattering (DLS) (Malvern Zetasizer Nano ZS). The photos of suspension samples were recorded by a camera.

6.2.2 Pin-on-disc test

The tribological properties of all lubricant samples were evaluated using a POD 2 Pin-on-disc tester (Teer Coatings Ltd.). All the tests were carried out with a 10N load and a sliding speed of 50 mm/s for a testing period of 60 minutes, under the experimental environment that has the ambient temperature of 22⁰C and humidity of 45%. In this study, a uniform concentration of 0.5% in weight fraction was applied for all friction and wear tests when the additive powders were employed. Some coupling agents have excellent tribological properties when they were used as lubricant additives [189-191]. OA and HS were combined with LP separately and tested with a pin-on-disc rig in order to validate if the effect of applying modification agents on the anti-wear results of surface modified particles could be eliminated. When either OA or HS was added into LP alone as an additive, the concentration was 0.1% in weight fraction. All additives (either particles or modification agents) were prepared following the procedure mentioned in section 5.5. The lubricants prepared in this study are presented in Table 6-1 in which the sample code and the associated fluids are defined.

6.2.3 Characterisation of the worn surfaces

Wear scars of the pins used in the pin-on-disc tests were observed using optical microscopy and scanning electron microscopy (SEM). Wear scar diameter of the pins were measured to the accuracy of 1 μ m. The topography of the wear scar surface was studied with atomic force microscopy (AFM). Energy dispersive X-ray spectroscopy (EDS) was conducted to examine the chemical features and elemental composition of the tribo-film generated on the worn surfaces of the pin.

Table 6-1 Different formulations with pure LP as control fluid.

Sample code	Constituent
LP	Liquid paraffin
LP + OA	Liquid paraffin with 0.1 wt% oleic acid
LP + HS	Liquid paraffin with 0.1 wt% hexadecyltrimethoxysilane
LP + CeO ₂	Liquid paraffin with 0.5 wt% original cerium oxide nanoparticles
LP + OA-CeO ₂	Liquid paraffin with 0.5 wt% oleic acid modified cerium oxide nanoparticles
LP + HS-CeO ₂	Liquid paraffin with 0.5 wt% hexadecyltrimethoxysilane modified cerium oxide nanoparticles

Mechanical properties of the tribo-film were determined with the nano-indentation facility. A Berkovich indenter with a tip diameter of 50 nm was employed throughout the nano-tests. For all indentation tests, a constant maximum indentation depth of 110 nm was applied with the loading/unloading duration of 15 seconds, and the initial load was set to be 0.05 mN. The distance between each indent was not less than 15 μm in order to avoid any possible interference between neighbouring indents.

6.3 Results and discussion

6.3.1 Characterisation of CeO₂ nanoparticles

Both composition and structure of the OA modified CeO₂ nanoparticles and HS modified CeO₂ nanoparticles were examined by FTIR spectroscopy.

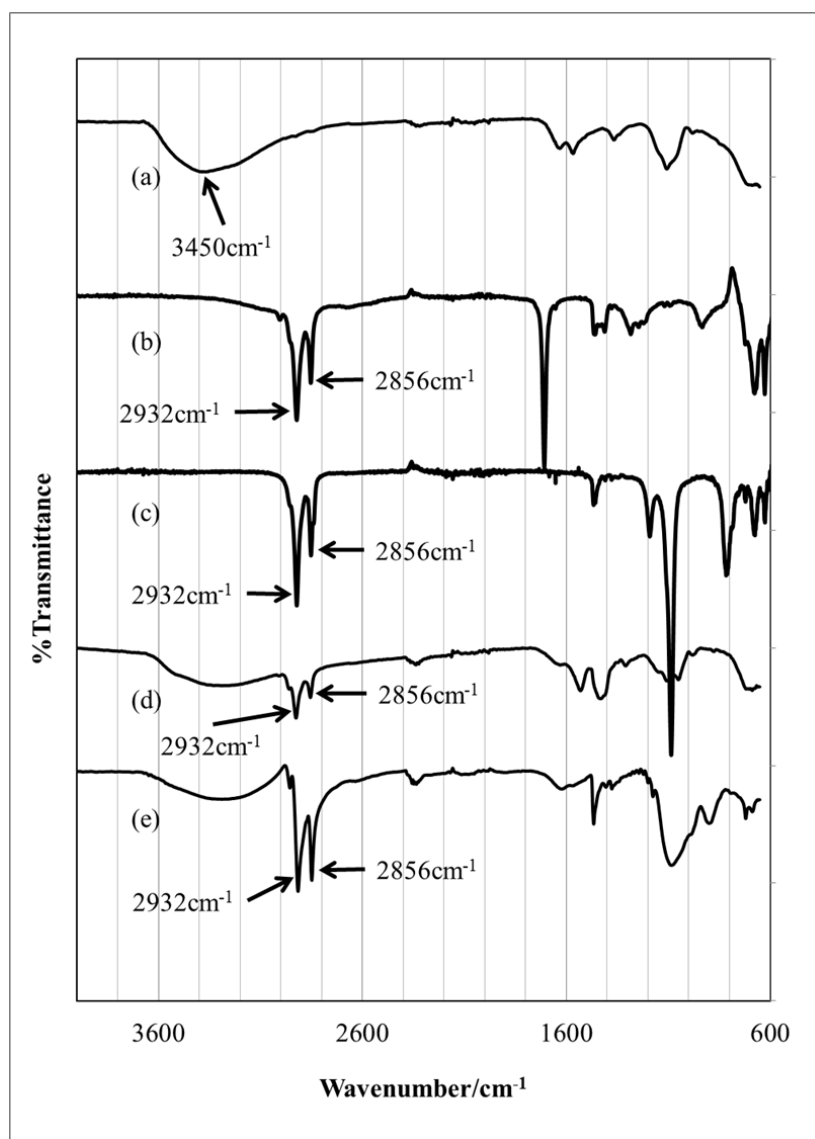


Figure 6-1 FT-IR spectra of: (a) unmodified CeO₂ nanoparticles; (b) OA; (c) HS; (d) OA modified CeO₂ nanoparticles; (e) HS modified CeO₂ nanoparticles.

Fig. 6-1 (a) shows the infrared spectrum of unmodified CeO₂ nanoparticles. The broad band at 3450 cm⁻¹ is assigned to stretching of –OH, which suggests the presence of –OH groups on the surfaces of cerium particles in the form of superficially adsorbed water before the surface modification. In the spectra of OA and HS displayed in Figs. 6-1 (b-c), two sharp peaks at 2923 and 2856 cm⁻¹ are attributed to the asymmetric and symmetric –CH₂ stretching vibrations respectively. Similar peaks were also found in the spectra of OA modified CeO₂ nanoparticles and HS modified CeO₂ nanoparticles shown in Figs. 6-1 (d-e). It is evident that the positions of the peaks for the distinctive functional groups observed in the spectra of OA modified CeO₂ nanoparticles and HS modified CeO₂ nanoparticles are identical with the pure modification agents of OA and HS. The infrared spectra results indicate that the surfaces of CeO₂ nanoparticles have been successfully modified by OA and HS.

6.3.2 Dispersibility of modified and unmodified cerium oxide nanoparticles

The dispersibility of the modified and unmodified CeO₂ nanoparticles was investigated by a zeta-potential tester. Table 6-2 displays the conglomerate size and values of zeta-potential of the unmodified and surface modified CeO₂ nanoparticles using methanol as a carrier. It is well known that at a very high or very low concentration, the data quality of zeta-potential tests cannot be trusted. Therefore, the samples with the concentration of 0.05 wt% for the zeta-potential tests were prepared according to the specification of Malvern's zeta-sizer. These samples were dispersed in methanol with an ultrasonic homogeniser (KINEMATICA PT 10-35 GT) for 5 minutes.

Table 6-2 The mean values of conglomerate size and Zeta-potential readings of CeO₂ nanoparticles dispersed in methanol.

	Cerium oxide nanoparticles		
	0.05% Original (mean)	0.05% OA modified CeO ₂ nanoparticles (mean)	0.05% HS modified CeO ₂ nanoparticles (mean)
Conglomerate size (in methanol)	1385nm	1254nm	672nm
Zeta-potential	4.5 mV	26.0mV	38.6mV

The average conglomerate size of original CeO₂ nanoparticles measured in methanol was 1385 nm in diameter. Under the same condition, OA modified CeO₂ nanoparticles demonstrated a smaller but still similar value of 1254 nm in diameter. It was observed that the values of conglomeration size of HS modified CeO₂ nanoparticles were reduced to 672 nm and a considerable reduction was achieved. Zeta-potential of the unmodified CeO₂ nanoparticles dispersed in methanol was measured to be 4.5 mV. In comparison, both OA modified CeO₂ nanoparticles and HS modified CeO₂ nanoparticles demonstrated high values of 26.0 mV and 38.6 mV respectively. It is well known that surface charges of the particles caused by absorption of ions and molecules generate an electrostatic repulsion force between particles. This electrostatic repulsion force can partially counteract gravitation and reduce agglomeration and sedimentation of particles [192, 193]. The physical stability of a colloidal system can be determined by the balance between the repulsive and attractive forces that are described quantitatively by the Deryaguin–Landau–Verwey–Overbeek (DLVO) theory [152]. Therefore, a higher absolute value of zeta-potential of a suspension presents a better dispersibility.

The Zeta potential results from this study shown in Table 6-2 suggest that surface modifications of CeO₂ nanoparticles using OA and HS have effectively improved the dispersibility of CeO₂ nanoparticles in the organic solvent. High zeta-potential value of HS modified CeO₂ nanoparticles also suggests that HS modified CeO₂ nanoparticles have better dispersibility than OA modified CeO₂ nanoparticles in methanol.

In this study, every material has been tested for three times, the detailed readings and standard deviations (s) of conglomerate size and Zeta-potential results have been listed in Table 6-3 and Table 6-4. The standard deviation s could be calculated by using the equations below, where x_i is the measurement reading for each time, \bar{x} is the arithmetic mean value, n is the number of measurements [194].

$$\bar{x} = \frac{\sum x_i}{n} \quad 6.3.2-1$$

$$s = \sqrt{\frac{\sum (x_i - \bar{x})^2}{(n - 1)}} \quad 6.3.2-2$$

Table 6-3 The standard deviations of conglomerate size results of cerium oxide nanoparticles dispersed in methanol. (Unit:nm)

	x_i	$(x_i - \bar{x})$	$(x_i - \bar{x})^2$	s
Original	1376	-9	81	-
	1399	14	196	-
	1380	-5	25	-
Σ	4155	0	302	12.28
	x_i	$(x_i - \bar{x})$	$(x_i - \bar{x})^2$	s
OA-CeO₂	1261	7	49	-
	1250	-4	16	-
	1251	-3	9	-
Σ	3762	0	74	6.08
	x_i	$(x_i - \bar{x})$	$(x_i - \bar{x})^2$	s
HS-CeO₂	664	-8	64	-
	679	7	49	-
	673	1	1	-
Σ	2016	0	114	7.55

Table 6-4 The standard deviations of Zeta-potential results of cerium oxide nanoparticles dispersed in methanol. (Unit:mV)

	x_i	$(x_i - \bar{x})$	$(x_i - \bar{x})^2$	s
Original	4.3	-0.2	0.04	-
	4.6	0.1	0.01	-
	4.6	0.1	0.01	-
Σ	13.4	0	0.06	0.17
	x_i	$(x_i - \bar{x})$	$(x_i - \bar{x})^2$	s
OA-CeO₂	24.9	-1.1	1.21	-
	25.7	-0.3	0.9	-
	27.4	1.4	1.96	-
Σ	78.0	0	4.07	1.43
	x_i	$(x_i - \bar{x})$	$(x_i - \bar{x})^2$	s
HS-CeO₂	39.2	0.6	0.36	-
	39.4	0.8	0.64	-
	37.2	-1.4	1.96	-
Σ	2016	0	2.96	1.22

The stability of modified and unmodified CeO₂ nanoparticle in LP can be reflected by Fig. 6-2. Fig. 6-2 shows the status of the sedimentation of LP + CeO₂, LP + OA-CeO₂, and LP + HS-CeO₂ at the different periods after the preparation, respectively. As shown in Figs. 6-2 (a-1), 6-2 (b-1) and 6-2 (c-1), at t=0, there was no significant difference of colour and transparency among the samples and all the samples were well dispersed into suspensions. At the 48th hour after the preparation, compared with Figs. 6-2 (b-2) and 6-2 (c-2), Fig. 6-2 (a-2) showed relatively clearer supernatant liquid paraffin which indicated that a complete deposition happened in sample LP + CeO₂. The notable sedimentation also was found in Fig. 6-2 (a-2) which had bigger size than sedimentation observed in Figs. 6-2 (b-2) and 6-2 (c-2). In sample LP + OA-CeO₂ and LP + HS-CeO₂, the accumulation of precipitate at the bottom of the container was much looser and thinner. And there was no clear boundary between the sedimentation and supernatant LP as shown in Figs. 6-2 (b-2) and 6-2 (c-2). Fig. 6-2 (c-2) shows that LP + HS-CeO₂ had the minimal deposition. It can also be seen that transparency in Figs. 6-2 (a-2), 6-2 (b-2) and 6-2 (c-2) decreased respectively. Based upon the aforementioned observations, it is suggested that the dispersibility and stability of CeO₂ nanoparticles in organic solvent can be greatly improved with the surface modification using OA and HS. The sample LP + HS-CeO₂ is the most stable colloidal system.

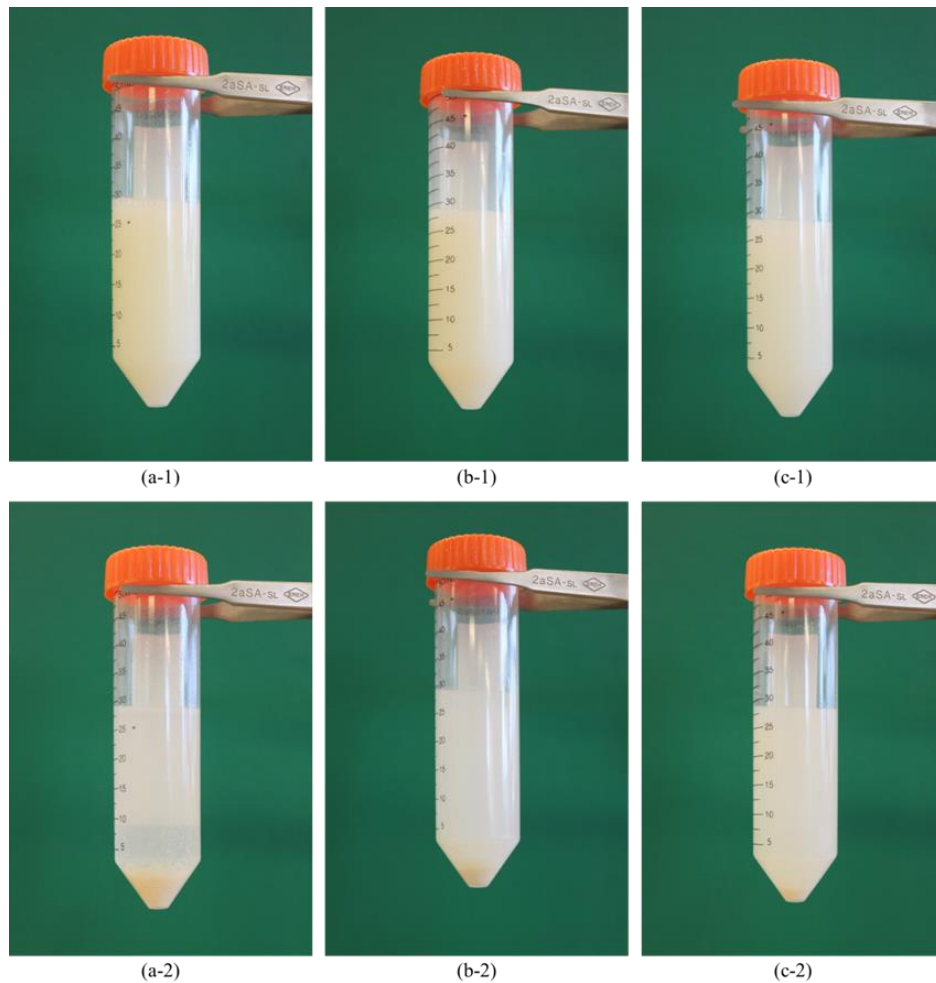


Figure 6-2 Status of the sedimentation of the lubricant samples at the different periods after the sample preparation: at zero hour: (a-1) LP + CeO₂, (b-1) LP + OA-CeO₂, (c-1) LP +HS-CeO₂, and at the 48th hour: (a-2) LP + CeO₂, (b-2) LP + OA-CeO₂, (c-2) LP +HS-CeO₂.

6.3.3 Anti-wear behaviour

Wear scars of the pins (bearing balls) used in pin-on-disc tests were firstly assessed using an optical microscope. The morphology and wear scar diameter (WSD) of the tested pins are shown in Fig 6-3. A smaller WSD indicates a less material loss, therefore, the superior wear resistance. It is evident that the applications of HS modified CeO₂ nanoparticles as lubricant additives in LP have significantly reduced the WSDs of the pins (bearing balls). Fig. 6-3 (a) shows the WSD measurement when pure LP was tested. As shown in Fig 6-3 (d), the smallest WSD (136 μm) was

obtained when LP with HS modified CeO₂ nanoparticles was used as a lubricant. This WSD is about 40% smaller than the wear scar obtained shown in Fig 6-3 (a). A relatively small reduction of WSD can be observed in Fig. 6-3 (c) when OA modified CeO₂ worked as a lubricant additive in LP. By contrast, without surface modification of the solid lubricant additive, LP with unmodified CeO₂ nanoparticles delivered the biggest WSD of 284 μm as shown in Fig 6-3 (b). A tribo-film that is uniform and tenacious was found on the wear scar lubricated with LP with HS modified CeO₂ nanoparticles, as shown in Fig 6-3 (d), the formation of this tribo-film appears to have played an important role in the outstanding anti-wear performance. In general, surface modification agents could also contribute to the improvement of the tribological properties of a lubricant, and therefore it is essential to identify the performance of the surface modification agent when they are employed in the lubricant base oil alone. Without CeO₂ nanoparticles, HS failed to deliver a noticeable anti-wear property, Fig 6-3 (f) shows a WSD of 242.5 μm. Fig. 6-3 (e) indicates that a smaller WSD was found when OA was added in LP alone compared with LP + OA-CeO₂.

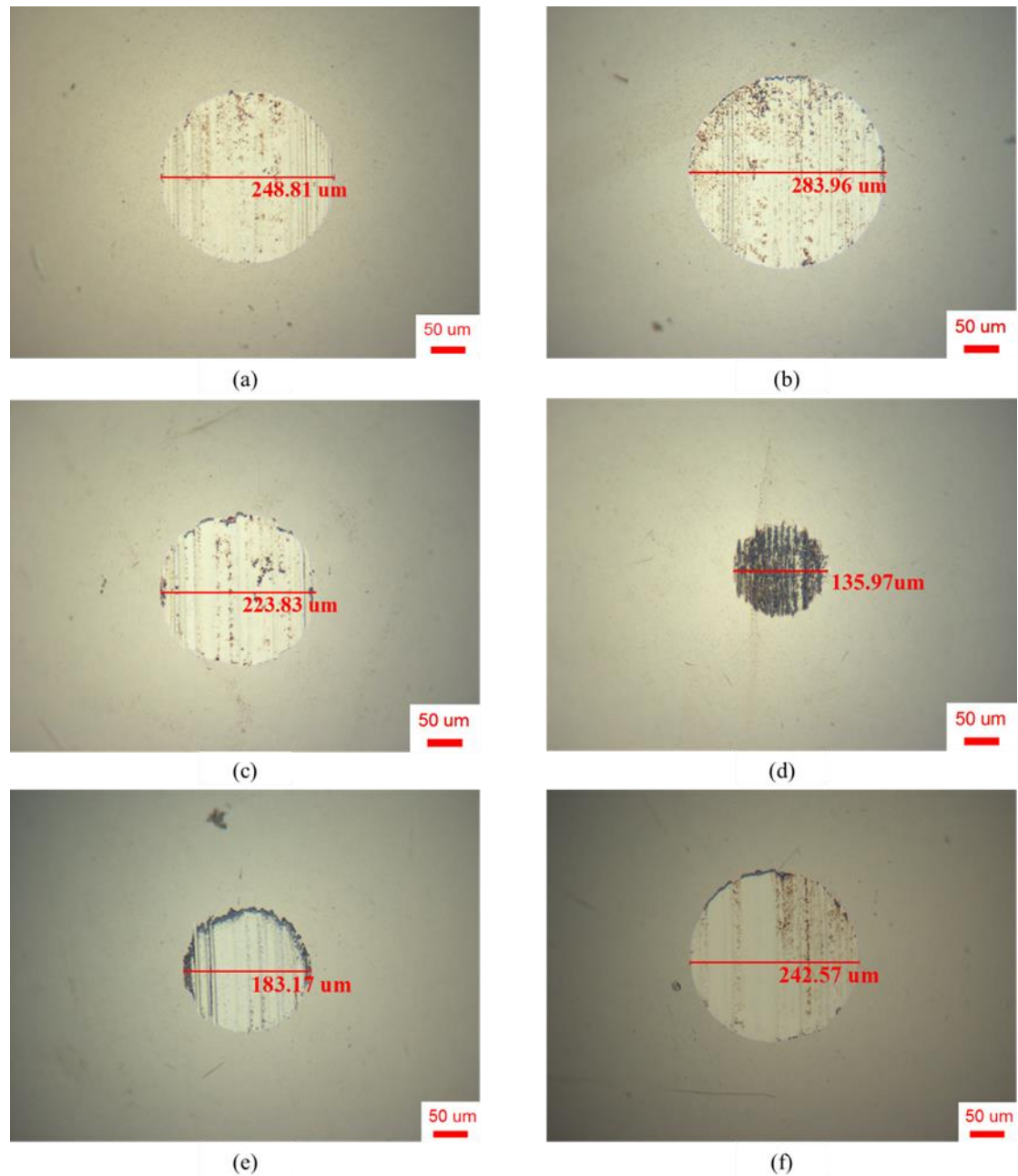


Figure 6-3 Optical micrographs of wear scars lubricated using: (a) LP, (b) LP with CeO₂ nanoparticles, (c) LP with OA modified CeO₂ nanoparticles, (d) LP with HS modified CeO₂ nanoparticles, (e) LP with OA, (f) LP with HS.

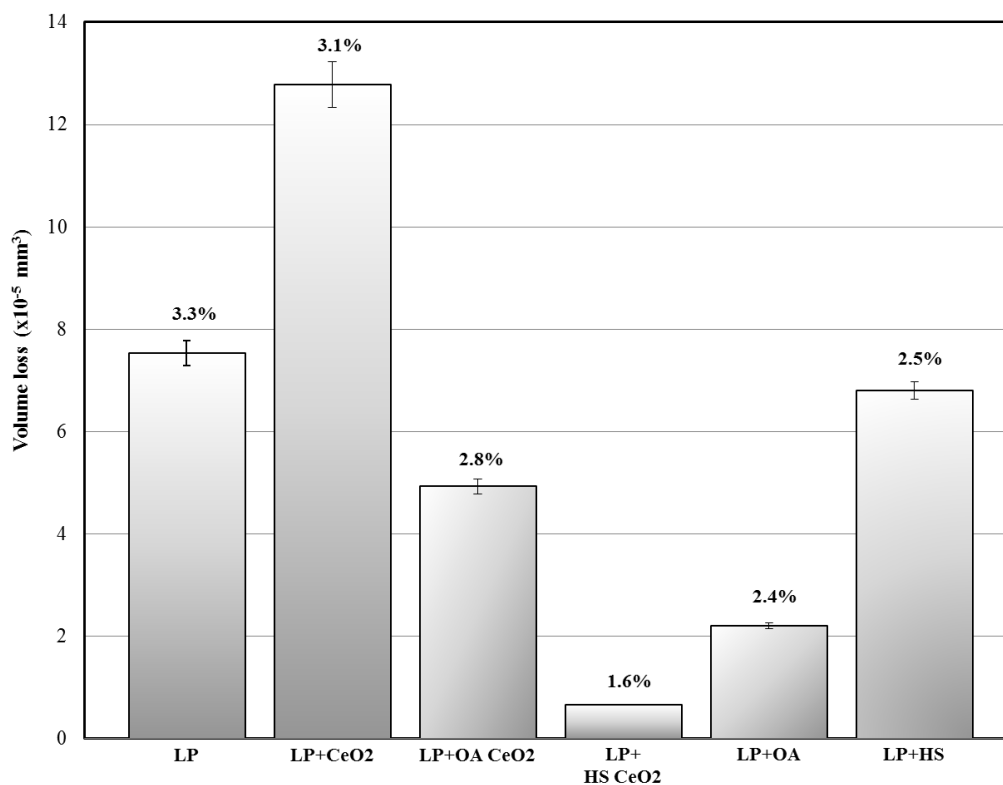


Figure 6-4 Effects of different lubricant additives on volume loss of the bearing balls.

Volume losses of the pins lubricated by different lubricant samples were also illustrated in Fig 6-4. The anti-wear property of a lubricant could be reflected by volume loss which was calculated geometrically based on the assumption that wear scar was a flat surface. As shown in Fig. 6-4, the volume loss of the upper pin lubricated by LP with 0.5% HS modified CeO₂ nanoparticles is over 11 times smaller than that lubricated by pure LP. As shown in Fig. 6-4, the maximum error value of volume loss was less than 3.3% which is within the limit of test tolerance so that the effect of WSD measurement system on errors could be ignored.

According to the zeta-potential results obtained above, surface modified CeO₂ nanoparticles have shown much greater dispersibility compared with unmodified CeO₂ nanoparticles. The dispersibility of additive particles in base oil plays an

important role in the formation of tribo-film. Compared with unmodified CeO₂ nanoparticles, both OA and HS modified CeO₂ nanoparticles have better dispersibility in LP. Additionally, HS modified CeO₂ nanoparticles have achieved the smallest conglomerate size. It is suggested that HS modified CeO₂ nanoparticles may have better compatibility with base oil and easier access to a contact interface.

6.4 Characterisation of the tribo-film

6.4.1 AFM and Nano-indentation results

The mechanical property of the tribo-film was measured with a nano-tester as shown in Fig. 6-5. The indentation tests were carried out on both the tribo-film and the substrate. Fig. 6-5 (a) shows a magnified optical image of Fig. 6-3 (d) which was the wear scar lubricated by LP with 0.5% HS modified CeO₂ nanoparticles. Figs. 6-5 (b-c) present the AFM images of tribo-film generated on wear scar surface as marked in Fig. 6-5 (a). It can be seen that a tribo-film with a good coverage does not show an entirely even distribution. The average thickness of the tribo-film was approximately 190 nm.

Corresponding load–depth curves are illustrated in Fig. 6-6. Mechanical properties of the worn surfaces of the tested bearing balls were derived from further analysing the load–depth curves.

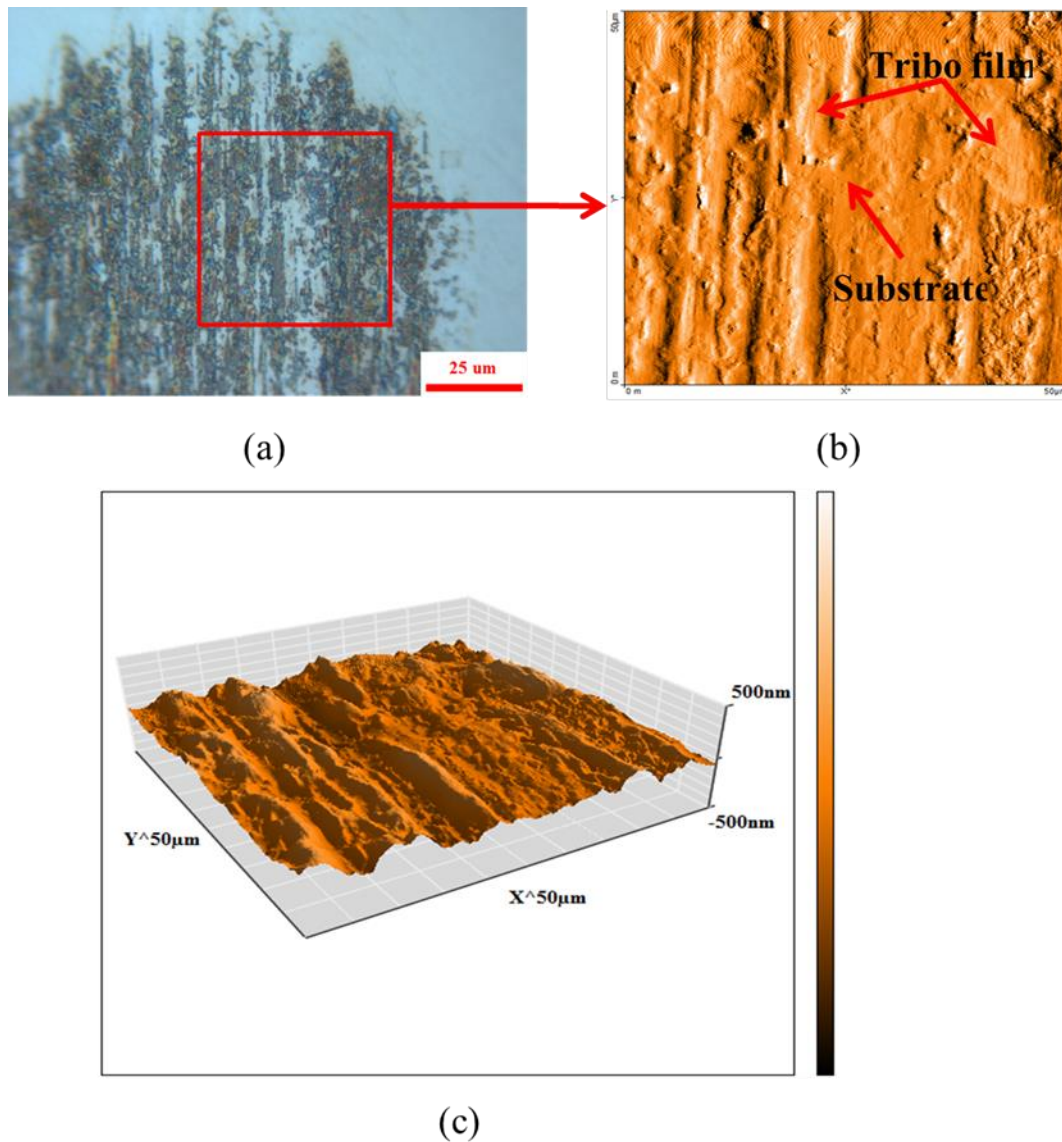


Figure 6-5 Morphologies of the tribo-film generated by LP with HS modified CeO₂ nanoparticles: (a) optical image, (b) AFM surface topographic image, (c) 3D AFM surface topographic image.

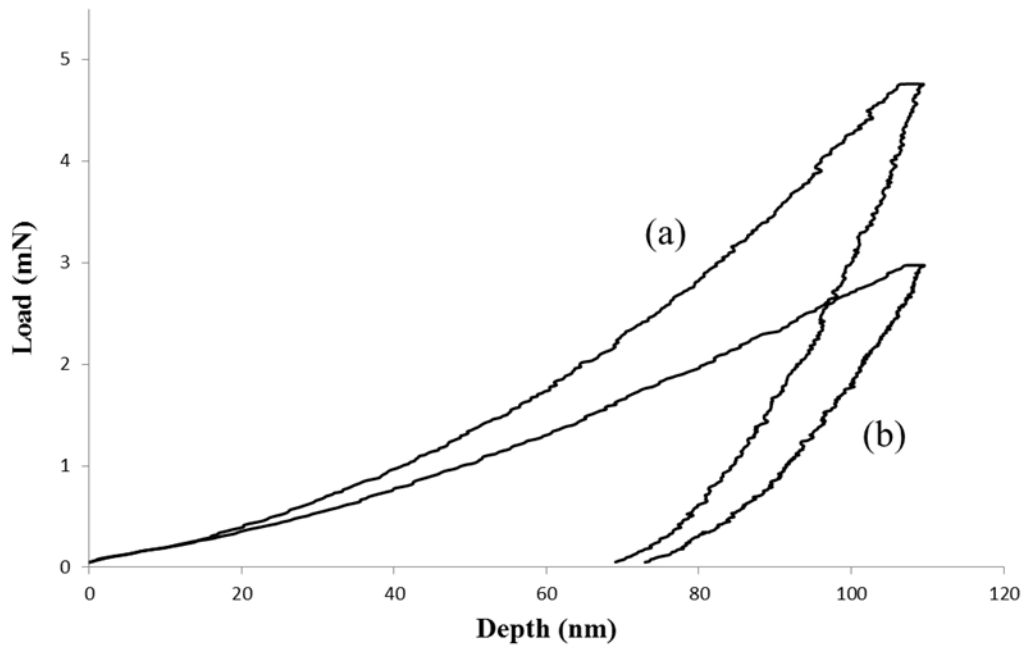


Figure 6-6 Indentation curves obtained at different domains on the worn surface lubricated by LP with HS modified CeO₂ nanoparticles: (a) on substrate, (b) on tribo-film.

As shown in Fig. 6-6, the maximum indentation depth was set to be 110 nm which was not higher than the thickness of the tribo-film. At this condition the mechanical properties of the tribo-film measured did not receive much interference from the substrate [195], and therefore it is suggested that the surface hardness and reduced modulus derived from this load-depth curve only represent the property of the tribo-film alone. In order to reach pre-set indentation depth, the indentation force required on tribo-film was 2.97×10^{-3} N (curve (b) in Fig. 6-6), whereas under the same condition the indentation force required on substrate steel was 4.75×10^{-3} N (curve (a) in Fig. 6-6). A comparison of the surface hardness and reduced modulus of the tribo-film and substrate steel is presented in Table 6-5. The test results suggest that tribo-film is much softer and less stiff compared with substrate steel.

Table 6-5 A comparison of mechanical properties of the tribo-film and the substrate.

Indentation position	Indentation force	Hardness	Reduced modulus
Tribo-film	2.97×10^{-3} N	8.3GPa	186GPa
Substrate	4.75×10^{-3} N	13.2GPa	304GPa

Fig. 6-7 shows AFM morphologies of the worn surfaces on the pins lubricated with different lubricant samples. Changes in the size and profile of the tribo-films were discovered when different lubricant samples were used.

When pure LP was used as the lubricant as shown in Fig. 6-7 (a), no complete tribo-film but only small patchy pieces were found scattering over the worn surface and some ploughing was also seen. A similar phenomenon was also observed when LP with the unmodified CeO₂ nanoparticles was employed, as shown in Fig. 6-7 (b). Heavy ploughing also took place on the worn surface lubricated by LP with the original CeO₂ nanoparticles, which indicated the abrasion effect contributed by the additional CeO₂ nanoparticles.

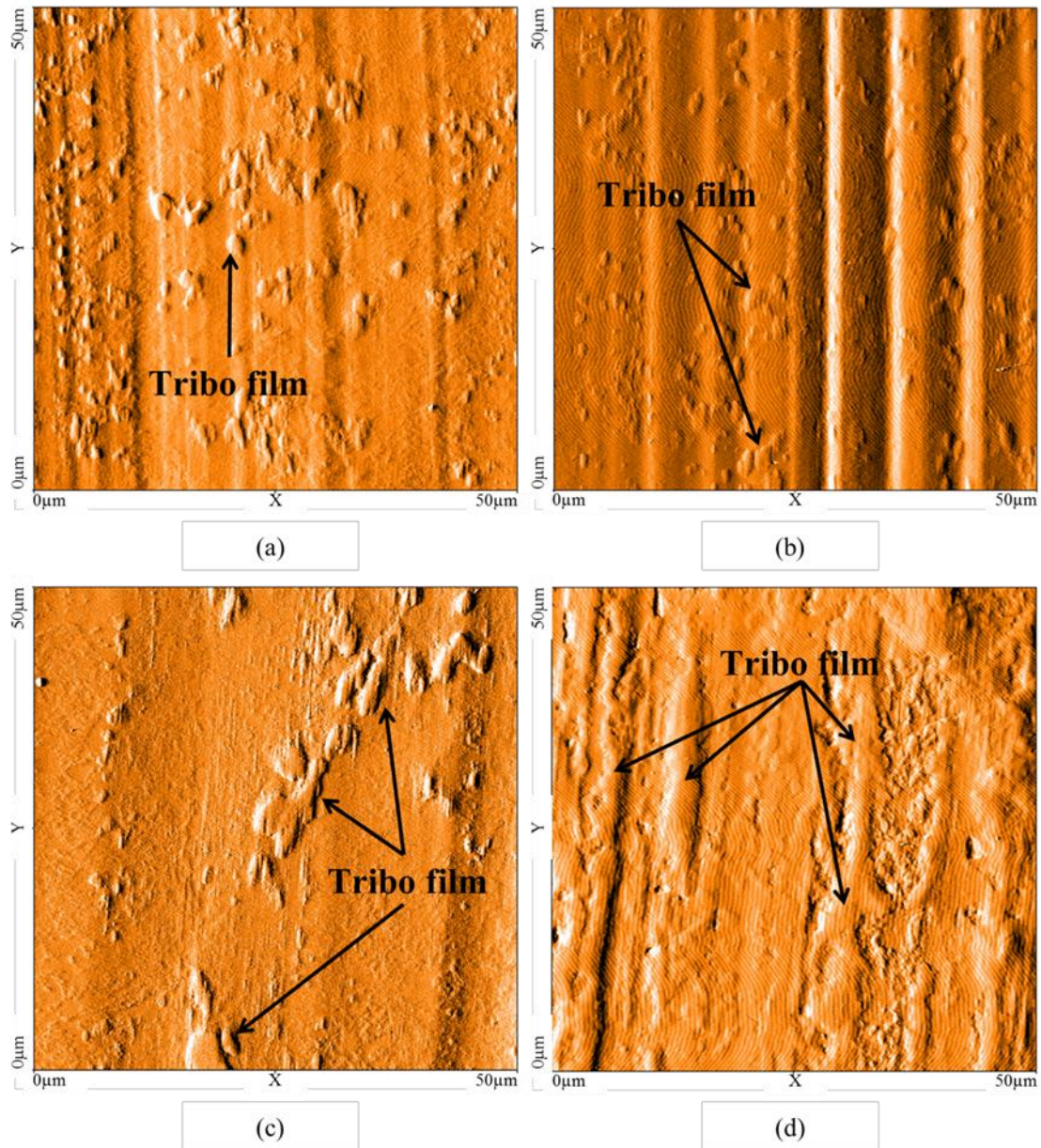


Figure 6-7 AFM surface topographic images of the worn surfaces lubricated with different lubricants: (a) LP; (b) LP with unmodified CeO₂ nanoparticles; (c) LP with OA modified CeO₂ nanoparticles; (d) LP with HS modified CeO₂ nanoparticles.

Very fine fragments of tribo-film can be seen spreading over the examined area. The tribo-film generated on the wear scar lubricated by LP with OA modified CeO₂ nanoparticles, as shown in Fig. 6-7 (c), had a bigger fragment size and elongated shape stretching along the direction of sliding. Among all the samples, the surface lubricated by LP with HS modified CeO₂ nanoparticles had the most widespread and

tenacious tribo-film. Almost the whole scanned surface was covered with the tribo-film, although the thickness of the tribo-film was not entirely uniform across the area, as shown in Fig. 6-7 (d). These results suggest that the employment of HS modified CeO₂ nanoparticles in LP enables a more complete and durable tribo-film to be generated on the contact surface, and this tribo-film can effectively protect the surface from serious wear damage.

6.4.2 SEM observations and EDS analysis

The worn surfaces lubricated by LP with 0.5% HS modified CeO₂ nanoparticles were analysed under a scanning electronic microscope (SEM) equipped with energy dispersive X-ray spectroscopy (EDS). Typical SEM images and EDS analyses are shown in Fig. 6-8. Distinctive topographical differences of the tribo-film and substrate can be seen clearly. The tribo-film displayed in Fig. 6-8 (a) appears in dark colour with a complex topography which makes a good contrast with the substrate displayed in brighter colour with smoother surface texture. The EDS patterns of the region highlighted on the tribo-film and the substrate are shown in Fig. 6-8 (d) and Fig. 6-8 (e) respectively. Quantified elemental analytical results are given in Table 6-6. It can be seen that a considerable increase of Oxygen and Silicon contents on the tribo-film compared with the element distribution on the substrate occurs. The further amount of oxygen and silicon was possibly derived from HS which is an important ingredient in the formation of the tribo-film.

No cerium element from CeO₂ nanoparticles was detected either on the substrate or on the tribo-film. It can be suggested that CeO₂ nanoparticles did not chemically contribute to the formation of tribo-film. However, the employment of HS-CeO₂

nanoparticles was an essential factor to produce a tenacious and continuous tribo-film with a good coverage on the worn surface.

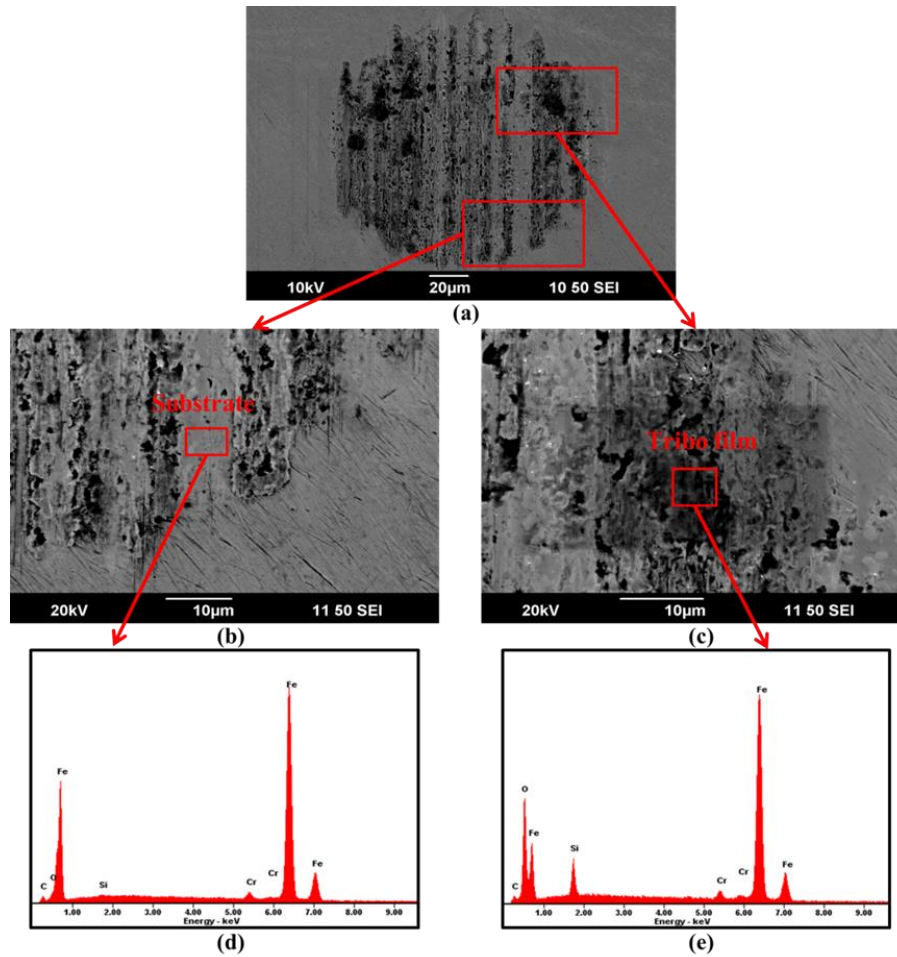


Figure 6-8 SEM images and EDS patterns of worn surfaces lubricated with LP with HS modified CeO₂ nanoparticles: (a) worn surface morphology, (b, c) magnified SEM image, (d) EDS patterns of the substrate, (e) EDS patterns of the tribo-film.

Table 6-6 Quantified elemental analysis on the worn surface shown in Figure 6-8.

Element	Spectrum (b) (at %)	Spectrum (c) (at %)
C	20.56	16.28
O	6.83	35.12
Si	0.50	5.22
Cr	1.36	1.08
Fe	70.76	42.31

6.5 Summary

In this chapter, the effects of surface modification of cerium oxide nanoparticles on the properties of the particles in liquid paraffin (LP) have been investigated. Based on the test results and discussion, the following conclusions can be drawn:

- The surface modification of oleic acid and hexadecyltrimethoxysilane modified CeO₂ nanoparticles were successfully carried out. It is evident that surface modifications of cerium oxide nanoparticles can significantly improve the dispersibility of CeO₂ nanoparticles in liquid paraffin. HS modified CeO₂ nanoparticles have demonstrated a reduction of more than 50% over the conglomerate size and a 34.1 mV increase in the zeta-potential value compared with the unmodified CeO₂ nanoparticles. HS modified CeO₂ nanoparticles have provided the most stable colloidal system in liquid paraffin compared with unmodified CeO₂ nanoparticles or OA modified CeO₂ nanoparticles.

- The modified CeO₂ nanoparticles as lubricant additives in LP displayed much greater anti-wear performance than LP only and LP with unmodified CeO₂ nanoparticles. Compared with OA modified CeO₂ nanoparticles, the HS modified CeO₂ nanoparticles demonstrated much greater improvement on the anti-wear property when it was used in LP. Without surface modification, the unmodified CeO₂ nanoparticles did not demonstrate any noticeable anti-wear performance.
- The outstanding anti-wear performance of HS modified CeO₂ nanoparticles can be attributed to the formation of a complete and tenacious tribo-film on worn surface. Modification agent HS is a crucial ingredient for the formation of the tribo-film which has a smaller hardness and reduced modulus than the substrate material.
- The changes on the size and profile of the tribo-films were discovered when different fluid samples were employed. It is evident that the coverage of the tribo-films on the worn surfaces has a good consistency with the intensity of wear. A good coverage of tribo-film can protect the surface from wear effectively. Only small patchy pieces of film were found on the worn surfaces lubricated by LP only and LP with unmodified CeO₂ nanoparticles. Tribo-film with larger fragment size was observed on the worn surface when LP with OA modified CeO₂ nanoparticles was used. The best coverage by tribo-film was achieved by using LP with HS modified CeO₂ nanoparticles as the lubricant.

Chapter 7 Effects of Surface Modified Zinc Borate Submicron Particles in Liquid Paraffin

7.1 Introduction

Surface modification of zinc borate submicron particles (ZB) can improve their dispersibility and tribological performance as a lubricant additive in liquid paraffin (LP) under certain experimental conditions [7, 68]. However, the influence on properties of hexadecyltrimethoxysilane (HS) and oleic acid (OA) modified zinc borate submicron particles (HS-ZB, OA-ZB) in LP under various experimental conditions have not been studied. This chapter presents the studies on properties of HS-ZB and OA-ZB under two experimental conditions. The outcomes will be compared with published results in order to evaluate the potential of surface modified ZB as lubricant additives under different working conditions. Identical HS-ZB and OA-ZB were synthesised by the method used in [7, 68] and tested with the procedure listed in chapter 5.

The preparations and detailed experimental conditions are presented in section 7.2. Tests results are included in section 7.3. The outcomes of experiments have been summarised in section 7.4. Further discussions of results will be included in chapter 9.

7.2 Experimental preparations

7.2.1 Characterisation apparatus

A Fourier transform infrared spectroscopy (FTIR) spectrometer (Perkin-Elmer Spectrum 100) in a transmission mode with a resolution of 4 cm^{-1} was employed and

the specimens were all powder-pressed KBr pellets. All data within the wave range from 600 cm^{-1} to 4000 cm^{-1} were collected. A Malvern Zetasizer Nano ZS measurer was employed in order to measure the conglomerate size of particles and zeta-potential results.

7.2.2 Procedures and experimental conditions for pin-on-disc tests

The tribological properties of all lubricant samples were evaluated using a POD 2 Pin-on-disc tester (Teer Coatings Ltd.). The details of different tribological test condition settings are listed in Table 7-1. As shown in Table 7-1, Setting (i) is the previous test condition used in a joint work [7]. On the purpose of studying the tribological behaviours of OA-ZB and HS-ZB in LP with a rather higher additive concentration, Setting (ii), the concentration of additives was increased from 0.5% to 1% and the rest of parameters were identical to setting (i). Setting (iii) was designed on the purpose to evaluate the tribological performance of OA-ZB and HS-ZB in LP under a harsher working condition, therefore, the load in Setting (iii) was increased to 30 N while other parameters were maintained as the same as Setting (i). In this chapter, on the purpose of comparison, all pin-on-disc tests were operated under Setting (ii) or Setting (iii) since the results of Setting (i) have already been published [7].

Table 7-1 The settings of experimental conditions.

Setting	Concentration	Load	Sliding speed	Testing period	Temperature	Humidity
(i) [7]	0.5 wt%	10 N	50 mm/s	3600 s	22 °C	45%
(ii)	1 wt%	10 N	50 mm/s	3600 s	22 °C	45%
(iii)	0.5 wt%	30 N	50 mm/s	3600 s	22 °C	45%

7.2.3 Preparations of lubricant samples

Table 7-2 presents sample codes of all lubricant samples that were tested and all samples will be denoted by the sample code in later sections of this chapter.

Table 7-2 Sample code and definition of associated fluid.

Sample code	Constituent
LP	Liquid paraffin
0.5% ZB + LP	Liquid paraffin with 0.5 wt% zinc borate submicron particles
0.5% OA-ZB + LP	Liquid paraffin with 0.5 wt% oleic acid modified zinc borate submicron particles
0.5% HS-ZB + LP	Liquid paraffin with 0.5 wt% hexadecyltrimethoxysilane modified zinc borate submicron particles
1% ZB + LP	Liquid paraffin with 1 wt% zinc borate submicron particles
1% OA-ZB + LP	Liquid paraffin with 1 wt% oleic acid modified zinc borate submicron particles
1% HS-ZB + LP	Liquid paraffin with 1 wt% hexadecyltrimethoxysilane modified zinc borate submicron particles

Lubricant samples for pin-on-disc tests were prepared by an ultrahigh shear homogeniser in order to fully disperse additive particles into LP. The detailed procedure of preparation of lubricant samples has been listed in chapter 5.

7.2.4 Characterisation of samples

To characterise the results of surface modification on zinc borate submicron particles, FTIR spectroscopy was employed to examine the composition and structure of both zinc borate submicron particles and surface modification agents. Table 7-3 shows the wave numbers and the corresponding assignments of absorption bands of zinc borate submicron particles (ZB, OA-ZB and HS-ZB) and surface modification agents (OA and HS) obtained in FTIR. The FTIR spectrums are shown in the Fig 7-1.

Table 7-3 Assignment of absorption bands and corresponding wave numbers from the FTIR spectrums shown in Figure 7-1.

Wavenumber (cm ⁻¹)	Assignment
986-1094	Stretching vibrations of BO ₄ units in various structural groups [196-198].
1390	B–O stretching vibration of trigonal BO ₃ units [196-198].
1630	H-O-H bending mode of H ₂ O [199].
2850	Stretching vibration of symmetrical CH ₂ [200].
2925	Stretching vibration of asymmetrical CH ₂ [200].
3200	Stretching vibration of –OH [201].

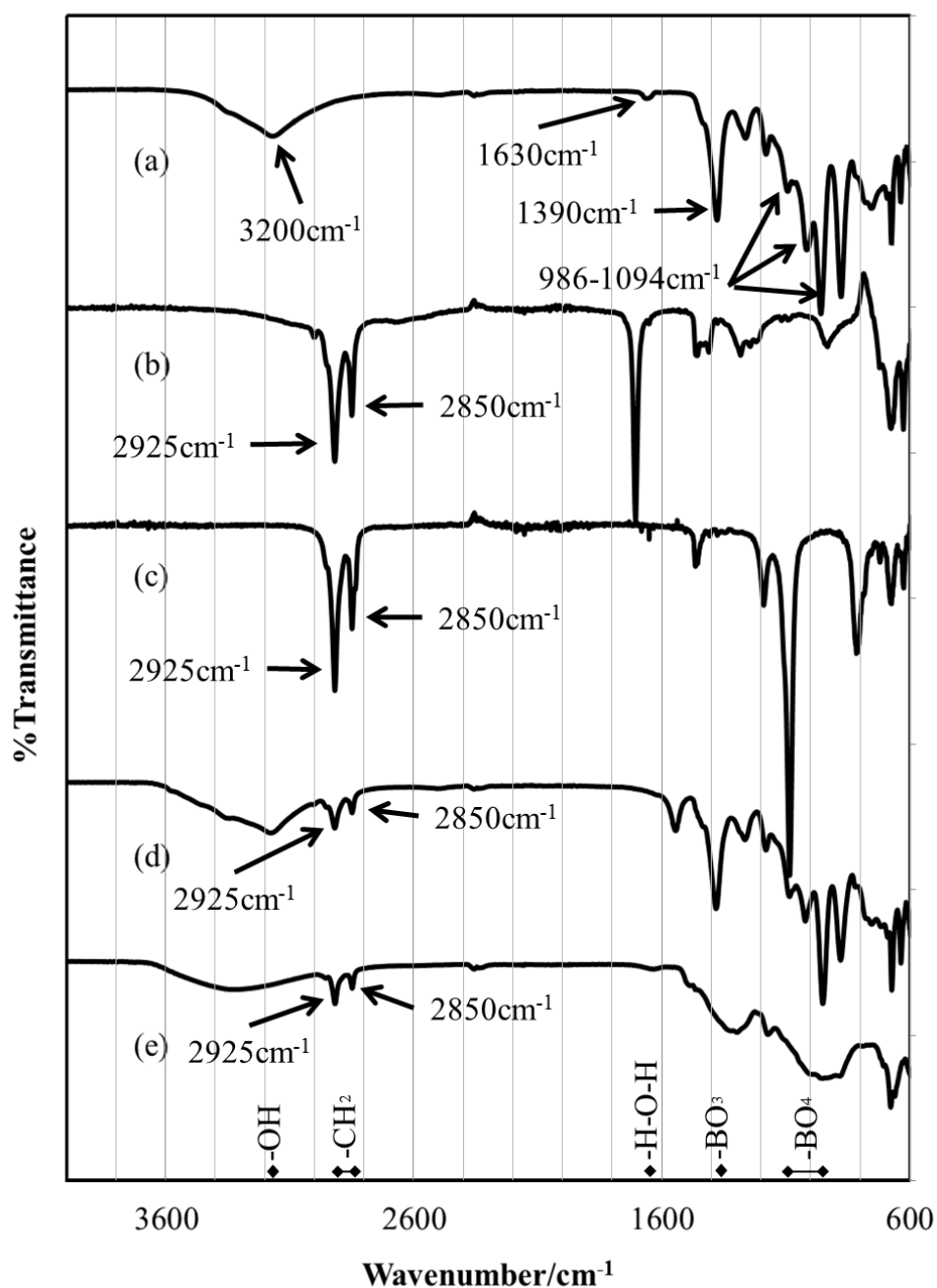


Figure 7-1 FTIR spectra of: (a) Unmodified zinc borate submicron particles; (b) OA; (c) HS; (d) OA zinc borate submicron particles; (e) HS zinc borate submicron particles.

Fig. 7-1(a) shows the spectrum of unmodified zinc borate submicron particles. The broad and strong band at approximately 3200 cm^{-1} is the stretching vibrations of $-\text{OH}$ [201]. The absorption band at 1630 cm^{-1} is attributed to the bending mode of H-O-H

[199]. This is the evidence that the zinc borate contains crystal water. B-O stretching vibration is observed at 1390 cm^{-1} . The peaks between 986 cm^{-1} to 1094 cm^{-1} are stretching vibrations of BO_4 units in different structural [196-198]. It is clear that before the surface modification, there is no any peak near the wave number range 2800 cm^{-1} to 3000 cm^{-1} . Fig. 7-1(b) and Fig. 7-1(c) are FTIR spectra of OA and HS, and two peaks at 2925 cm^{-1} and 2850 cm^{-1} can be observed in both Fig. 7-1(b) and Fig. 7-1(c). The peak at 2925 cm^{-1} is the stretching vibration of asymmetrical CH_2 [200] and the peak at 2850 cm^{-1} is the stretching vibration of symmetrical CH_2 [200]. The same peaks appeared in Fig. 7-1(d) and Fig. 7-1(e) are spectra of OA modified zinc borate submicron particles and HS modified zinc borate submicron particles. The fact that Figs. 7-1(b), (c), (d) and (e) have the same distinctive functional groups at the same positions on spectra confirms that the particle surfaces have been modified by either OA or HS. The infrared spectrum results indicate that the surface modification of zinc borate submicron particles was conducted successfully.

7.3 Results and discussion

7.3.1 Dispersibility of surface modified zinc borate submicron particles

The dispersibility of the modified and unmodified zinc borate submicron particles was investigated by a zeta-potential tester. Table 7-4 displays the zeta-potential and conglomerate size reading of modified/unmodified zinc borate submicron particles in methanol. By the recommendation of the instruction from the equipment provider, for the best accuracy of results, all suspensions for zeta tests were prepared with additive concentration of 0.05wt% and dispersed into methanol. An average conglomerate size reading of 2580 nm was obtained when the unmodified ZB was measured. OA-ZB demonstrated an average conglomerate size 2230 nm in methanol which was slightly

smaller than that of the unmodified ZB. A comparatively smaller value of 1070 nm was generated by the HS-ZB in methanol. Compared with first two readings, the reduction of conglomerate size is significant.

Table 7-4 Conglomerate size and zeta-potential readings of ZB, OA-ZB and HS-ZB.

	Zinc borate ultrafine powders		
	0.05%ZB	0.05% OA-ZB	0.05 % HS-ZB
Conglomerate size (in methanol)	2580 nm	2230 nm	1070 nm
Zeta-potential	6.63 mV	9.41mV	33.2mV

Based upon Deryaguin–Landau–Verwey–Overbeek (DLVO) theory, the stability (physical) of a colloidal system is related to the balance between the repulsive and attractive forces [152]. Zeta-potential measurement is an important factor to reflect this balance. The greater absolute zeta-potential value of a suspension system leads to a better dispersibility of particles in the solute [202]. It is well known that an electrostatic repulsion force between particles is a result of the surface charges which can be created by the absorption of molecules and ions. And this electrostatic repulsion force can be a resistance of the formation of agglomeration and sedimentation due to the partially counteract of gravitation [192, 193]. As shown in Table 7-4, the zeta-potential values of OA and HS modified zinc borate particles are 9.41 mV and 33.2 mV respectively while that of unmodified zinc borate submicron particles only reached 6.63 mV. Based upon the zeta-potential results, it can be suggested that the HS modified zinc borate submicron particles have the strongest ability to disperse themselves into organic solvents, compared with the other two

samples. According to Table 7-4, when HS was used as the modification agent, the lowest conglomerate size and the highest zeta-potential value of HS-ZB have been achieved. HS modified zinc borate submicron particles have demonstrated the most significant improvement on dispersibility in organic solvents.

The standard deviations of conglomerate size results and Zeta-potential measurements are calculated based on the equation that is mentioned in section 6.3.2. The calculation results are listed in table 7-5 and Table 7-6 respectively.

Table 7-5 The standard deviations of conglomerate size results of zinc borate submicron-particles dispersed in methanol. (Unit:nm)

	x_i	$(x_i - \bar{x})$	$(x_i - \bar{x})^2$	s
Original	2839	-11	121	-
	2856	6	36	-
	2855	5	25	-
Σ	8550	0	182	9.54
	x_i	$(x_i - \bar{x})$	$(x_i - \bar{x})^2$	s
OA-ZB	2237	7	49	-
	2231	1	1	-
	2222	-8	64	-
Σ	6690	0	114	7.55
	x_i	$(x_i - \bar{x})$	$(x_i - \bar{x})^2$	s
HS-ZB	1067	-3	9	-
	1076	6	36	-
	1067	-3	9	-
Σ	3210	0	54	5.20

Table 7-6 The standard deviations of Zeta-potential results of of zinc borate submicron-particles dispersed in methanol. (Unit:mV)

	x_i	$(x_i - \bar{x})$	$(x_i - \bar{x})^2$	s
Original	6.78	0.15	0.0225	-
	6.61	-0.02	0.0004	-
	6.50	-0.13	0.0169	-
Σ	19.89	0	0.0398	0.14
	x_i	$(x_i - \bar{x})$	$(x_i - \bar{x})^2$	s
OA- ZB	9.29	-0.12	0.0144	-
	9.42	0.01	0.0001	-
	9.52	0.11	0.0121	-
Σ	28.23	0	0.0266	0.12
	x_i	$(x_i - \bar{x})$	$(x_i - \bar{x})^2$	s
HS- ZB	32.6	-0.6	0.36	-
	32.9	-0.3	0.09	-
	34.1	0.9	0.81	-
Σ	99.6	0	1.26	0.79

7.3.2 Wear property of surface modified zinc borate submicron particles in LP

7.3.2.1 WSD results under Experimental Condition (ii)

Four suspension samples LP, LP+ZB, LP+OA-ZB and LP+HS-ZB with the concentration 1 wt% have been tested by a pin-on-disc tester under Experimental Condition (ii) as shown in Table 7-1. Fig. 7-2 shows the pictures and WSD measurements of wear scars taken by a camera equipped with an optical microscope. As mentioned in chapter 2, the smaller WSD, the better the anti-wear performance of the lubricant. It can be seen that the smallest WSD of 250.06 μm was generated by LP. The samples of 1% ZB + LP demonstrated 325.02 μm , a nearly 50% increase of WSD compared to LP. Samples of 1% HS-ZB + LP and 1% LP+OA-ZB have shown similar results which are 281.08 μm and 297.88 μm respectively. Although the wear

scar lubricated by 1% HS-ZB + LP has a WSD value that is 13% smaller than the WSD value of 1% ZB + LP, however, compared with solely LP, the adding of surface modified ZB in LP results in a worse anti-wear property. As shown in Fig. 7-2, no evidence on formation of tenacious tribo-films can be found among the surfaces of four wear scars. Therefore, it is suggested that under the Experimental Condition (ii), when the concentration was increased to 1 wt%, both OA and HS modified zinc borate submicron particles failed to archive any improvement on anti-wear performance in LP.

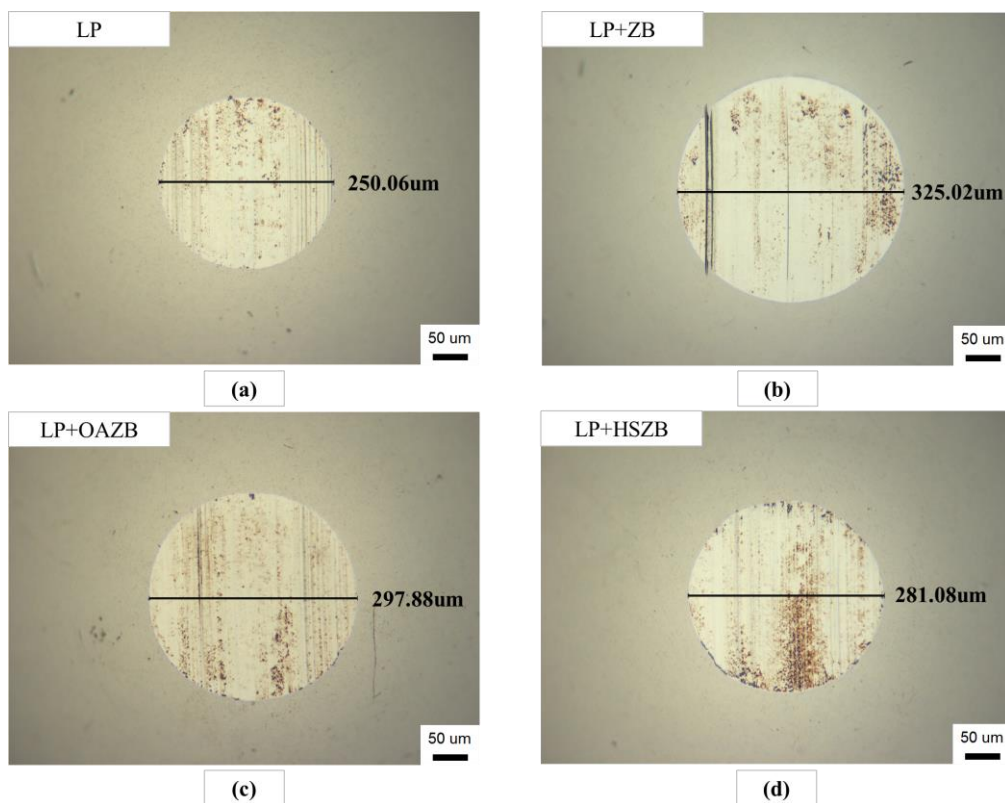


Figure 7-2 Images of wear scars taken by optical microscope and WSD measurements of, (a) LP; (b) 1% ZB +LP; (c) 1% OA-ZB + LP; (d) 1% HS-ZB + LP.

7.3.2.2 WSD results under Experimental Condition (iii)

Four suspension samples, LP, LP+ZB, LP+OA-ZB and LP+HS-ZB with the concentration 0.5wt%, have been tested by a pin-on-disc tester under Experimental Condition (iii) listed in Table 7-1. The loading applied on the pin of the tester was 30 N. Fig. 7-3 (a) shows that the value of wear scar from the LP lubricated pin ball is 336.63 μm . A close but bigger WSD of 377.36 μm was demonstrated by the sample of 0.5 wt% ZB + LP. It appears that surface modified ZB did not contribute any improvements on anti-wear performance of LP, the WSD values of 0.5% OA-ZB + LP and 0.5% HS-ZB + LP are 353.51 μm and 351.22 μm respectively. There also is no trace of the formation of tenacious tribo-films. The failure of generating a strong tribo-film could be the main reason of the poor anti-wear performance of modified zinc borate submicron particles.

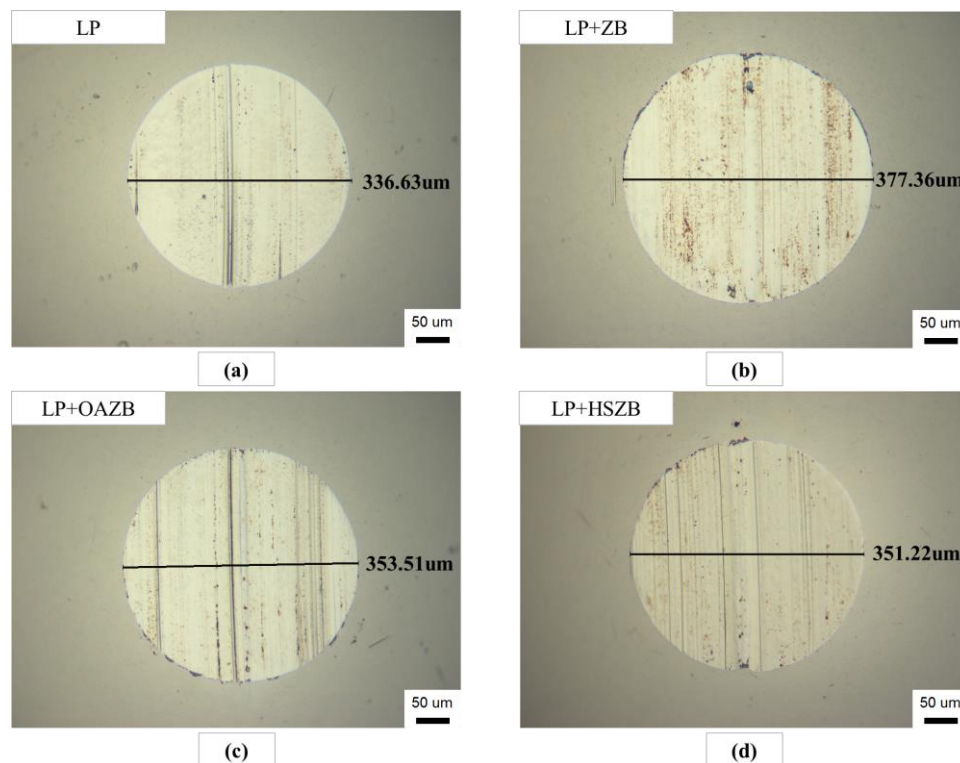


Figure 7-3 Images of wear scars taken by optical microscope and WSD measurements of, (a) LP; (b) 0.5% ZB + LP; (c) 0.5% OA-ZB + LP; (d) 0.5% HS-ZB + LP.

7.3.3 Coefficient of friction

7.3.3.1 Coefficient of friction under Experimental Condition (ii)

Fig. 7-4 illustrated the coefficient of friction versus time curves of four lubricant samples under Experimental Condition (ii).

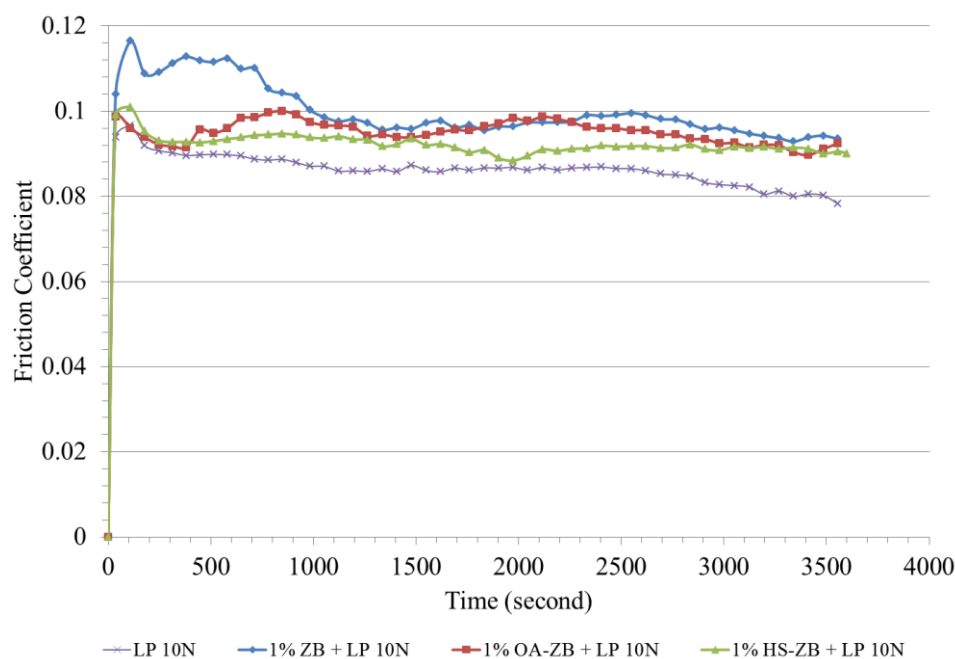


Figure 7-4 Coefficient of friction versus time curves of 1% HS-ZB + LP, 1% OA-ZB + LP, 1% ZB + LP and LP recorded during pin-on-disc test under Experimental Condition (ii).

As showed in Fig. 7-4, sample LP delivered the lowest values of coefficients of friction among all samples. The coefficients of friction of LP maintained at 0.09 through the most test period and gradually down below to 0.08 at 3600s. The sample of HS-ZB demonstrated better friction reducing ability than samples of OA-ZB and ZB and the overall coefficient of friction is approximately 0.094. Unmodified ZB derived the highest reading of coefficient of friction 0.116 during first 900 s and the trend of its curve was similar as the curve of OA-ZB which fluctuated between 0.095 and 0.1.

7.3.3.2 Coefficient of friction under Experimental Condition (iii)

Fig. 7-5 showed the coefficient of friction versus time curves of different lubricant samples under Experimental Condition (iii). It can be seen that the sample of HS-ZB displayed the best results this time compared with other samples and the overall coefficient of friction is approximately 0.09. The values of coefficients of friction of OA-ZB were stable at 0.1 in the first 2800 s and then decreased to 0.092. The coefficient of friction of LP started to drop at 450 s, and then was maintained at 0.1. The sample of ZB+LP failed to perform better than pure LP sample and the overall coefficient of friction is 0.112.

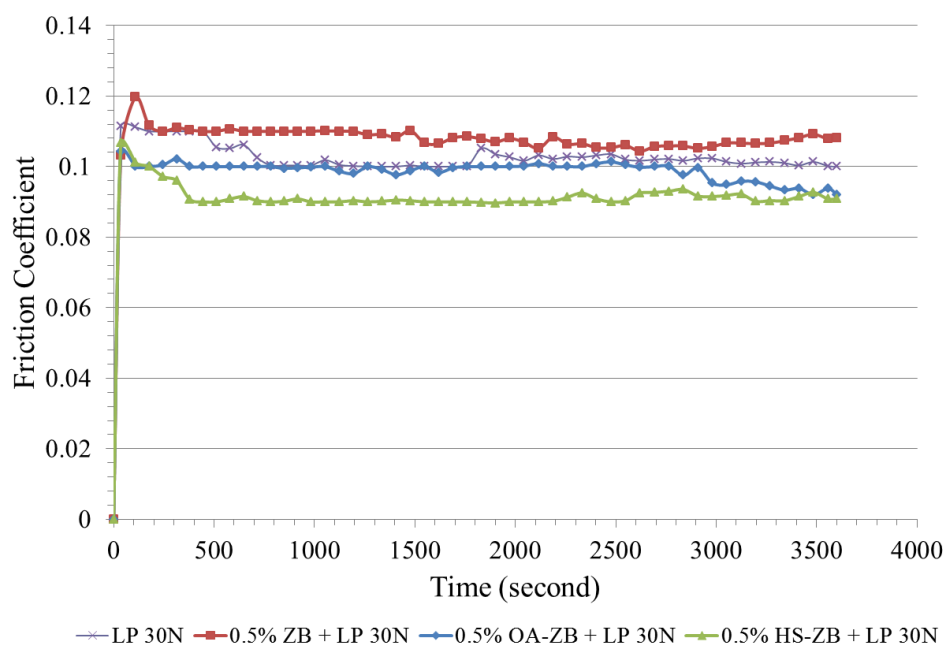


Figure 7-5 Coefficient of friction versus time curves of 0.5% HS-ZB + LP, 0.5% OA-ZB + LP, 0.5% ZB + LP and LP recorded during pin-on-disc test under Experimental Condition (iii).

7.4 Summary

Results indicated that using OA and HS as surface modification agents could improve dispersibility of ZB and reduce ZB's conglomerate size. HS performed better than OA

as a surface modification agent. Under Experimental Condition (ii), HS-ZB and OA-ZB fail to deliver notable improvement on anti-wear and friction reducing performance in LP. Under Experimental Condition (iii), HS-ZB has the best friction reducing ability among all samples; however, no enhancement on anti-wear properties of LP could be found when HS-ZB and OA-ZB were added. ZB, HS-ZB and OA-ZB as solid lubricant additives, fail to show great potential under various testing conditions when it combined with in LP. The summary of results is listed as follows:

- Oleic acid (OA) and hexadecyltrimethoxysilane (HS) modified zinc borate submicron particles (ZB) have been synthesised successfully.
- Surface modification on ZB improves the dispersibility of ZB in organic solvent. HS modified ZB demonstrated best zeta potential results and the smallest conglomerate size.
- Under Experimental Conditions (ii) and (iii), OA-ZB and HS-ZB did not deliver satisfied performance on anti-wear and friction reduction in LP compared to published results which were obtained under Experimental Condition (i).
- HS demonstrates outstanding performance as a surface modification agent. Under various working conditions, HS-ZB demonstrated the best anti-wear performance and dispersibility compared with OA-ZB and ZB. HS has great potential to improve performance of particle lubricant additives.

Chapter 8 Effects of Surface Modified Lanthanum Fluoride Nanoparticles in Liquid Paraffin

8.1 Introduction

The results gained from chapters 6 and 7 proved that even under variety of experimental conditions, HS surface modifier played a vital role in improving the oil solubility and tribological performance of solid lubricant additive particles in LP. In order to investigate the properties of HS, especially to learn the behaviour when HS is adapted with other rare earth nanoparticles, HS modified LaF₃ nanoparticles were synthesised and tested with similar procedure of the tests that presented in section 5.4, chapter 5.

This chapter includes three following sections: experimental preparations, test results and a brief summary of results. The experimental conditions and details of procedure will be introduced in the section of preparation of experiments. A preliminary analysis of results will be included into the test result section. Further discussion will be presented in chapter 9. With the pin-on-disc results, the pre-test sample characterisation and post-test analyse of worn surfaces were also included in the test result section.

8.2 Experimental preparations

8.2.1 Sample characterisation

The conglomerate size and zeta-potential measurements of all lubricant samples were obtained by using Dynamic Light Scattering (DLS) (Malvern Zetasizer Nano ZS). The photos of suspension samples were recorded by a camera.

8.2.2 Pin-on-disc testing

The tribological properties of all lubricant samples were evaluated using the POD 2 Pin-on-disc tester as shown in Fig. 5-7. The lab had constant humidity and temperature which was 45% and 22 °C respectively. All parameters were decided on the purpose for a comparison. The sliding speed of the disc is 50 mm/s and every single test lasts for 60 minutes. Loadings and detailed experimental conditions are shown in Table 8-1. The lubricants prepared in this study are presented in Table 8-2 in which the sample code and the associated fluids are defined. All samples will be denoted by sample code in this chapter.

Table 8-1 Experimental conditions of pin-on-disc test.

Setting	Load	Sliding speed	Testing period	Additive concentration	Ambient Temperature	Ambient Humidity
i	10N	50mm/s	3600s	1%, 2%, 3%	22 ⁰ C	45%
ii	30N	50mm/s	3600s	1%	22 ⁰ C	45%

Table 8-2 Different formulations with pure LP as controlled fluid.

Sample code	Constituent
LP	Liquid paraffin
LP + HS	Liquid paraffin with 0.1 wt% hexadecyltrimethoxysilane
1% LaF ₃ + LP	Liquid paraffin with 1 wt% original LaF ₃ nanoparticles
2% LaF ₃ + LP	Liquid paraffin with 2 wt% original LaF ₃ nanoparticles
3% LaF ₃ + LP	Liquid paraffin with 3 wt% original LaF ₃ nanoparticles
1% HS-LaF ₃ + LP	Liquid paraffin with 1 wt% HS modified LaF ₃ nanoparticles
2% HS-LaF ₃ + LP	Liquid paraffin with 2 wt% HS modified LaF ₃ nanoparticles
3% HS-LaF ₃ + LP	Liquid paraffin with 3 wt% HS modified LaF ₃ nanoparticles

8.3 Results and discussions

8.3.1 Dispersibility and stability

8.3.1.1 Conglomerate size and zeta-potential results

According to the specification and instruction of the zeta-potential measurer, on the purpose to obtain the most accurate results, a recommended concentration of 0.05 wt% of unmodified and HS modified LaF₃ nanoparticles was dispersed into methanol respectively for tests. Before the tests, all mixtures of fluids were sheared by an

ultrasonic homogeniser (KINEMATICA PT 10-35 GT) for five minutes. The readings from zeta-potentials tester are displayed in Table 8-3.

Table 8-3 Conglomerate size and Zeta-potential of CeO₂ nanoparticles dispersed in methanol with a concentration of 0.05%.

	Lanthanum fluoride nanoparticles	
	Unmodified	HS modified
Conglomerate size (in methanol)	1145 nm	583 nm
Zeta-potential	5.2 mV	41.2mV

As shown in Table 8-3, the unmodified LaF₃ nanoparticles in methanol have an average conglomerate size of 1145 nm. HS modified LaF₃ nanoparticles have demonstrated relatively smaller reading of 583 nm and a nearly 50% reduction was achieved. The zeta-potential readings indicate that the HS modified LaF₃ nanoparticles have better dispersibility in an organic solvent, compared with the unmodified nanoparticles. Similar to results from chapters 6 and 7, HS shows strong ability to improve particles' dispersibility in organic solvents when it is used as a surface modifier. It is observed that dispersibility of LaF₃ nanoparticles in organic solvents was promoted significantly by the surface modification.

The standard deviations of conglomerate size results and Zeta-potential measurements are calculated based on the equation that is mentioned in section 6.3.2. The calculation results are listed in table 8-4 and Table 8-5 respectively.

Table 8-4 The standard deviations of conglomerate size results of lanthanum fluoride nanoparticles dispersed in methanol. (Unit:nm)

	x_i	$(x_i - \bar{x})$	$(x_i - \bar{x})^2$	s
Original	1144	-1	1	-
	1139	-6	36	-
	1152	7	49	-
Σ	3435	0	86	6.56
	x_i	$(x_i - \bar{x})$	$(x_i - \bar{x})^2$	s
HS-ZB	588	5	25	-
	580	-3	9	-
	581	-2	4	-
Σ	1749	0	38	4.36

Table 8-5 The standard deviations of Zeta-potential results of lanthanum fluoride nanoparticles dispersed in methanol. (Unit:mV)

	x_i	$(x_i - \bar{x})$	$(x_i - \bar{x})^2$	s
Original	5.4	0.2	0.04	-
	5.6	0.4	0.16	-
	4.6	-0.6	0.36	-
Σ	15.6	0	0.56	0.53
	x_i	$(x_i - \bar{x})$	$(x_i - \bar{x})^2$	s
HS-LaF₃	40.6	-0.6	0.36	-
	41.9	0.7	0.49	-
	41.1	-0.1	0.01	-
Σ	123.6	0	0.86	0.66

8.3.1.2 Status of the sedimentation

Fig. 8-1 demonstrates the status of the sedimentation of LaF₃ + LP and HS - LaF₃ + LP in different periods after a preparation.

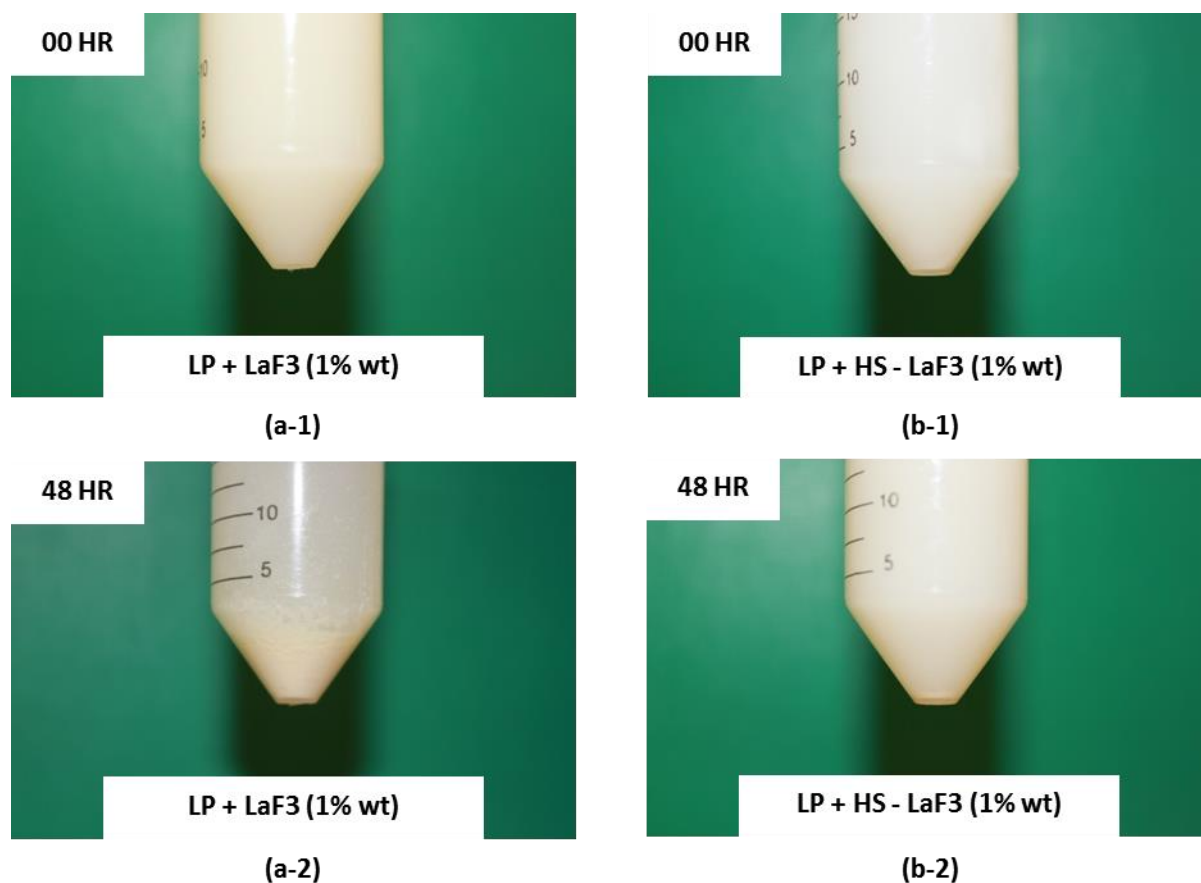


Figure 8-1 Status of the sedimentation of the lubricant samples at the different periods after the sample preparation: at 00 hour: (a-1) LP + LaF₃ (1% wt), (b-1) LP + HS-LaF₃ (1% wt), and at the 48th hour: (a-2) LP + LaF₃ (1% wt), (b-2) LP + HS- LaF₃ (1% wt).

Fig. 8-1 (a-1) and Fig. 8-1 (b-1) present the colour and transparency of both samples at $t=00$ hour. The sample of LaF₃ + LP shown in Figs. 8-1 (a-1) appears slightly darker and yellower, compared with the sample HS - LaF₃ + LP shown in Figs. 8-1 (b-1). No sedimentations are found in Figs. 8-1 (a-1) and (b-1) at $t=00$ hour and this indicates that the nanoparticles have been well dispersed into LP. At $t=48^{\text{th}}$ hour, as showed in Fig. 8-1 (a-2), the upper half of the suspension is relatively more transparent than the bottom half and the depositions are clearly visible at the bottom of the container. The sedimentation with remarkable size can be observed. There is a clear boundary between the sedimentation and suspension. Fig. 8-1 (b-2), by contrast, shows much smaller sedimentation size and also the sample colour is more uniform.

No clear boundary between sedimentation and suspension can be observed. However, the difference between Fig. 8-1 (a-1) and Fig. 8-1 (a-2) is significant. Large sized sedimentations happened in 48 hours after the preparation and the unmodified LaF₃ nanoparticles do not have a good stability in LP. Compared with Fig. 8-1 (b-1), the sample in Fig. 8-1 (b-2) has slightly yellower and darker colour. However, there is no obvious sedimentation formed. It is suggested that HS - LaF₃ nanoparticles can slow down the formation of sedimentation once it has been well dispersed into LP.

Based upon the aforementioned observations, it is logical to suggest that HS can improve both dispersibility and stability of LaF₃ nanoparticles significantly in LP. The sample of HS - LaF₃ + LP has the most stable colloidal system.

8.3.2 Results of tribological tests

8.3.2.1 Tribological properties of LP with HS-LaF₃ nanoparticles (Load=10 N)

8.3.2.1.1 Anti-wear properties

HS-LaF₃+LP samples with three different concentrations were tested by the pin-on-disc test rig with a loading 10 N. Wear scars of the pins (bearing balls) used in pin-on-disc tests were firstly assessed using an optical microscope. The wear scar diameter (WSD) and surface morphology of the tested pins are shown from Fig. 8-2 to Fig. 8-6. As mentioned in chapter 2, the measurements of WSD of the pin can reflect the volume loss of material since the volume that worn off from the pin can be calculated with WSD values. In this case, a smaller WSD means that less material has been worn off from the pin ball during a test, therefore, means a better anti-wear property of the lubricant. The results indicate that HS-LaF₃ in LP demonstrated greater anti-wear

performance compared with a mixture of LP and unmodified LaF_3 . The anti-wear ability of LP can be improved significantly by adding HS- LaF_3 nanoparticles into LP.

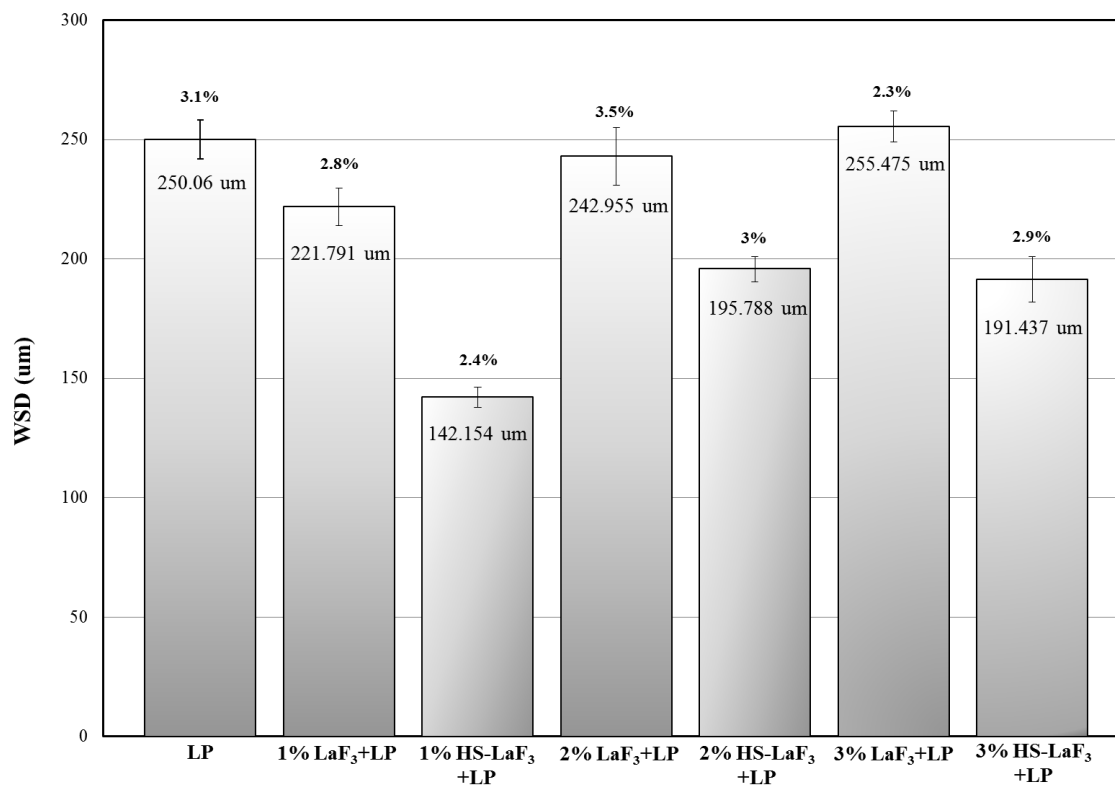
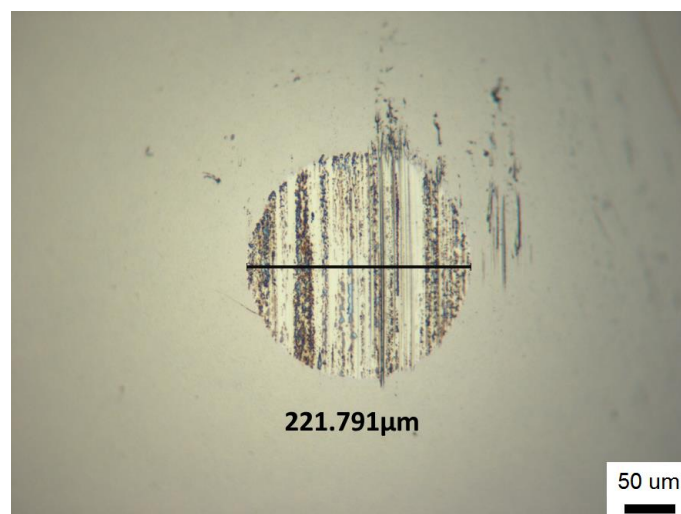


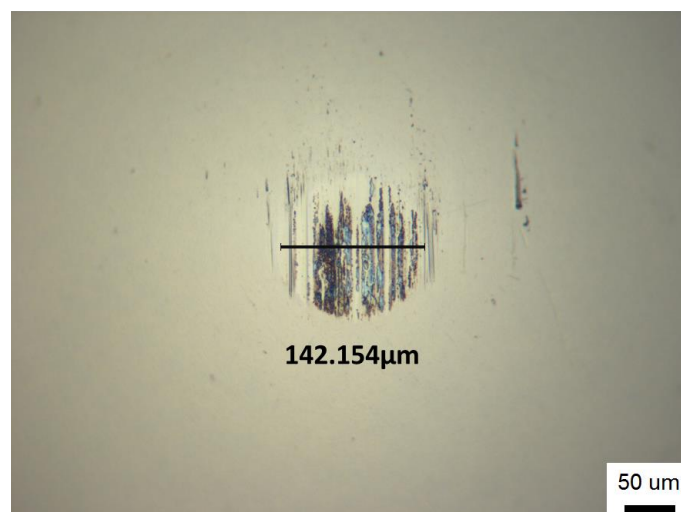
Figure 8-2 WSD values obtained after pin-on-disc tests with an applied loading of 10 N.

Fig. 8-2 demonstrates the WSD values of all samples tested. It can be seen that the WSD value is 250.06 μm when pure LP was used. WSD decreased significantly when the HS modified LaF_3 nanoparticles were applied. The smallest WSD of 142.154 μm was generated when 1% HS- LaF_3 + LP was tested. The WSD value stayed at around 190 μm as the concentration of HS- LaF_3 nanoparticles was increased. WSD values of 2% HS- LaF_3 + LP and 3% HS- LaF_3 + LP were 195.788 μm and 191.437 μm respectively. Among all samples which with unmodified LaF_3 nanoparticles, both 1% LaF_3 + LP and 2% LaF_3 + LP contributed to a reduction of WSD values, compared with the WSD value of the pin ball lubricated by LP alone. The WSD values rose

gradually with an increase of concentrations of unmodified LaF_3 nanoparticles. The largest WSD value of $255.475 \mu\text{m}$ was observed by using 3% $\text{LaF}_3 + \text{LP}$.



(a) 1% $\text{LaF}_3 + \text{LP}$

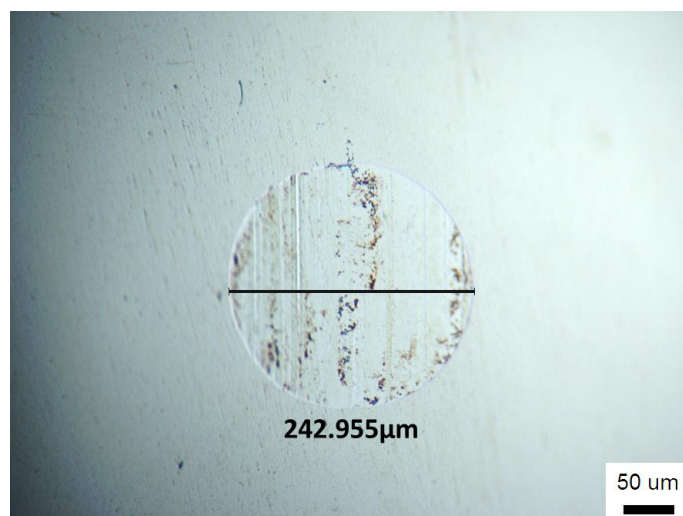


(b) 1% HS- $\text{LaF}_3 + \text{LP}$

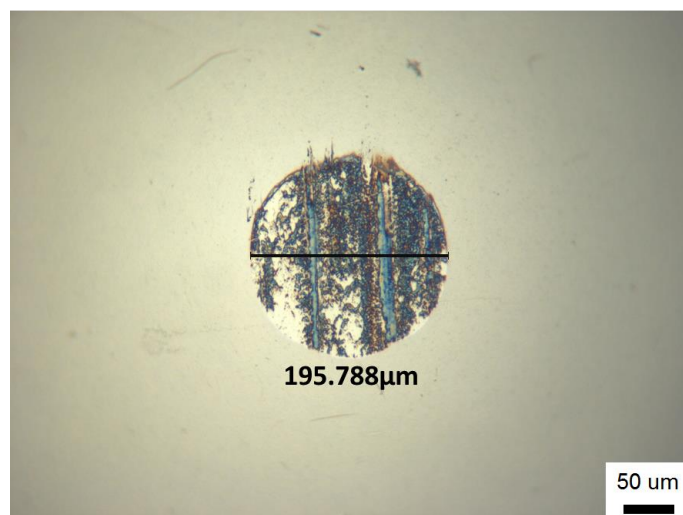
Figure 8-3 Optical micrographs of wear scars (pin balls) with WSD measurements.

As shown in Fig. 8-3, compared with 1% $\text{LaF}_3 + \text{LP}$, a reduction over 35% of WSD has been achieved when 1% HS- $\text{LaF}_3 + \text{LP}$ was tested. The reduction rises to 44% compared with the results of pure LP shown in Fig. 8-2. In Fig. 8-3 (a) and Fig. 8-3 (b), tribo-films can be observed on the contact area of worn surfaces. However, the pattern of tribo-films in Fig. 8-3 (a) was fragmented. It can be seen in Fig. 8-3 (b)

that relatively more complete and widespread tribo-films were formed when 1% HS-LaF₃ + LP had been used.



(a) 2% LaF₃ + LP

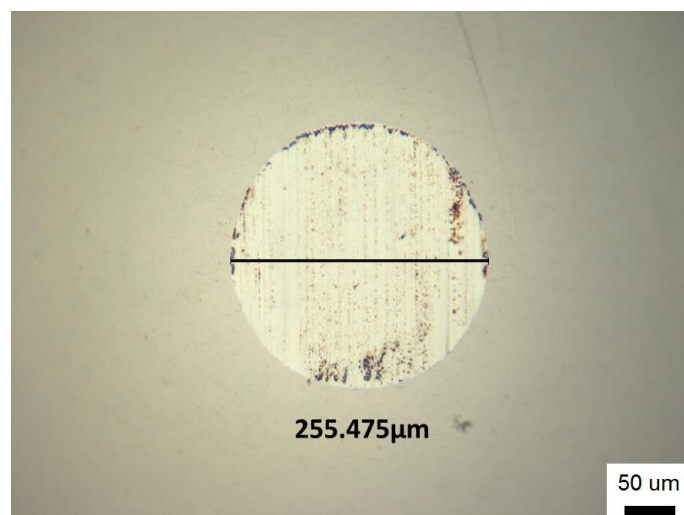


(b) 2% HS-LaF₃ + LP

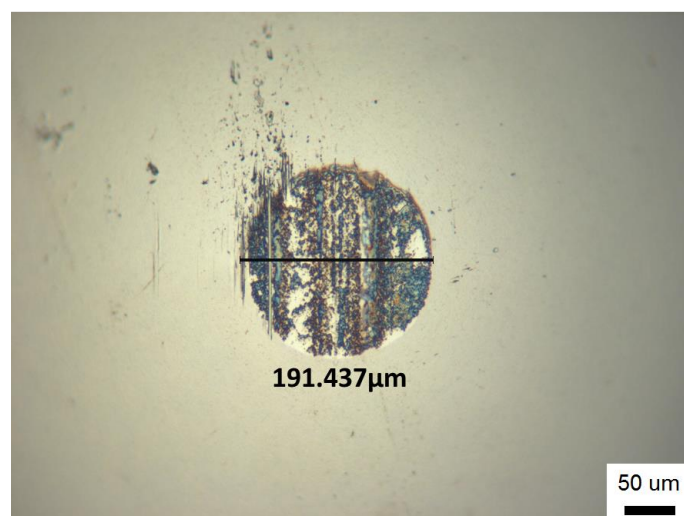
Figure 8-4 Optical micrographs of wear scars (pin balls) with WSD measurements.

Fig. 8-4 shows the images of post-test worn surfaces of the pin balls which were lubricated with 2% LaF₃+ LP and 2% HS-LaF₃ + LP. As can be seen, the WSD value was 242.955 µm when 2% LaF₃ + LP was applied, similar to the result when LP was used. Also there is no solid evidence of formation of tribo-films on the top of the worn surface. In contrast, Fig. 8-4 (b) illustrates that the tribo-films covered wear scar

which was generated by 2% HS-LaF₃ + LP. A reduction on WSD nearly 19.5% is achieved compared with 2% LaF₃ + LP and the reduction is approximately 22% compared with LP.



(a) 3% LaF₃ + LP



(b) 3% HS-LaF₃ + LP

Figure 8-5 Optical micrographs of wear scars (pin balls) with WSD measurements.

As increasing the concentration of LaF₃/HS-LaF₃ nanoparticles in LP, there is no sign of further decrease on WSD measurements. Compared with Fig. 8-4, similar outcomes can be obtained in Fig. 8-5. The highest WSD value of 255.475 µm occurred when 3% LaF₃ + LP was employed. The formation of a relatively stronger

tribo-film happened after applying HS-LaF₃ nanoparticles. It can be seen that the WSD generated by 3% HS-LaF₃ + LP is approximately 25% smaller than the results of 3% LaF₃ + LP and pure LP. However, based upon the above results, the largest improvement on anti-wear properties of LP occurred when 1% wt HS-LaF₃ was applied. It is suggested that the optimum concentration of HS-LaF₃ is 1% wt.

8.3.2.1.2 Generation and transition of tribo-films

Fig. 8-6 shows changes of the wear scar on the pin ball that was lubricated by the sample of 1% HS-LaF₃ + LP. The images have been taken at a different period during the test with 1% HS-LaF₃ + LP.

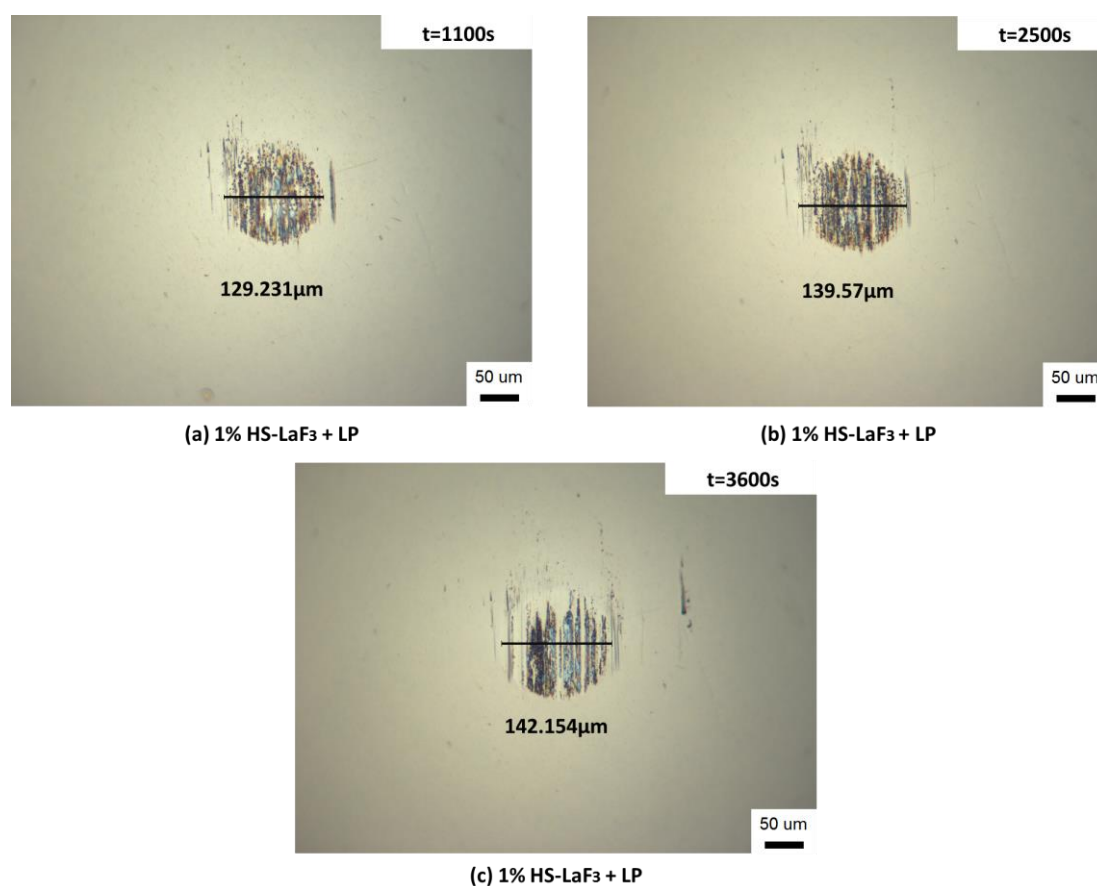


Figure 8-6 Optical microscope images and WSD measurements of wear scars on the pin-ball lubricated by 1% HS-LaF₃ + LP, taken at different period during the pin-on-disc test, (a) 1100s after test started; (b) 2500s after test started; (c) 3600s after test started.

It was observed in Fig. 8-6 (a) that at 1100 s after the beginning of test, most area of the wear scar was covered by tribo-films. Many large tribo-film pieces were distributed in the central area of the wear scar. As the test was continued, it can be found in Fig. 8-6 (b) that the tribo-films were fragmented into smaller pieces and even worn off from some areas. At the end of test, as shown in Fig. 8-6 (c), the area covered by the tribo-films was much less compared with that in Fig. 8-6 (a). However, the WSD was only increased 13 μm after 2500 seconds. Based upon Fig. 8-6, it is suggested that tribo-films generated by HS-LaF₃ have a self-replenishing capability. The self-replenishing tribo-films could protect mating surfaces from a direct contact and reduce wear.

8.3.2.1.3 Coefficient of friction

Coefficient of friction is one of the major parameters to evaluate the friction reduction property of lubricants. Coefficients of friction that generated by using 1% HS-LaF₃ + LP, 1% LaF₃ + LP and LP are showed in Fig. 8-7. These results were obtained from pin-on-disc tests which were conducted with a normal load of 10 N.

As illustrated in Fig. 8-7, in the first 650 s, coefficients of friction results when LP was used were the lowest compared with those of the rest two samples shown in Fig. 8-7. At approximately 650 s, the coefficients of friction of 1% HS-LaF₃ + LP and 1% LaF₃ + LP dropped from 0.1 to 0.09. From 650 s to 1500 s, same trends of declines occurred on the curves of all three samples. After 1500 s, the curve of 1% HS-LaF₃ + LP started to show a sharper fall in coefficients of friction compared with other two curves. The coefficient of friction finally was reduced to 0.073. During the same period, the coefficient of friction of LP and 1% LaF₃ + LP was fluctuated in between 0.08 to 0.09. In overall, 1% HS-LaF₃ + LP demonstrated superior friction reduction

ability to LP and 1% LaF₃ + LP. The results indicate that HS-LaF₃ nanoparticles could improve the friction reduction properties of LP effectively.

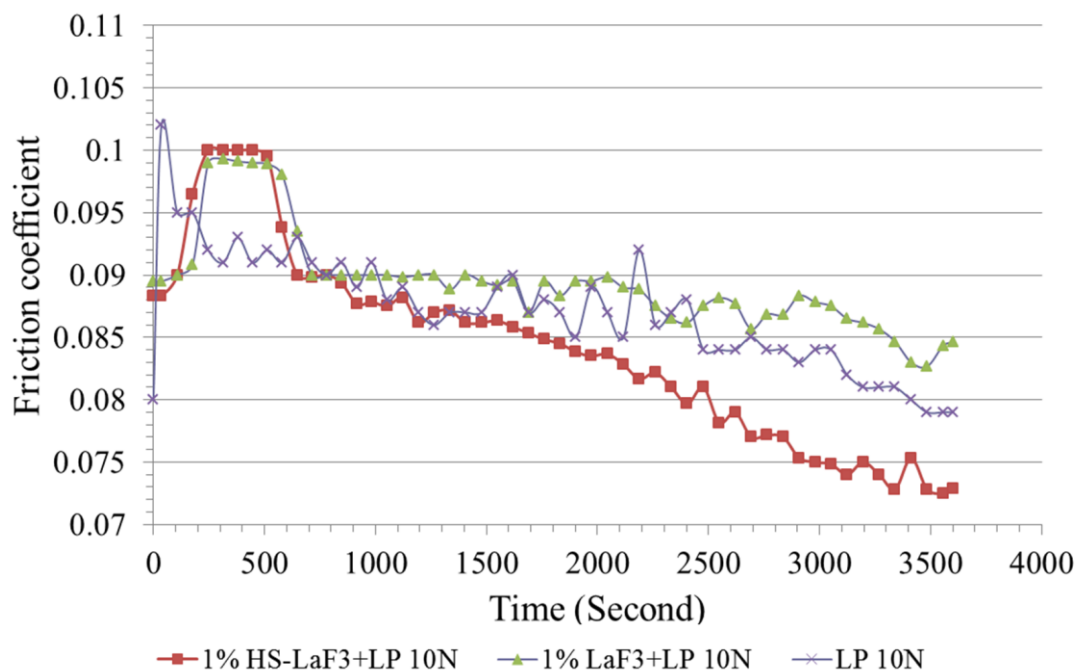


Figure 8-7 Coefficient of friction versus time curves of 1% HS-LaF₃ + LP, 1% LaF₃ + LP and LP recorded during pin-on-disc tests.

It can be seen in Fig.8-7 that all curves are of similar trends. The friction coefficients went up at the first stage of the tests and then maintained at a level for a while before they start to drop gradually until the ends. The fluctuation of the coefficients of friction at the beginning of the tests could be explained as the running-in of metal surfaces. At the start of the contact, the oxidation layer on the top of the surfaces have not been penetrated, the relatively higher hardness of the oxidation layers gives coefficients of friction a dramatic jump up. As the sliding continues, the oxidation layers are penetrated and the beneath softer layers are exposed. Therefore, the coefficients of friction start to decrease. As shown in Fig. 8.7, when the LaF₃ and HS-LaF₃ are tested, the fluctuation appeared later and takes longer time compared to the results of LP. The better lubricity of 1% HS-LaF₃ + LP and 1% LaF₃ + LP slowed

down the process of the oxidation layers been worn off. This is evidence that LaF_3 and HS- LaF_3 increased the anti-wear ability of the LP.

Based upon the above results, unmodified LaF_3 nanoparticles can improve the anti-wear property of LP when the concentration is below 3%. However, the improvement is small and highly limited. The possible reason is that the intrinsic poor dispersibility of LaF_3 nanoparticles has stunted the chance of LaF_3 nanoparticles to access the contact surfaces. The unmodified LaF_3 nanoparticles were accumulated to bigger groups and failed to reach the contact surfaces. A shortage of LaF_3 nanoparticles on the contacting surfaces leads to the lack of material for tribo-films formation. The intermittent process of tribo-films formation cannot provide enough protection to the surface of pin ball. When the concentration of unmodified LaF_3 reaches to the certain level, the conglomerated LaF_3 might play a role as abrasive particles that accelerate the wear loss on mating surfaces. This might be the reason in some case that the applying of unmodified LaF_3 even result in a bigger WSD value than using solely LP.

Compared with the unmodified LaF_3 nanoparticles, HS- LaF_3 nanoparticles can improve the anti-wear properties of LP significantly. Tribo-films could be found on top of the worn surfaces which were lubricated by HS- LaF_3 combined with LP. It is suggested that the superior dispersibility and stability of HS modified LaF_3 in LP is the key factor of forming healthy self-replenishing tribo-films on the contact surface. These self-replenishing tribo-films could protect the rubbing surfaces from wear effectively. In addition, reduce material loss of working component. The using of 1% HS- LaF_3 + LP contributes to the generation of the smallest WSD among all samples. Compared with results of LP, 1% HS- LaF_3 + LP lubricated worn scar has a 44% smaller WSD and it is 35% smaller than the WSD generated by using 1% LaF_3 + LP.

As shown in Fig. 8-2, Fig. 8-4 and Fig. 8-5, 2% HS-LaF₃ + LP and 3% HS-LaF₃ + LP can also improve the anti-wear ability of LP. However, an increase of concentration did not trigger further growing on the ratio of WSD reduction. For all samples tested, it can be found that the optimum concentration of adding HS-LaF₃ nanoparticles is 1% wt.

HS-LaF₃ nanoparticles also showed their excellent ability to improve friction reduction properties of LP. According to Fig. 8-7, the coefficient of friction of lubricant with HS-LaF₃ nanoparticles starts to decrease after 1000 s since it takes time to form tribo-films. Once the films were generated, they are able to separate the mating surfaces and also to fill the ploughings on the contact area, therefore, reduce the friction force.

8.3.2.2 Tribological properties of HS-LaF₃ (Load=30 N)

8.3.2.2.1 Anti-wear properties

Another group of tests has been conducted in order to study the anti-wear property of HS-LaF₃ under a higher loading. The LP combined with an optimum concentration 1% of HS-LaF₃ nanoparticles was tested. Also, as cross references, LP and 1% LaF₃+LP were also investigated. Fig. 8-8 shows the WSD measurements of tested pins when a load of 30 N was applied. As shown in Fig. 8-8, under the applied load of 30 N, a wear scar with 351.175 μm in diameter was resulted by using 1% LaF₃ + LP, approximately equal to the WSD (359.91 μm) of the pin ball lubricated by LP. As shown in Fig. 8-8 (c), the worn surface lubricated by 1% HS-LaF₃ + LP has the smallest WSD of 208.71 μm, over 40% smaller than the WSD values presented in Fig. 8-8 (a) and Fig. 8-8 (b). The morphology of worn surface in Fig. 8-8 (c) is clearly different from those of the other two. It was difficult to find tribo-films in Figs. 8-8 (a)

and (b). Under the loading of 30 N, it appears that the HS-LaF₃ nanoparticles have demonstrated excellent ability to improve anti-wear property of LP, unmodified LaF₃ failed to contribute a better performance than solely LP and LP with HS-LaF₃ nanoparticles demonstrated great anti-wear property under various experimental conditions.

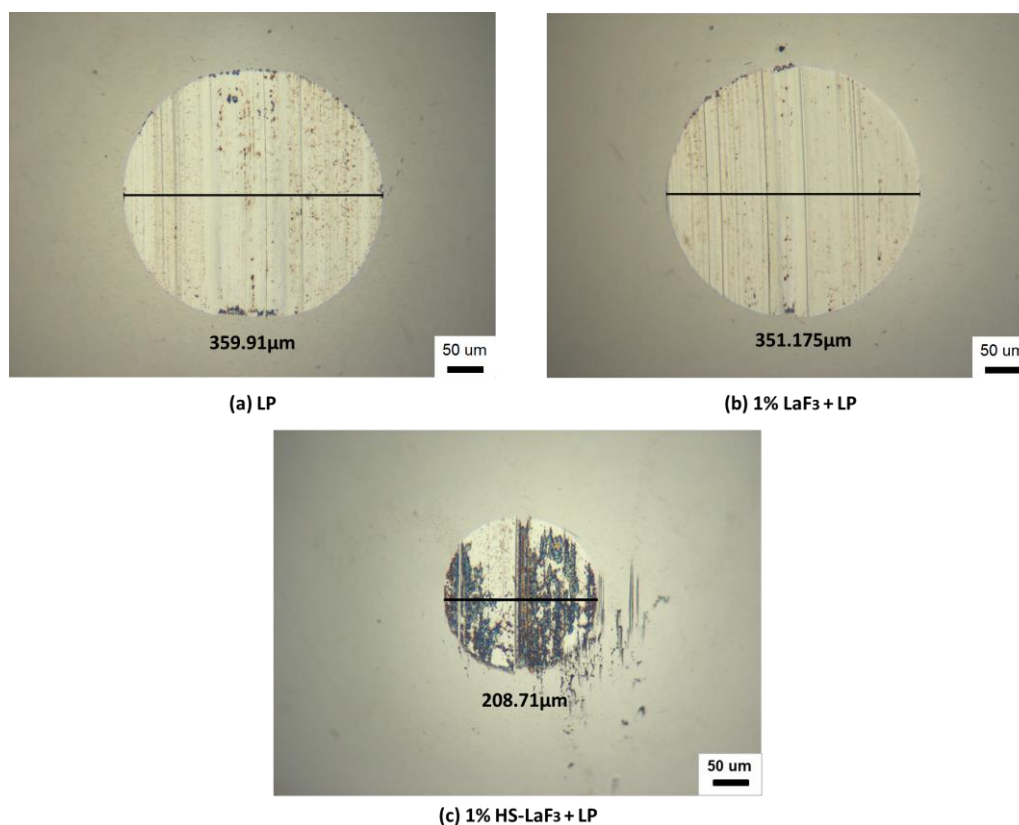


Figure 8-8 Images of wear scars (pin balls) with WSD measurements, taken by optical microscope.

8.3.2.2.2 Coefficient of friction

The coefficients of friction of three different lubricant samples have been obtained and illustrated in Fig. 8-9. As can be seen, the lubricant of 1% LaF₃+LP has the highest coefficient of friction among three samples. The coefficients of friction of 1% LaF₃+LP were approximately 0.115 in the first 2200 s and then slowly increased to 0.12 at the end of the test. After the fluctuation in the first 2000 s, the coefficients of friction of LP were maintained at 0.118 in the rest period of test. The lowest

coefficient of friction was obtained when 1% HS-LaF₃+LP was tested. The coefficients of friction were below 0.1 in the first 1500 s and were stabilised around 0.116 – 0.118. The results indicate that HS-LaF₃ could improve the friction reducing ability of LP under the loading of 30 N. However, the unmodified LaF₃ nanoparticles failed to show any satisfied reduction of friction coefficient under the same testing condition.

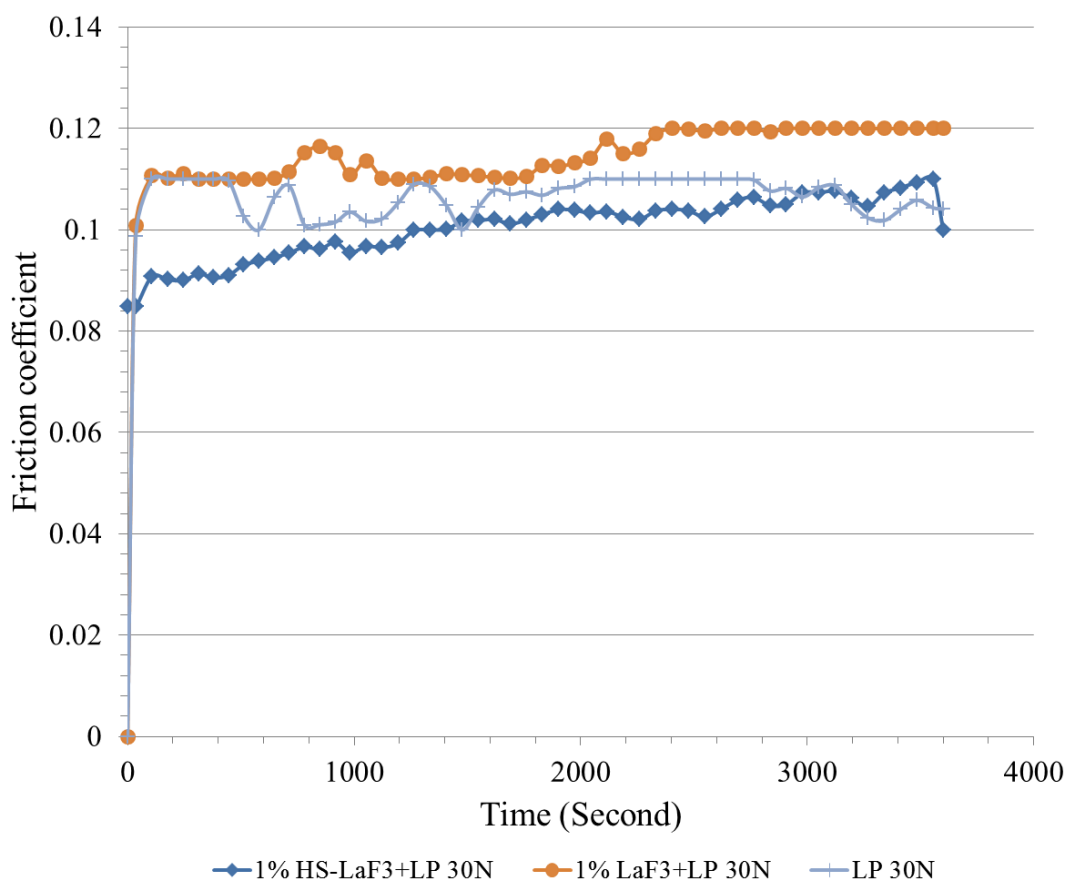


Figure 8-9 Coefficient of friction versus time curves of 1% HS-LaF₃ + LP, 1% LaF₃ + LP and LP recorded during pin-on-disc tests.

When the applied loading was 30 N, the HS-LaF₃ showed remarkable performance in improving tribological properties of LP. The anti-wear ability of LP can be ameliorated significantly by adding HS-LaF₃, at the meanwhile, the friction reduction properties of LP have been improved by adding HS-LaF₃ too. The characterisations and analysis of tribo-films will be presented in next section.

8.3.3 Characterisation of one typical worn surfaces

After the pin-on-disc test, the post-test pin-ball was studied with an AFM and a nano-indentation tester respectively for further examining. Relatively more complete and tenacious tribo-films were observed on top of the worn surface of the pin ball that was lubricated by HS-LaF₃. It was difficult to find healthy tribo-films on the worn surfaces lubricated by solely LP and unmodified LaF₃ in LP. Normally, it takes higher strength for the tribo-film to stay on the worn surface when the applied load was increased. Therefore, in order to investigate the topography and to obtain the hardness of the strongest tribo-film generated by HS-LaF₃ in this study, the worn surface of the pin-ball lubricated by 1% HS-LaF₃ (tested by pin-on-disc with 30 N loading for 3600 s) was selected. Fig. 8-10 shows the optical and AFM images of the worn surface. It can be found that the areas covered by tribo-films demonstrate unique texture and different morphology, and the distribution of tribo-films is random. According to the results obtained by AFM scanning shown in Fig. 8-10 (c), the average thickness of the tribo-film is around 140 nm to 150 nm.

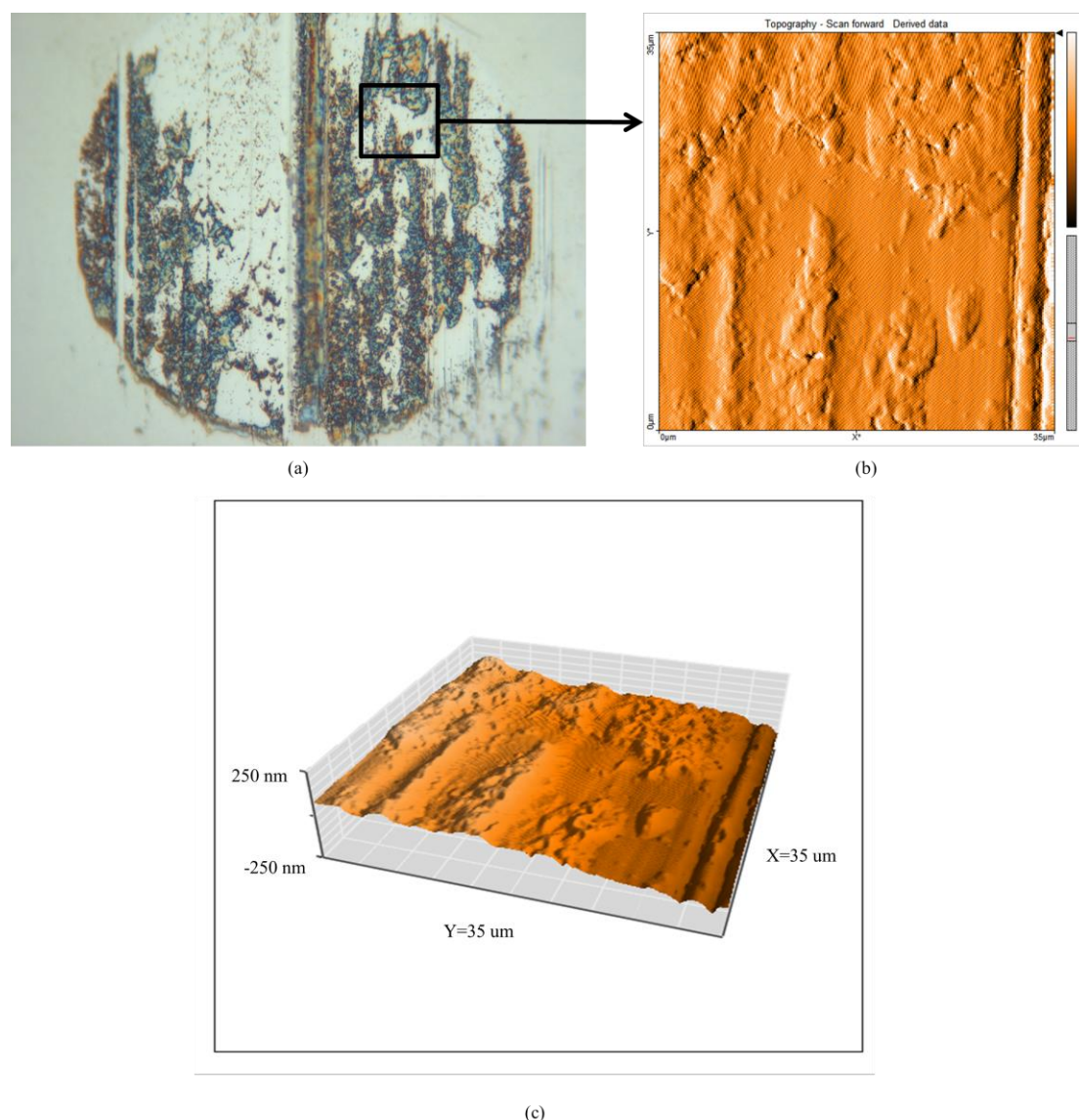


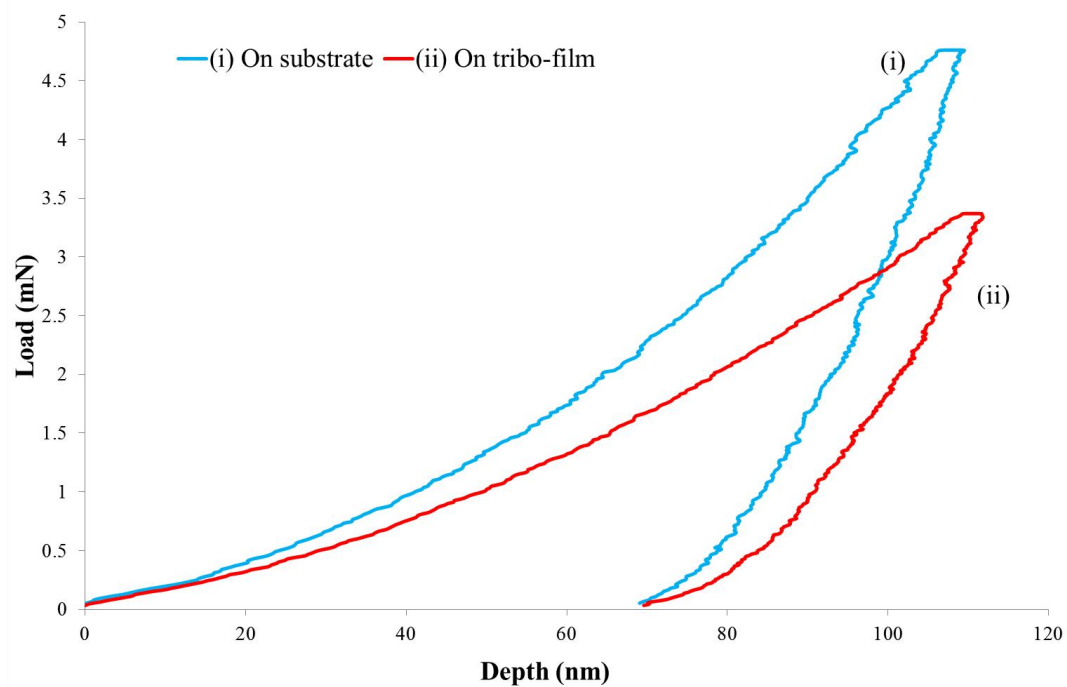
Figure 8-10 The images of worn surface of pin-ball (1% HS-LaF₃, 30 N, 3600s); (a) optical image; (b) AFM topography; (c) AFM 3-D view.

After the thickness of the tribo-film has been measured, nano-indentation tests were conducted on the worn surface. The indent positions have been set on both the tribo-film and substrate to compare their physical properties. Fig. 8-11 illustrated the load versus depth curve obtained during the indentation. Curve (i) is the result of indentation on the substrate, and curve (ii) is the result of indentation on the tribo-film. The hardness of the tribo-film and substrate were calculated from these curves by the system of nano-tester. To prevent any penetration on the tribo-film, the maximum

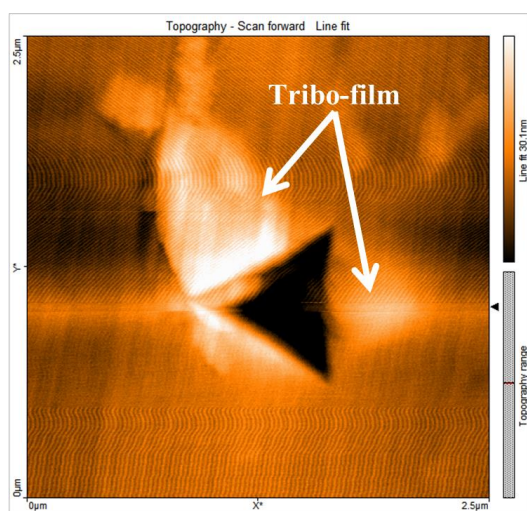
indentation depth of curve (ii) was set to be 110 nm. Figs. 8-11 (b) and (c) are the AFM images of indents left on the worn surface by the Berkovich tip of nano-indentation tester. It is clear that the indent in Fig. 8-11 (b) was surrounded by tribo-film. The value of an indentation force depends on the values of pre-set indentation depth. As shown in Fig. 8-11 (a) it takes 3.35×10^{-3} N to achieve the depth of 110 nm on tribo-film, while 4.82×10^{-3} N was applied to reach the same depth on substrate. Table 8-6 presented the results that were derived from the load versus depth curves in Fig. 8-11 (a). It has been reported that when thin-films are analysed by nano-indentation method, the 'substrate effect' is the main factor that may affect the result accuracy [203-205]. However, R Saha claimed that the substrate effect on film hardness was negligible when softer films were on a harder substrate [195]. The results as shown in Table 8-6 indicate that the tribo-film is much softer than substrate; therefore in this case, the influence of 'substrate effect' can be ignored. In a summary, the tribo-film formed by HS-LaF₃ + LP has an average film thickness of 140 nm and the tribo-film is much softer than the substrate.

Table 8-6 Hardness of tribo-film and substrate obtained by nano-indentation tester.

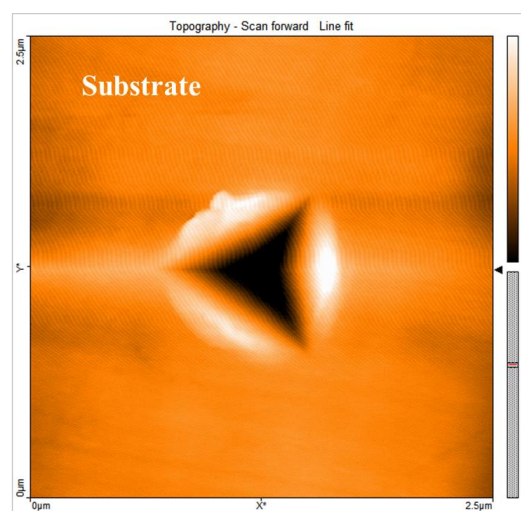
Indentation position	Indentation force	Hardness
Tribo-film	3.35×10^{-3} N	8.9 GPa
Substrate	4.82×10^{-3} N	13.4 GPa



(a)



(b)



(c)

Figure 8-11 (a) Load versus depth curves of tribo-film and substrate; (b) An AFM image of the indent that left by a Berkovich tip of nano-tester on tribo-film; (c) An AFM image of the indent that left by a Berkovich tip of nano-tester on substrate.

8.4 Summary

The results have indicated that HS can improve the dispersebility and stability of LaF₃ nanoparticles greatly in an organic solvent. HS modified LaF₃ nanoparticles have excellent anti-wear and friction reduction ability in LP under various working conditions. When a mixture of 1 wt% HS modified LaF₃ nanoparticles and LP was used as a lubricant, the smallest WSD and lowest coefficient of friction were observed.

The main founds of this chapter have been listed as follows;

- Hexadecyltrimethoxysilane (HS) modified lanthanum fluoride nanoparticles (LaF₃) have been synthesised successfully.
- HS-LaF₃ nanoparticles have superior zeta-potential results and smaller conglomerate size, compared with unmodified LaF₃. The surface modifications of LaF₃ nanoparticles improve the dispersibility and stability of LaF₃ significantly in organic solvent.
- HS-LaF₃ nanoparticles demonstrated excellent anti-wear ability in LP under different experimental conditions. The optimum concentration of 1%wt HS-LaF₃ was obtained.
- When 1% HS-LaF₃+LP tested under a loading of 10 N, The WSD was 44% smaller than that tested with LP and the reduction on WSD was 35%, compared with unmodified LaF₃ tested. When 1% HS-LaF₃+LP tested under a normal force 30 N loading, the reduction on WSD was 40% compared with LP and 1% LaF₃+LP.
- HS-LaF₃ nanoparticles demonstrated great friction reducing performance under different experimental conditions. The smallest overall coefficients of friction were observed when HS-LaF₃ contained with LP was tested.

- HS-LaF₃ nanoparticles can generate self-replenishing tribo-film on top of the sliding surface during contact. The tribo-film separates sliding surfaces and helps to reduce wear and friction as a third body [206]. The tribo-film is softer than the substrate and it has an average film thickness of 140 nm.

Chapter 9 Discussion

9.1 Introduction

Surface modified zinc borate submicron particles, cerium oxide nanoparticles and lanthanum fluoride nanoparticles were synthesised, characterised and tested in this project. The results and brief explanations were presented in chapters 6, 7 and 8. This chapter includes general discussions and further analysis based on results gained from the above chapters. The effects of using surface modifier HS and OA on dispersibility and tribological properties of three different types of particles will be covered. The reduction mechanisms of wear and friction of surface modified particles will be discussed.

9.2 Effects of surface modified cerium oxide nanoparticles in liquid paraffin

As shown in Fig. 6-3, Fig. 6-4 and Fig. 6-7, surface modification of cerium oxide nanoparticles have significant effects on the tribological properties of liquid paraffin. Typically, surface modified CeO₂ nanoparticles have shown much greater dispersibility and anti-wear properties, compared with unmodified CeO₂ nanoparticles. It is observed from the above results that the dispersibility of additive nanoparticles in base oil could play a very important role in the formation of tribo-film. Compared with unmodified CeO₂ nanoparticles, both of OA and HS modified CeO₂ nanoparticles have better dispersibility in LP. Additionally, HS modified CeO₂ nanoparticles have achieved the smallest conglomerate size. It is suggested that HS

modified CeO₂ nanoparticles may have better compatibility with base oil and easier access to a contact interface.

The HS modified CeO₂ nanoparticles with LP have also demonstrated the best anti-wear property. A tenacious and continuous tribo-film on the worn surface of pin ball can be observed when HS surface modified CeO₂ combined with LP is employed. SEM and EDS results have indicated that CeO₂ nanoparticles were most likely not chemically involved in the reaction of tribo-film generation. All results are inclined to attribute the key ingredient for generating a healthy tribo-film to the HS. However, the employment of solely HS in LP failed to demonstrate any contribution to either a reasonable anti-wear performance or the generation of a tenacious tribo-film. Therefore, based on the test results and facts aforementioned, a hypothesis can be proposed that CeO₂ nanoparticles are acted as a role of physical carrier to effectively deliver the HS to contact surfaces. Due to the superior dispersibility compared with unmodified and OA modified CeO₂ nanoparticles, HS modified CeO₂ nanoparticles can access to contact interface easily and be entrapped into it under the influence of shear effect [207]. With a continuously sliding, more and more HS modified CeO₂ nanoparticles can be deposited on the worn surface which may lead to a high localised concentration of CeO₂ nanoparticles on the surface. While the direct metal contact was reduced because of the third body effect of the CeO₂ nanoparticles [207], tribo-chemical reactions also could take place during the sliding process due to the local high pressure concentration and temperature caused by the collision and rupture of the asperities between the mating surfaces [117]. As a result of interactions between chemical components of the lubricant, lubricated surface and debris, a tribo-film was formed.

The results shown in Fig. 6-3, Fig. 6-5 and Fig. 6-7 have indicated that the reduction of wear can be attributed to the formation of an enduring tribo-film. It has been observed that high volume losses of materials occurred with small and patchy tribo-film fragments on the worn surface. Conversely, the low volume losses of material were associated with that more tenacious tribo-films were generated. It is evident that the formation of tribo-film has been influenced by surface modification carried out on CeO₂ nanoparticles. That unmodified CeO₂ nanoparticles failed to improve the anti-wear property of base oil may be due to their poor dispersibility in an organic solvent. Poor dispersibility will lead to the agglomeration in the base lubricant and formation of bulk clusters with many particles. Under the abrasive effect of those clusters, tribo-films may be destructed and worn out quickly. Consequently, the exposed contact surfaces were in contact directly and metal wear will be increased. As a result, the unmodified CeO₂ nanoparticles have demonstrated the highest volume loss of pin ball material.

9.3 Effects of surface modified zinc borate ultrafine particles in liquid paraffin

In general, the dispersibility of zinc borate ultrafine powders (ZB) in an organic solvent can be improved by the surface modification according to the zeta-potential results. However, both OA and HS modified ZB ultrafine particles did not show satisfied tribological performance in liquid paraffin (LP) regardless a variation of particle concentrations and applied loadings.

Compared with the results published in [7], the FT-IR and zeta-potential results that presented in this thesis has no notable difference from the previous work [7, 68]. It can be seen that the particles used and synthesised in this thesis are identical to the

particles that tested in the previous work. In both studies, HS-ZB has demonstrated the strongest dispersibility in the organic solvent.

However, unlike the reported results [7], surface modified zinc borate submicron particles fail to deliver significant improvement on the anti-wear performance of LP neither when the concentration of additives was increased to 1% (Experimental Conditions ii), nor with a higher loading 30 N (Experimental Conditions iii). No evidence of formation of tribo-film has been found on the post-test worn surface.

Table 9-1 lists a comparison of WSD measurements between published results and results presented in this thesis.

Table 9-1 A comparison of WSD measurements between published results and results presented in section 7.3.

	LP	ZB + LP	OA-ZB + LP	HS-ZB + LP
Experimental condition (i)	248.81 μm	373.67 μm	226.61 μm	123.76 μm
Experimental condition (ii)	250.06 μm	325.02 μm	297.88 μm	281.08 μm
Experimental condition (iii)	336.63 μm	377.36 μm	353.51 μm	351.22 μm

As shown in Table 9-1, under experimental condition (ii), OA-ZB+LP and HS-ZB+LP all demonstrated smaller WSD than the ZB+LP. However, samples contained additives have shown bigger WSD values than LP. Compared to results obtained under Experimental Condition (i), anti-wear performance of both OA-ZB + LP and

HS-ZB + LP is poor. As reported, the tribo-chemical reactions between zinc borate particles and environment is the key of tribo-film formation in oil [18]. Increasing of content concentration of additive particles to 1% leads to an accumulation of particles on contact surfaces. The conglomerated particle group might penetrate the tribo-film when the size of particle group is bigger than the thickness of tribo-film[208]. The penetration affects tribo-chemical reactions and stops the self-replenishment of tribo-film. Under this circumstance, the conglomerated zinc borate particles could behave as abrasive particles to accelerate surface wear and also remove any potential tribo-films, therefore, lead to unsatisfied anti-wear performance. The destruction of tribo-film and the abrasion effect encourage the high coefficient of friction at the same time.

Under experimental condition (iii), all WSD results are in a similar level. As contrast of results obtained under Experimental Condition (i), OA-ZB+LP and HS-ZB+LP fail to improve the anti-wear performance of LP. It requires greater adhesive force to maintain the tribo-film on the rubbing surface under a higher applied load, in another word, stronger tribo-chemical reactions is desired. However, higher loading leads to more debris, this changing of environment might cause undesired influence on the tribo-chemical reactions of additive particles that prevent from the formation of tribo-film. The higher contact pressure also creates obstructions on tribo-film formations [206]. Under Experimental Condition (iii), OA-ZB and HS-ZB enhanced the friction reducing ability of LP. Even no signs of tribo-film formation could be found, but the superior dispersibility of OA-ZB and HS-ZB helps additive particles well distributed onto contact surfaces. The uniform distributed surface modified ZB particles could separate the rubbing surfaces, reduce metal to metal contacts and also fill ploughings. As a result, the coefficient of friction was decreased. Surface modification of zinc borate submicron particles could improve their dispersibility in LP. However, results

indicated that OA-ZB and HS-ZB could only contribute excellent tribological performance under certain conditions.

The possible reason of the poor performance of the OA-ZB and HS-ZB under certain experimental conditions is the failure on tribo-film generation. Under the experimental condition ii, the increased concentration of particles may speed the conglomerate process of particle groups. Big particle groups cannot access to the contact surfaces effectively to form tribo-film. Under the experimental condition iii, the increased load leads to a higher local contact pressure on the contact point. When the contact pressure was increased, the tribo-film was easily worn off from the top of the contact surfaces. Once the speed of the tribo-film generation is slower than the speed of material loss, the tribo-film is difficult to remain on the contact surfaces which results in unsatisfied tribological performance.

9.4 Effects of surface modified lanthanum fluoride nanoparticle in liquid paraffin

Based on results from previous chapters, HS has shown its excellent potential as a surface modifier for solid particles. In particular, HS modified LaF_3 nanoparticles (HS- LaF_3) have demonstrated stronger ability to disperse themselves in liquid paraffin (LP) compared with unmodified LaF_3 nanoparticles (LaF_3). The zeta-potential results and status of sedimentation approved that the stability of LaF_3 in LP has been improved significantly due to the surface modification on particles. It is suggested HS could improve dispersibility and stability of LaF_3 nanoparticles in LP.

An effect of HS on tribological properties of LaF_3 in LP has been reflected by pin-on-disc results presented in chapter 8. HS- LaF_3 has improved the tribological properties

of LP greatly under various experimental conditions while unmodified LaF_3 fail to show such improvement. Under Experimental Condition (i) (listed in Table 8-1), as shown in Fig. 8-3, Fig. 8-4 and Fig. 8-5, tribo-films generated by using HS- LaF_3 +LP clearly have covered more areas of the worn scar. Compared with tribo-films that were generated by LaF_3 +LP, using HS- LaF_3 +LP leads to formation of the more tenacious tribo-films. Results presented in Fig. 8-6 indicate that HS- LaF_3 +LP could enforce the self-replenish property of tribo-film. Using HS- LaF_3 +LP also contributes to the lowest coefficient among other samples. Under Experimental Condition (ii) (listed in Table 8-1), HS- LaF_3 have demonstrated greater anti-wear property and friction reducing property than unmodified LaF_3 in LP too. The tribo-film generated by using HS- LaF_3 +LP has been proved that it has much lower hardness than the metal substrate of worn surface.

According to published studies [115], the tribol-chemical reactions triggered by surface modifier are main mechanism of tribo-film formation of surface modified LaF_3 in LP. No evidence has been found to support that LaF_3 is chemically involved to tribo-film generation [115, 175]. Therefore, similar to CeO_2 , LaF_3 more likely played a role as a physical carrier during the formation of tribo-film. The superior dispersibility of HS- LaF_3 in LP leads to high deposition of surface modified LaF_3 nanoparticles on the rubbing surfaces. The deposition of HS- LaF_3 ensures enough integrant of tribo-chemical reactions during contact. As the tribo-chemical reactions continued, a tribo-film that much softer than substrate was formed on top of the worn surface. This tribo-layer reduced metal-to-metal contacts and material loss of the worn surface. Therefore, the wear of metal has been reduced. During the sliding, the well dispersed HS- LaF_3 nanoparticles were much easier to fill into ploughings on the contact surface and carry load as a third body to reduce the friction force. By contrast,

adding unmodified LaF_3 fails to deliver a healthy tribo-film. The possible reason for this is conglomerated unmodified LaF_3 nanoparticle groups could penetrate the tribo-film and interrupt the tribo-chemical reactions once their size exceeds the thickness of tribo-film [1]. The failure of tribo-film formation leads to poor tribological performance.

It is suggest that the surface modification using HS could improve the dispersibility and tribological performance of LaF_3 nanoparticles in LP significantly, even under various working conditions.

9.5 The role of the tribo-film

Results of this study indicate that the formation of the healthy tribo-film which with self-replenish feature has made significant contributions to reducing sliding friction and wear of the tribo-system. The tribo-film played a role as a third body which efficiently separated the tribo-pair. Due to the different physical structure and chemical deposition from the substrate metal surface, the tribo-film could support partially the load. The self-replenish property of the tribo-film protected the metal surface effectively too. However, for the better understanding of the role of the tribo-film, further investigations on the chemical deposition of the tribo-film and the debris would be ideal. This would be included into the future works.

Chapter 10 Conclusions and Suggestions for Future Work

10.1 Introduction

This thesis presented the outcomes of the investigation on effects of surface modification on particle materials. Two surface modification agents (OA, HS) and three different types of particle materials (CeO₂, ZB, and LaF₃) were tested. The effects of surface modification of nanoparticles on their dispersibility and tribological properties were reflected through a series of experimental studies. This chapter is a summary of the findings of this study and a suggestion of work that needs to be focused in future.

10.2 Conclusions

10.2.1 Dispersibility of surface modified particles in an organic solvent

In this study, to improve the dispersibility of particles in an organic solvent is one of the major purposes of surface modification. According to zeta-potential results presented in previous chapters, surface modified particles all have shown higher zeta-potential value and smaller conglomerate size compared to unmodified particles. This indicates that surface modification has improved the dispersibility of particles successfully. Compared with the results of OA modified particles, HS modified particles demonstrate higher zeta-potential values and smaller conglomerate size. The status of sedimentation results has also confirmed that HS modified particles have the best stability in LP among all samples. It is essential that surface modification could

improve the dispersibility of particles in the organic solvent significantly, HS has stronger ability to reduce conglomerate size and to improve the dispersebility and stability of particles in the organic solvent compared with OA.

10.2.2 Effects of surface modified particles on tribological performance of liquid paraffin

10.2.2.1 Anti-wear property

OA-CeO₂+LP and HS-CeO₂+LP both have shown smaller WSD results compared with unmodified CeO₂+LP and solely LP. The smallest WSD was created by adding HS-CeO₂ into LP. Without surface modification, unmodified CeO₂ nanoparticles fail to demonstrate any improvement on anti-wear performance of LP. HS modified LaF₃ have the delivered excellent anti-wear property under different working conditions in LP and the maximum reduction on WSD was 44% compared to that from LP. Tenacious tribo-films were observed on the worn surface when HS-CeO₂ or HS-LaF₃ was used. The formation of tribo-film protects metal surface from the contact and reduces wear. Results have indicated that HS is an essential ingredient for the formation of a health tribo-film. However, under certain experimental conditions, surface modification did not improve the anti-wear property of ZB particles in LP. Both OA-ZB and HS-ZB have failed to show any improvement on anti-wear performance of LP under Experimental Conditions (ii) and (iii) (listed in Table 7-1).

In general, surface modification could improve the anti-wear performance of particles significantly. However, in some cases, the changing of working conditions must be controlled due to the great influence it might cause. Compared to results of OA modified particles, the particles modified by HS have shown superior ability to

improve anti-wear property of LP. HS has delivered a better perform as a surface modifier compared with OA in this study.

10.2.2.2 Coefficient of friction

Surface modified particles have demonstrated lower coefficient of friction compared with unmodified particles and LP under most circumstances of this study. Under Experimental Condition (ii) (Table 7-1), both OA-ZB and HS-ZB have shown higher coefficient of friction than LP. Under the Experimental Condition (iii) (Table 7-1), HS-ZB combined LP resulted in the lowest coefficient of friction while rest results were at same level. The lowest coefficient of friction was also detected when HS-LaF₃ nanoparticles were tested under two different experimental conditions. HS modified particles have shown smaller coefficient of friction results compared with OA modified particles. Surface modification by using OA and HS could improve the friction reduction property of particles under certain working conditions and HS has shown superior ability of improving friction reduction property of particles in LP in a comparison with OA.

10.2.3 Effects of surface modified particles on formation of tribo-film

Tribo-film was observed on the worn surfaces which were lubricated by HS-CeO₂ and HS-LaF₃ contained LP. The results from nano-indentation tester suggest that the hardness of tribo-film is much less than the metal substrate. EDS results indicated that HS encouraged the tribo-chemical reactions on worn surfaces. The observation that presented in chapter 8 has demonstrated the self-replenish property of tribo-film was generated by HS-LaF₃. It can be concluded that surface modification would change

the tribological mechanism of particles in LP. HS is the crucial ingredient of formation a self-replenish tribo-film which is much softer than the metal substrate.

10.3 Suggestions for future work

This thesis presented the outcomes of a systematically investigation of effects of surface modification on properties of particle materials. Two types of surface modifiers and three types of particles have been tested and numerous results were obtained and analysed. However, author believes there is still plenty of work worth to be focused in future. The suggestions are outlined below:

Surface modification

To study the effects of surface modification on dispersebility and tribological properties of particles is the theme of this thesis. However, the influence of surface modification on other material properties of particles is still an open question. The study of tribological performance of HS with particles have different sizes would be another meaningful topic.

Working conditions

It has been found that surface modified particles could behave totally differently under various working conditions. The variation of parameters such as temperature, surface roughness and sliding distance would also influence the performance of lubricant additives. Also it is important to industry to explore the limitation of materials.

Characterisation of tribo-film

The mechanical properties of tribo-films were characterised by SEM, AFM and nano-indentation tester in this study. Hardness, reduced modulus and thickness of tribo-films were measured. It is suggested that the further analysis of tribo-film could focus on the chemical basis on the purpose to fully understand the tribological mechanism of lubricant. X-ray photoelectron spectroscopy (XPS) has been proved that it is the most common method to exam the chemical deposition of tribo-film by the work of many scholars.

Friction coefficient results

In this study, some of the typical coefficient of friction results have been selected and presented, for example, in chapter 8, only the coefficient of friction of samples that with 1% concentration is presented. This is because of the results of other concentrations all show similar trends and outcomes, for the consideration of presenting and less confusion, therefore, only selective results of coefficient of friction have been included. However, it would be a great enforcement of this piece of thesis to present all results. It would include as a future work.

References

1. Hernández Battez, A., et al., *CuO, ZrO₂ and ZnO nanoparticles as antiwear additive in oil lubricants*. *Wear*, 2008. **265**(3): p. 422-428.
2. Xue, Q., W. Liu, and Z. Zhang, *Friction and wear properties of a surface-modified TiO₂ nanoparticle as an additive in liquid paraffin*. *Wear*, 1997. **213**(1): p. 29-32.
3. Hu, Z., et al., *Preparation and tribological properties of nanoparticle lanthanum borate*. *Wear*, 2000. **243**(1-2): p. 43-47.
4. Li, Z. and Y. Zhu, *Surface-modification of SiO₂ nanoparticles with oleic acid*. *Applied Surface Science*, 2003. **211**(1): p. 315-320.
5. Bakunin, V.N., et al., *Synthesis and Application of Inorganic Nanoparticles as Lubricant Components – a Review*. *Journal of Nanoparticle Research*, 2004. **6**(2): p. 273-284.
6. Yu, H., et al., *Effect of thermal activation on the tribological behaviours of serpentine ultrafine powders as an additive in liquid paraffin*. *Tribology International*, 2011. **44**(12): p. 1736-1741.
7. Zhao, C., et al., *The preparation and tribological properties of surface modified zinc borate ultrafine powder as a lubricant additive in liquid paraffin*. *Tribology International*, 2014. **70**: p. 155-164.
8. Li, B., et al., *Tribochemistry and antiwear mechanism of organic–inorganic nanoparticles as lubricant additives*. *Tribology Letters*, 2006. **22**(1): p. 79-84.

9. Sperling, R.A. and W.J. Parak, *Surface modification, functionalization and bioconjugation of colloidal inorganic nanoparticles*. Philosophical Transactions of the Royal Society A: Mathematical, Physical and Engineering Sciences, 2010. **368**(1915): p. 1333-1383.
10. Veriansyah, B., et al., *Characterization of surface-modified ceria oxide nanoparticles synthesized continuously in supercritical methanol*. The Journal of Supercritical Fluids, 2009. **50**(3): p. 283-291.
11. Liu, W. and S. Chen, *An investigation of the tribological behaviour of surface-modified ZnS nanoparticles in liquid paraffin*. Wear, 2000. **238**(2): p. 120-124.
12. Zhou, J., et al., *Study on the structure and tribological properties of surface-modified Cu nanoparticles*. Materials Research Bulletin, 1999. **34**(9): p. 1361-1367.
13. Xu, T., et al., *Study on the structure of surface-modified MoS₂ nanoparticles*. Materials Research Bulletin, 1996. **31**(4): p. 345-349.
14. Kolodziejczyk, L., et al., *Surface-modified Pd nanoparticles as a superior additive for lubrication*. Journal of Nanoparticle Research, 2007. **9**(4): p. 639-645.
15. Ye, Y.-P., J.-M. Chen, and H.-D. Zhou, *Influence of nanometer lanthanum fluoride on friction and wear behaviors of bonded molybdenum disulfide solid lubricating films*. Surface and Coatings Technology, 2009. **203**(9): p. 1121-1126.
16. Zhang, Z.-F., W.-M. Liu, and Q.-J. Xue, *The tribological behaviors of succinimide-modified lanthanum hydroxide nanoparticles blended with zinc*

-
- dialkyldithiophosphate as additives in liquid paraffin*. *Wear*, 2001. **248**(1–2): p. 48-54.
17. Evans, D.R. *Cerium Oxide Abrasives—Observations and Analysis*. in *MRS Proceedings*. 2004. Cambridge Univ Press.
 18. Dong, J. and Z. Hu, *A study of the anti-wear and friction-reducing properties of the lubricant additive, nanometer zinc borate*. *Tribology International*, 1998. **31**(5): p. 219-223.
 19. Tian, Y., et al., *Synthesis of hydrophobic zinc borate nanodiscs for lubrication*. *Materials Letters*, 2006. **60**(20): p. 2511-2515.
 20. Hutchings, I.M., *Tribology: friction and wear of engineering materials*. 1992: p. 1-2.
 21. Bhushan, B., *Introduction to tribology*. 2002, John Wiley & Sons: New York. p. 331.
 22. Hutchings, I.M. and P. Shipway, *Tribology: friction and wear of engineering materials*. 1992: Edward Arnold. p.2-3.
 23. Khonsari, M.M. and E.R. Booser, *Applied tribology: bearing design and lubrication*. Vol. 12. 2008: John Wiley & Sons.
 24. Ludema, K.C., *Friction, wear, lubrication: a textbook in tribology*. 1996: CRC press.
 25. Burwell Jr, J.T., *Survey of possible wear mechanisms*. *Wear*, 1957. **1**(2): p. 119-141.
 26. Bhushan, B., *Introduction to Tribology*. 2013: John Wiley & Sons. p. 347.

27. Hutchings, I.M. and P. Shipway, *Tribology: friction and wear of engineering materials*. 1992: Edward Arnold. p.200.
28. Rabinowicz, E., *The least wear*. Wear, 1984. **100**(1–3): p. 533-541.
29. Stachowiak, G. and A.W. Batchelor, *Engineering tribology*. 2013: Butterworth-Heinemann.
30. Mee, M. and A.A. Torrance, *A study of the lubricated wear of plain bearing materials in a ZDDP-containing lubricant*. Wear, 1988. **128**(2): p. 201-217.
31. Barnes, A.M., K.D. Bartle, and V.R.A. Thibon, *A review of zinc dialkyldithiophosphates (ZDDPS): characterisation and role in the lubricating oil*. Tribology International, 2001. **34**(6): p. 389-395.
32. Lin, Y. and H. So, *Limitations on use of ZDDP as an antiwear additive in boundary lubrication*. Tribology International, 2004. **37**(1): p. 25-33.
33. Bhushan, B., *Introduction to Tribology*. 2013: John Wiley & Sons. p. 346.
34. Misra, A. and I. Finnie, *Some observations on two-body abrasive wear*. Wear, 1981. **68**(1): p. 41-56.
35. Sin, H., N. Saka, and N. Suh, *Abrasive wear mechanisms and the grit size effect*. Wear, 1979. **55**(1): p. 163-190.
36. Hokkirigawa, K., K. Kato, and Z. Li, *The effect of hardness on the transition of the abrasive wear mechanism of steels*. Wear, 1988. **123**(2): p. 241-251.
37. Bakshi, S.D., P. Shipway, and H. Bhadeshia, *Three-body abrasive wear of fine pearlite, nanostructured bainite and martensite*. Wear, 2013. **308**(1): p. 46-53.
38. Alen John, D.Y.V.K.S.R., Jerin Sabu, Rajeev V. R *Stress Analysis of Polyoxymethylene which Leads to Wear in Pin on Disc Configuration using*

-
- Finite Element Method*. International Journal of Research in Advent Technology, 2014. **2**(4).
39. Vingsbo, O., *Wear and wear mechanisms*. Wear of Materials, 1979: p. 620-635.
40. Szolwinski, M.P. and T.N. Farris, *Mechanics of fretting fatigue crack formation*. Wear, 1996. **198**(1): p. 93-107.
41. Bhushan, B., *Introduction to Tribology*. 2013: John Wiley & Sons. p. 380.
42. Davis, J.R., *Surface engineering for corrosion and wear resistance*. 2001: ASM international.
43. de Baets, P., K. Strijckmans, and A.P. van Peteghem, *A comparative study of different wear measurement techniques applied to fretting wear of a spherical against a flat steel specimen*. Tribotest, 1997. **4**(2): p. 129-143.
44. Kuo, W.-F., Y.-C. Chiou, and R.-T. Lee, *A study on lubrication mechanism and wear scar in sliding circular contacts*. Wear, 1996. **201**(1): p. 217-226.
45. Committee, A.I.H., *ASM handbook: Friction, lubrication, and wear technology*. Vol. 18. 1992: ASM International.
46. Bhushan, B., *Introduction to Tribology*. 2013: John Wiley & Sons. p. 207-209.
47. Hutchings, I.M. and P. Shipway, *Tribology: friction and wear of engineering materials*. 1992: Edward Arnold. p.22-25.
48. Amontons, G., *De la résistance causée dans les machines*. Mémoires de l'Académie des Sciences, 1699: p. 257-282.

49. Coulomb, *Théorie des machines simples, en ayant égard au frottement de leurs parties et la roideur des cordages*. Mémoires de Mathématique et de Physique, présentés à L'Académie Royales des Sciences, 1785. **10**: p. 161-342.
50. Bhushan, B., *Introduction to Tribology*. 2013: John Wiley & Sons. p. 214.
51. Popova, E. and V.L. Popov, *The research works of Coulomb and Amontons and generalized laws of friction*. Friction, 2015. **3**(2): p. 183-190.
52. Bowden, F. and D. Tabor, *The friction and lubrication of solids, part II*. 1964, Clarendon Press, Oxford.
53. Bhushan, B., *Principles and applications of tribology*. 2013: John Wiley & Sons.
54. Bhushan, B., *Introduction to Tribology*. 2013: John Wiley & Sons. p. 216.
55. Greenwood, J. and D. Tabor, *The friction of hard sliders on lubricated rubber: the importance of deformation losses*. Proceedings of the Physical Society, 1958. **71**(6): p. 989.
56. Rigney, D.A. and J.P. Hirth, *Plastic deformation and sliding friction of metals*. Wear, 1979. **53**(2): p. 345-370.
57. Bhushan, B., *Introduction to Tribology*. , 2013: John Wiley & Sons. p. 225.
58. Bhushan, B., *Introduction to tribology*. 2002: Wiley.
59. Hutchings, I.M., *Tribology: friction and wear of engineering materials*. 1992: Butterworth-Heinemann Ltd.
60. Suh, N.P. and H.C. Sin, *The genesis of friction*. Wear, 1981. **69**(1): p. 91-114.
61. Bhushan, B., *Introduction to Tribology*. , 2013: John Wiley & Sons. p. 226.

-
62. Buckley, D.H., *Surface films and metallurgy related to lubrication and wear*. Progress in Surface Science, 1982. **12**(1): p. 1-153.
 63. Rabinowicz, E., *Friction and wear of materials*. Vol. 2. 1965: Wiley New York.
 64. Blau, P.J., *On the nature of running-in*. Tribology International, 2005. **38**(11–12): p. 1007-1012.
 65. Blau, P.J., *Friction and wear transitions of materials*. 1989.
 66. Bartels, T., et al., *Lubricants and Lubrication*. Ullmann's Encyclopedia of Industrial Chemistry, 2005.
 67. Hutchings, I.M. and P. Shipway, *Tribology: friction and wear of engineering materials*. 1992: Edward Arnold. p.58.
 68. Zhao, C., *The Influence of Solid Additives on the Tribological Properties of Lubricants*. 2013: p. 119 -137.
 69. Bhushan, B., *Introduction to Tribology*. 2013: John Wiley & Sons. p. 424.
 70. Bisson, E.E. and W.J. Anderson, *Advanced bearing technology*. 1964, NASA. Adm. George C. Marshall Space Flight Cent.
 71. Bhushan, B., *Introduction to Tribology*. 2013: John Wiley & Sons. p. 426.
 72. Zhu, D. and Q.J. Wang, *EHL History (Elastohydrodynamic Lubrication)*, in *Encyclopedia of Tribology*, Q.J. Wang and Y.-W. Chung, Editors. 2013, Springer US: Boston, MA. p. 832-847.
 73. Bhushan, B., *Introduction to Tribology*. 2013: John Wiley & Sons. p. 427.
 74. Hutchings, I.M. and P. Shipway, *Tribology: friction and wear of engineering materials*. 1992: Edward Arnold. p.67-69.

-
75. Woydt, M. and R. Wäsche, *The history of the Stribeck curve and ball bearing steels: The role of Adolf Martens*. *Wear*, 2010. **268**(11–12): p. 1542-1546.
76. Hardy, W. and I. Doubleday, *Boundary lubrication. The paraffin series*. Proceedings of the Royal Society of London. Series A, Containing Papers of a Mathematical and Physical Character, 1922: p. 550-574.
77. Spikes, H.A., *Boundary Lubrication and Boundary Films*, in *Tribology Series*, C.M.T.T.H.C.C.M.G. D. Dowson and G. Dalmaz, Editors. 1993, Elsevier. p. 331-346.
78. Hsu, S.M. and R.S. Gates, *Boundary lubricating films: formation and lubrication mechanism*. *Tribology International*, 2005. **38**(3): p. 305-312.
79. Bieber, H., E. Klaus, and E. Tewksbury, *A study of tricresyl phosphate as an additive for boundary lubrication*. *ASLE TRANSACTIONS*, 1968. **11**(2): p. 155-161.
80. Cann, P. and A. Cameron, *Studies of thick boundary lubrication — influence of zddp and oxidized hexadecane*. *Tribology International*, 1984. **17**(4): p. 205-208.
81. Heyes, D.M., *Molecular aspects of boundary lubrication*. *Tribology International*, 1996. **29**(8): p. 627-629.
82. Zhang, Y., *Boundary lubrication—An important lubrication in the following time*. *Journal of Molecular Liquids*, 2006. **128**(1–3): p. 56-59.
83. Swalen, J.D., et al., *Molecular monolayers and films. A panel report for the materials sciences division of the department of energy*. *Langmuir*, 1987. **3**(6): p. 932-950.

-
84. Anghel, V., P. Cann, and H. Spikes, *Direct measurement of boundary lubricating films*. Tribology Series, 1997. **32**: p. 459-466.
 85. Guangteng, G. and H.A. Spikes, *Boundary Film Formation by Lubricant Base Fluids*. Tribology Transactions, 1996. **39**(2): p. 448-454.
 86. Choa, S.-H., et al., *A model of the dynamics of boundary film formation*. Wear, 1994. **177**(1): p. 33-45.
 87. Bruce, R.W., *Handbook of Lubrication and Tribology, Volume II: Theory and Design*. Vol. 2. 2012: CRC press. p.20-7.
 88. Cabrera, N. and N. Mott, *Theory of the oxidation of metals*. Reports on progress in physics, 1949. **12**(1): p. 163.
 89. Liu, Y., et al., *Structure and frictional properties of self-assembled surfactant monolayers*. Langmuir, 1996. **12**(5): p. 1235-1244.
 90. Lansdown, A.R., *Molybdenum disulphide lubrication*. Vol. 35. 1999: Elsevier. p.33.
 91. Martin, J., et al., *Superlubricity of molybdenum disulphide*. Physical Review B, 1993. **48**(14): p. 10583.
 92. Winer, W., *Molybdenum disulfide as a lubricant: a review of the fundamental knowledge*. Wear, 1967. **10**(6): p. 422-452.
 93. Zhao, C., *The influence of solid additives on the tribological properties of lubricants*. 2013: p. 32 - 33.
 94. Guangteng, G. and H.A. Spikes, *The control of friction by molecular fractionation of base fluid mixtures at metal surfaces*. Tribology Transactions, 1997. **40**(3): p. 461-469.

-
95. Erdemir, A., O. Eryilmaz, and G. Fenske, *Self-replenishing solid lubricant films on boron carbide*. Surface Engineering, 1999. **15**(4): p. 291-295.
 96. Chen, S.-H., *Self-replenishing hydrodynamic bearing*. 1995, Google Patents.
 97. Stribeck, R., *Kugellager für beliebige Belastungen*. 1901: Buchdruckerei AW Schade, Berlin N.
 98. Kondo, Y., T. Koyama, and S. Sasaki, *Tribological properties of ionic Liquids*, in *Ionic liquids-New aspects for the future*. 2013, InTech.
 99. Kondo, Y., S. Sasaki, and T. Koyama, *Tribological properties of ionic liquids*. 2013: INTECH Open Access Publisher.
 100. Stribeck, P., *Die wesentlichen Eigenschaften der Gleit-und Rollenlager*. Z. Ver. Dt. Ing, 1902. **46**(38): p. 1341-1348.
 101. Stachowiak, G.W. and A.W. Batchelor, *Engineering tribology*. 2005: Butterworth-Heinemann.
 102. Wu, Y. and B. Dacre, *Effects of lubricant-additives on the kinetics and mechanisms of ZDDP adsorption on steel surfaces*. Tribology International, 1997. **30**(6): p. 445-453.
 103. Mourhatch, R. and P.B. Aswath, *Nanoscale properties of tribofilms formed with zinc dialkyl dithiophosphate (ZDDP) under extreme pressure condition*. Journal of nanoscience and nanotechnology, 2009. **9**(4): p. 2682-2691.
 104. Ma, Y., et al., *The effect of oxy-nitrided steel surface on improving the lubricating performance of tricresyl phosphate*. Wear, 1997. **210**(1-2): p. 287-290.

-
105. Godfrey, D., *The lubrication mechanism of tricresyl phosphate on steel*. ASLE TRANSACTIONS, 1965. **8**(1): p. 1-11.
 106. Mortier, R.M., M.F. Fox, and S.T. Orszulik, *Chemistry and technology of lubricants*. 2010: Springer Verlag.
 107. Zhang, M., et al., *Performance and anti-wear mechanism of CaCO₃ nanoparticles as a green additive in poly-alpha-olefin*. Tribology International, 2009. **42**(7): p. 1029-1039.
 108. Sunqing, Q., D. Junxiu, and C. Guoxu, *Wear and friction behaviour of CaCO₃ nanoparticles used as additives in lubricating oils*. Lubrication Science, 2000. **12**(2): p. 205-212.
 109. Hernández Battez, A., et al., *CuO, ZrO₂ and ZnO nanoparticles as antiwear additive in oil lubricants*. Wear, 2008. **265**(3–4): p. 422-428.
 110. Huang, H., et al., *An investigation on tribological properties of graphite nanosheets as oil additive*. Wear, 2006. **261**(2): p. 140-144.
 111. Sliney, H.E., *Rare earth fluorides and oxides used as solid lubricants at high temperatures*. NASA-TN-D-5301, 1969.
 112. Aldorf, H.E., *Rare earth halide grease compositions*. 1985, Google Patents.
 113. Yu, L., M. Nie, and Y. Lian, *The tribological behaviour and application of rare earth lubricants*. Wear, 1996. **197**(1–2): p. 206-210.
 114. Sliney, H.E., *Rare-earth fluorides and oxides—their use as solidlubricants at temperature to 1000 °C*. NASA Technical Note, NASA-TN-D-5301 (1969), 1969.

115. Zhang, Z., et al., *The effect of LaF₃ nanocluster modified with succinimide on the lubricating performance of liquid paraffin for steel-on-steel system*. Tribology International, 2001. **34**(2): p. 83-88.
116. Wang, L., et al., *The preparation of CeF₃ nanocluster capped with oleic acid by extraction method and application to lithium grease*. Materials Research Bulletin. **43**(8-9): p. 2220-2227.
117. Gu, C., et al., *Study on application of CeO₂ and CaCO₃ nanoparticles in lubricating oils*. Journal of Rare Earths, 2008. **26**(2): p. 163-167.
118. Ru Yang, J.L., Ming Li, *Synthesis of mesoporous ceria using a non-surfactant template approach*. Journal of the Chinese Rare Earth Society, 2004. **22**(6).
119. Tian, Y., et al., *Self-assembly of monodisperse SiO₂-zinc borate core-shell nanospheres for lubrication*. Materials Letters, 2007. **61**(2): p. 506-510.
120. Schubert, D.M., et al., *Structural characterization and chemistry of the industrially important zinc borate, Zn [B₃O₄ (OH) ₃]*. Chemistry of materials, 2003. **15**(4): p. 866-871.
121. Hu, Z. and J. Dong, *Study on antiwear and reducing friction additive of nanometer titanium borate*. Wear, 1998. **216**(1): p. 87-91.
122. Zeng, Y., et al., *Synthesis of magnesium borate (Mg₂B₂O₅) nanowires, growth mechanism and their lubricating properties*. Materials Research Bulletin. **43**(8-9): p. 2239-2247.
123. Hu, Z.S., et al., *Preparation and tribological properties of nanometer magnesium borate as lubricating oil additive*. Wear, 2002. **252**(5-6): p. 370-374.

-
124. Li-Feng, H., et al., *Preparation and Tribological Properties of Surface-modified Borate Magnesium Nanoparticles*. Journal of Inorganic Materials. **25**.
125. Jia, Z. and Y. Xia, *Hydrothermal Synthesis, Characterization, and Tribological Behavior of Oleic Acid-Capped Lanthanum Borate with Different Morphologies*. Tribology Letters, 2011. **41**(2): p. 425-434.
126. Kong, L., et al., *Synthesis and surface modification of the nanoscale cerium borate as lubricant additive*. Journal of Rare Earths, 2011. **29**(11): p. 1095-1099.
127. Zhao, C., *The Influence of Solid Additives on the Tribological Properties of Lubricants*. 2013: p. 137-153.
128. Hu, Z.S., J.X. Dong, and G.X. Chen, *Study on antiwear and reducing friction additive of nanometer ferric oxide*. Tribology International, 1998. **31**(7): p. 355-360.
129. Jiao, D., et al., *The tribology properties of alumina/silica composite nanoparticles as lubricant additives*. Applied Surface Science, 2011. **257**(13): p. 5720-5725.
130. Pourjavadi, A., et al., *Improving the performance of cement-based composites containing superabsorbent polymers by utilization of nano-SiO₂ particles*. Materials & Design, 2012. **42**(0): p. 94-101.
131. Arumugam, S. and G. Sriram, *Preliminary Study of Nano and Micro-Scale TiO₂ Additives on Tribological Behavior of Chemically Modified Rapeseed Oil*. Tribology Transactions, 2013: p. null-null.
132. Hernandez Battez, A., et al., *The tribological behaviour of ZnO nanoparticles as an additive to PAO6*. Wear, 2006. **261**(3): p. 256-263.

-
133. Hernández Battez, A., et al., *Friction reduction properties of a CuO nanolubricant used as lubricant for a NiCrBSi coating*. *Wear*, 2010. **268**(1): p. 325-328.
134. *The lubrication mechanism of tricresyl phosphate on steel* : D. Godfrey, *ASLE Trans.*, 8 (1965) in press; Paper No. 64 LC-1; 8 figs., 2 tables, 45 refs. *Wear*, 1965. **8**(5): p. 412.
135. *Effects of P32 impurities on the behavior of tricresyl phosphate-32 as an antiwear additive* : E. E. Klaus and H. E. Bieber, *ASLE Trans.*, 8 (1965) in press; Paper No. 64 LC-2; 4 figs., 9 tables, 14 refs. *Wear*, 1965. **8**(5): p. 412.
136. *Neopentyl polyol esters for jet engine lubricants—effect of tricresyl phosphate on thermal stability and corrosivity* : R. L. Cottingham and H. Ravner, *Naval Res. Lab. Rept. 6667, Feb. 1968, 20 pp.* *Wear*, 1968. **12**(4): p. 300.
137. Sheasby, J.S., T.A. Caughlin, and J.J. Habeeb, *Observation of the antiwear activity of zinc dialkyldithiophosphate additives*. *Wear*, 1991. **150**(1–2): p. 247-257.
138. Wu, H., Y.-G. Wang, and T.-H. Ren, *The tribological properties and action mechanism of non-active organic molybdate ester and its combination with ZDDP*. *Tribology International*, 2012. **49**(0): p. 90-95.
139. Hu, J.-Q., et al., *Tribological behaviors and mechanism of sulfur- and phosphorus-free organic molybdate ester with zinc dialkyldithiophosphate*. *Tribology International*, 2008. **41**(6): p. 549-555.
140. Pidduck, A. and G. Smith, *Scanning probe microscopy of automotive anti-wear films*. *Wear*, 1997. **212**(2): p. 254-264.

-
141. Li, J., et al., *The tribological study of a tetrazole derivative as additive in liquid paraffin*. *Wear*, 2000. **246**(1–2): p. 130-133.
142. Peng, D., et al., *Tribological properties of diamond and SiO₂ nanoparticles added in paraffin*. *Tribology International*, 2009. **42**(6): p. 911-917.
143. Zhang, Z., W. Liu, and Q. Xue, *Study on lubricating mechanisms of La(OH)₃ nanocluster modified by compound containing nitrogen in liquid paraffin*. *Wear*, 1998. **218**(2): p. 139-144.
144. Zhang, J., et al., *Investigation of the friction and wear behaviors of Cu(I) and Cu(II) dioctyldithiophosphates as additives in liquid paraffin*. *Wear*, 1998. **216**(1): p. 35-40.
145. Igari, S., S. Mori, and Y. Takikawa, *Effects of molecular structure of aliphatic diols and polyalkylene glycol as lubricants on the wear of aluminum*. *Wear*, 2000. **244**(1-2): p. 180-184.
146. Asadauskas, S., J.M. Perez, and J.L. Duda, *Lubrication properties of castor oil - Potential basestock for biodegradable lubricants*©. *Lubrication Engineering*, 1997. **53**(12): p. 35-40.
147. Fox, N.J. and G.W. Stachowiak, *Vegetable oil-based lubricants—A review of oxidation*. *Tribology International*, 2007. **40**(7): p. 1035-1046.
148. Hamdan, S., et al., *Influence of fatty acid methyl ester composition on tribological properties of vegetable oils and duck fat derived biodiesel*. *Tribology International*, 2017. **113**: p. 76-82.
149. Allawzi, M., et al., *Physicochemical characteristics and thermal stability of Jordanian jojoba oil*. *Journal of the American Oil Chemists' Society*, 1998. **75**(1): p. 57-62.

-
150. Choi, U.S., et al., *Tribological behavior of some antiwear additives in vegetable oils*. Tribology International, 1997. **30**(9): p. 677-683.
151. Booker, M.L., et al., *Effects of dietary cholesterol and triglycerides on lipid concentrations in liver, plasma, and bile*. Lipids, 1997. **32**(2): p. 163-172.
152. Yu, W., H. Xie, and L.H. Liu, *A Review on Nanofluids: Preparation, Stability Mechanisms, and Applications*. Journal of Nanomaterials, 2011. **2012**(711): p. 128.
153. Chen, L., et al., *Nanofluids containing carbon nanotubes treated by mechanochemical reaction*. Thermochemica acta, 2008. **477**(1-2): p. 21-24.
154. Kopperud, H.M., F.K. Hansen, and B. Nyström, *Effect of surfactant and temperature on the rheological properties of aqueous solutions of unmodified and hydrophobically modified polyacrylamide*. Macromolecular Chemistry and Physics, 1998. **199**(11): p. 2385-2394.
155. Plueddemann, E.P., *Chemistry of Silane Coupling Agents*, in *Silane Coupling Agents*. 1991, Springer US: Boston, MA. p. 31-54.
156. Arkles, B., *Tailoring Surfaces with Silanes*. Chem Tech, 1977. **7**: p. 13.
157. Hegde, N.D. and A.V. Rao, *Organic modification of TEOS based silica aerogels using hexadecyltrimethoxysilane as a hydrophobic reagent*. Applied Surface Science, 2006. **253**(3): p. 1566-1572.
158. Gomathi, A. and C.N.R. Rao, *Hexadecyltriethoxysilane-induced Dispersions of Metal Oxide Nanoparticles in Nonpolar Solvents*. Journal of Cluster Science, 2008. **19**(1): p. 247-257.

-
159. Zhang, Z., W. Liu, and Q. Xue, *Study on lubricating mechanisms of La (OH) 3 nanocluster modified by compound containing nitrogen in liquid paraffin*. *Wear*, 1998. **218**(2): p. 139-144.
160. Fekete, E., et al., *Surface modification and characterization of particulate mineral fillers*. *Journal of Colloid and Interface Science*, 1990. **135**(1): p. 200-208.
161. Papirer, E., J. Schultz, and C. Turchi, *Surface properties of a calcium carbonate filler treated with stearic acid*. *European polymer journal*, 1984. **20**(12): p. 1155-1158.
162. Gao, Y., et al., *Study on tribological properties of oleic acid-modified TiO₂ nanoparticle in water*. *Wear*, 2002. **252**(5-6): p. 454-458.
163. Kang, X., et al., *Synthesis and tribological property study of oleic acid-modified copper sulfide nanoparticles*. *Wear*, 2008. **265**(1-2): p. 150-154.
164. Li, Z. and Y. Zhu, *Surface-modification of SiO₂ nanoparticles with oleic acid*. *Applied Surface Science*, 2003. **211**(1-4): p. 315-320.
165. Jiao, D., et al., *The tribology properties of alumina/silica composite nanoparticles as lubricant additives*. *Applied Surface Science*, 2011.
166. Alecrim, L., et al., *Sliding wear behavior of Al₂O₃-NbC composites obtained by conventional and nonconventional techniques*. *Tribology International*, 2017. **110**: p. 216-221.
167. Gui, S., X. Shen, and B. Lin, *Surface organic modification of Fe₃O₄ nanoparticles by silane-coupling agents*. *Rare Metals*, 2006. **25**(6): p. 426-430.

-
168. Zhou, X., et al., *Study on the tribological properties of surfactant-modified MoS₂ micrometer spheres as an additive in liquid paraffin*. Tribology International, 2007. **40**(5): p. 863-868.
169. Xu, Z., et al., *Formation and tribological properties of hollow sphere-like nano-MoS₂ precipitated in TiO₂ particles*. Tribology International, 2015. **81**: p. 139-148.
170. Hong, R., et al., *Synthesis and surface modification of ZnO nanoparticles*. Chemical Engineering Journal, 2006. **119**(2): p. 71-81.
171. Salameh, S., et al., *Contact behavior of size fractionated TiO₂ nanoparticle agglomerates and aggregates*. Powder Technology, 2014. **256**(0): p. 345-351.
172. Liu, Y., J. Zhou, and T. Shen, *Effect of nano-metal particles on the fracture toughness of metal–ceramic composite*. Materials & Design, 2013. **45**(0): p. 67-71.
173. Yu, H., et al., *Tribological properties and lubricating mechanisms of Cu nanoparticles in lubricant*. Transactions of Nonferrous Metals Society of China, 2008. **18**(3): p. 636-641.
174. Ye, W., et al., *Preparation and tribological properties of tetrafluorobenzoic acid-modified TiO₂ nanoparticles as lubricant additives*. Materials Science and Engineering: A, 2003. **359**(1): p. 82-85.
175. Zhou, J., et al., *Study on an antiwear and extreme pressure additive of surface coated LaF₃ nanoparticles in liquid paraffin*. Wear, 2001. **249**(5–6): p. 333-337.
176. Durst, R.A., *Ion-selective electrodes: proceedings*. 1969: US National Bureau of Standards; for sale by the Supt. of Docs., US Govt. Print. Off., Washington.

-
177. Zhao, C., Y.K. Chen, and G. Ren, *A Study of Tribological Properties of Water-Based Ceria Nanofluids*. Tribology Transactions, 2013. **56**(2): p. 216-223.
178. Braun, U., et al., *Flame retardancy mechanisms of aluminium phosphinate in combination with melamine polyphosphate and zinc borate in glass-fibre reinforced polyamide 6, 6*. Polymer degradation and stability, 2007. **92**(8): p. 1528-1545.
179. Gurrappa, I. and L. Binder, *Electrodeposition of nanostructured coatings and their characterization—A review*. Science and Technology of Advanced Materials, 2008. **9**(4): p. 043001.
180. Carpentier, F., et al., *Charring of fire retarded ethylene vinyl acetate copolymer—magnesium hydroxide/zinc borate formulations*. Polymer degradation and stability, 2000. **69**(1): p. 83-92.
181. Durin-France, A., et al., *Magnesium hydroxide/zinc borate/talc compositions as flame-retardants in EVA copolymer*. Polymer international, 2000. **49**(10): p. 1101-1105.
182. Hu, Z.S. and J.X. Dong, *Study on antiwear and reducing friction additive of nanometer titanium oxide*. Wear, 1998. **216**(1): p. 92-96.
183. Saikko, V., *Effect of contact area on the wear of ultrahigh molecular weight polyethylene in noncyclic pin-on-disk tests*. Tribology International, 2017. **114**: p. 84-87.
184. Verma, P.C., et al., *Role of the friction layer in the high-temperature pin-on-disc study of a brake material*. Wear, 2016. **346**: p. 56-65.

-
185. Johnson, K.L. and K.L. Johnson, *Contact mechanics*. 1987: Cambridge university press.
186. Ajayi, O. and R. Erck. *Variation of nominal contact pressure with time during sliding wear*. in *International Joint Tribology Conference*. 2001.
187. Reichelt, R., *Scanning electron microscopy*, in *Science of microscopy*. 2007, Springer. p. 133-272.
188. Oyen, M.L. and R.F. Cook, *A practical guide for analysis of nanoindentation data*. *Journal of the mechanical behavior of biomedical materials*, 2009. **2**(4): p. 396-407.
189. Fox, N., B. Tyrer, and G. Stachowiak, *Boundary lubrication performance of free fatty acids in sunflower oil*. *Tribology Letters*, 2004. **16**(4): p. 275-281.
190. Zhang, P., et al., *The tribological behavior of LB films of fatty acids and nanoparticles*. *Wear*, 2000. **242**(1): p. 147-151.
191. Ren, S.-L., et al., *Preparation and tribological studies of stearic acid self-assembled monolayers on polymer-coated silicon surface*. *Chemistry of materials*, 2004. **16**(3): p. 428-434.
192. Schmid, G., *Nanoparticles*. 2004: Wiley-vch Weinheim.
193. Evans, D.R., *Cerium Oxide Abrasives – Observations and Analysis*. *MRS Online Proceedings Library*, 2004. **816**: p. null-null.
194. Miller, J.C. and J.N. Miller, *Basic statistical methods for analytical chemistry. Part I. Statistics of repeated measurements. A review*. *Analyst*, 1988. **113**(9): p. 1351-1356.

-
195. Saha, R. and W.D. Nix, *Effects of the substrate on the determination of thin film mechanical properties by nanoindentation*. Acta Materialia, 2002. **50**(1): p. 23-38.
196. Kamitsos, E.I., et al., *Infrared reflectance spectra of lithium borate glasses*. Journal of Non-Crystalline Solids, 1990. **126**(1-2): p. 52-67.
197. Doweidar, H. and Y.B. Saddeek, *FTIR and ultrasonic investigations on modified bismuth borate glasses*. Journal of Non-Crystalline Solids, 2009. **355**(6): p. 348-354.
198. Kamitsos, E.I., M.A. Karakassides, and G.D. Chryssikos, *Vibrational spectra of magnesium-sodium-borate glasses. 2. Raman and mid-infrared investigation of the network structure*. The Journal of Physical Chemistry, 1987. **91**(5): p. 1073-1079.
199. Zecchina, A., et al., *FTIR investigation of the formation of neutral and ionic hydrogen-bonded complexes by interaction of H-ZSM-5 and H-mordenite with CH₃CN and H₂O: Comparison with the H-NAFION superacidic system*. The Journal of Physical Chemistry, 1996. **100**(41): p. 16584-16599.
200. Lis, G.P., et al., *FTIR absorption indices for thermal maturity in comparison with vitrinite reflectance R₀ in type-II kerogens from Devonian black shales*. Organic Geochemistry, 2005. **36**(11): p. 1533-1552.
201. Carrillo, F., et al., *Structural FTIR analysis and thermal characterisation of lyocell and viscose-type fibres*. European Polymer Journal, 2004. **40**(9): p. 2229-2234.
202. Hunter, R.J., *Zeta potential in colloid science: principles and applications*. Vol. 2. 2013: Academic press.

-
203. Tsui, T.Y. and G.M. Pharr, *Substrate effects on nanoindentation mechanical property measurement of soft films on hard substrates*. Journal of Materials Research, 1999. **14**(1): p. 292-301.
204. Li, C., et al., *Substrate effect on the growth of monolayer dendritic MoS₂ on LaAlO₃ (100) and its electrocatalytic applications*. 2D Materials, 2016. **3**(3): p. 035001.
205. Rebec, S., et al. *ARPES Studies on the substrate effect on monolayer FeSe*. in *APS Meeting Abstracts*. 2016.
206. Luo, Q., *Tribofilms in solid lubricants*. Encyclopedia of Tribology, 2013: p. 3760-3767.
207. Godet, M., *The third-body approach: a mechanical view of wear*. Wear, 1984. **100**(1-3): p. 437-452.
208. Battez, A.H., et al., *CuO, ZrO₂ and ZnO nanoparticles as antiwear additive in oil lubricants*. Wear, 2008. **265**(3): p. 422-428.

